DOE/BC/14951-10
Distribution Category UC-122

INTEGRATED APPROACH TOWARDS THE APPLICATION OF HORIZONTAL WELLS TO IMPROVE WATERFLOODING PERFORMANCE

Annual Report

By
Mohan Kelkar
Chris Liner
Dennis Kerr

May 1995

Work Performed Under Contract No. DE-FC22-93BC14951

Prepared for
U.S. Department of Energy
Assistant Secretary for Fossil Energy

Rhonda P. Lindsey, Project Manager
Bartlesville Project Office
P.O. Box 1398
Bartlesville, OK 74005

Prepared by
The University of Tulsa
Tulsa, OK 74104

Acknowledgment

The research effort described in this report was supported by the U.S. Department of Energy under Contract DE-FC22-93BC14951. Additional support was provided by Amoco Production Company and Uplands Resources, Inc. The computer facilities were provided by the University of Tulsa.

We would like to thank Dan Richmond from Uplands Resources, Inc. for his valuable insights and for his contributions to our work. We also would like to acknowledge the guidance provided by Rich Chambers, Henry Tan, John Eager and Chandra Rai from Amoco Production Co. Lastly, our special thanks go to Rhonda Lindsey, representative of the contracting officer of the project, for her enthusiasm and valuable suggestions.

January 1995

DISCLAIMER

DISCLAIMER

Portions of this document may be illegible in electronic image products. Images are produced from the best available original document.

Abstract

This annual report describes the progress during the second year of the project on Integrated Approach Towards the Application of Horizontal Wells to Improve Waterflooding Performance. This project is funded under the Department of Energy's Class I program which is targeted towards improving the reservoir performance of mature oil fields located in fluvial-dominated deltaic deposits. The project involves an integrated approach to characterize the reservoir followed by the drilling of horizontal injection wells to improve production performance. The type of data we have integrated include cross bore hole seismic surveys, geological interpretation based on logs and cores, and engineering information.

This report covers the second phase of the project which includes a detailed reservoir description of the field by integrating all the available information, followed by flow simulation of the Self Unit under various operating conditions. Based on an examination of the various operating parameters, we observed that the best possible solution to improve the Self Unit performance is to recomplete and stimulate most of the wells followed by an increase in the water injection rate. Drilling of horizontal injection well, although helpful in improving the performance, was not found to be economically feasible. The proposed reservoir management plan will be implemented shortly.

Executive Summary

This annual report discusses the proposed reservoir management plan to improve the production performance of the Self Unit. Based on the preliminary evaluation, a test well (Self Well No. 82) was drilled and cored. Additional log data including FMI (Formation Microscanner Imaging) data were collected from the same well. Using this well as a source well, three cross bore hole tomography surveys were conducted between Self Well No. 82 and the surrounding three wells. With the help of a modified geological description as well as geophysical and engineering data, a detailed reservoir description was constructed. After validating the description by comparing the simulated flow performance with the historical data, several operating scenarios were simulated to optimize the flow performance under modified conditions. A combination of recompletion and stimulation of most wells followed by increasing the water injection rate in the field was observed to be the most optimal change to improve the flow performance of the Self Unit.

This report is divided in four sections. The first section discusses the background and the available data from the Self Unit. The second section discusses the geological description of the Self Unit based on the old data as well as newly acquired data from the Self Well No. 82. The third section provides the geophysical data collection and processing of the tomographic data. The final section discusses the integration of the geological, geophysical and engineering data to generate the reservoir description. The last section also explains the procedure used for selecting the optimal method of reservoir management. The last three sections are briefly summarized below.

The original geological description divided the Self Unit into seven discrete genetic intervals (DGIs). However, based on the newly acquired data from Self Well No. 82, the geological description was modified to include only 6 DGI's to describe the Self Unit. In addition, using the detailed log and FMI information, a detailed facies interpretation and reservoir architecture reconstruction was conducted for each DGI. Petrophysical properties were evaluated to understand the relationship between the facies/subfacies and the petrophysical properties.

The geophysical data collection involved cross bore hole seismic data between Self Well No. 82 and three surrounding wells. Based on the data, cross well tomograms were computed using different software packages. Each software package uses a different method and assumptions. This would allow us to evaluate the minimum capabilities needed to properly process the cross well seismic data. Using the tomograms, a porosity velocity relationship was established. This relationship is useful in generating the petrophysical properties distribution.

Using the geological, geophysical and engineering data (log and core data as well as production data) data, alternative reservoir descriptions were constructed using three approaches: deterministic modeling, stochastic modeling using only geological and engineering data, and stochastic modeling using tomography information. It was observed that the addition of new data always improves the reservoir description. Also, the deterministic model predicts more optimistic results compared to the stochastic models. Using the generated reservoir descriptions, the historical performance was matched with the simulated performance and the future production was predicted under different scenarios. The simulated performances were evaluated using an economic criterion and the best scenario was selected. We hope to have the best scenario implemented in the near future.

Annual Report

Introduction

The overall report is divided into four sections. In this section, we provide the background of the field which is the subject of the investigation. In the second section, we discuss the development of the geological description based on wireline log data and the newly acquired FMI and core data. In the third section, we discuss the geophysical data acquisition and processing. In the last section, we present a method to incorporate geological, geophysical and engineering data to generate the reservoir description. This section also describes the procedure used for selecting the optimum reservoir management plan to improve the production performance of the Self Unit.

Background

The DOE Class I Program is targeted towards improvement of the production performance of existing mature oil fields located in fluvial-dominated deltaic sandstone reservoirs. This project was selected under the near-term program which requires that existing new technologies be applied in these fields to prevent any premature abandonment of these mature fields. The Glenn Pool field selected for this project fits the specific profile under this program.

The Glenn Pool field is located in portions of Tulsa and Creek Counties of Oklahoma. The field was discovered in 1905, and it is estimated to have produced 330 MM barrels of oil from the Middle Pennsylvanian (Desmoinesian) age Bartlesville Sandstone. The field is near the center of the Northeast Oklahoma platform which is situated between the Ozark uplift to the east, the Nemaha ridge to the west, and the Arkoma basin to the south (**Figure 1**). The field encompasses 27,440 acres. Initial production from the wells ranged from 75-500 BOPD to 4,000 BOPD. After discovery in 1905, the field reached peak production in 1907.

The first well in the field was drilled in the Fall of 1905. The well was located on the Ida Glenn farm near the center of the SE/4 of section 10, T17N, R12E, in Tulsa County (Figure 1). The well was 1458 ft. deep and produced at a flowing rate of 75 BOPD. The producing interval was called "Glenn Sandstone" and in the subsequent years became the target pay zone. The average producing thickness was estimated to be close to 240 ft. and was the most productive when compared to the other nearby fields.

Initially, wells were drilled by cable tools. Surface casing of 8-5/8 inch size was set at 275 ft. and open hole drilling was carried out to the top of the Bartlesville reservoir. The hole size was reduced to 6 inches through the pay zone interval. The producing interval was shot with 250-300 quarts of

nitroglycerine, casing set to the top of the sandstone, and the shot hole cleaned out. By 1906, well drilling averaged at the rate of 3 wells per day and in this process orderly spacing of the wells was neglected. Subsequently, the completion was on a ten-acre pattern. Earthen lakes were used for storage on many leases, and oil was shipped to the Texas Gulf Coast by railroad. In 1908, one hundred companies were operating in the field. By 1912, several BCF of natural gas is estimated to have been flared, vented or used as fuel for lighting field operations. The field limits had been defined by 1920. A pipeline through Coffeyville, Kansas connected the field to Chicago and Great Lakes markets. By 1926, twenty-two refineries served the area.

With depletion of production, gas injection was introduced in 1940, and gas collected at producing wells was recycled to injection wells. Waterflooding operations began in 1944. Cumulative oil production records prior to field-wide waterflooding are incomplete. By 1943, it was estimated that the production throughout the field was between 222 and 236 MMBO. Over 100 MMBO had been produced up to 1990 by secondary gas repressuring, waterflooding, and tertiary recovery methods bringing the total production to 330 MMBO. The field is being depleted at present. Several large production units are under waterflood, and a few units have undergone testing and implementation of micellar-polymer enhanced recovery methods. Results have shown the possibility for significant additional volumes of recoverable oil.

Reservoir

The Glenn Sand has been conventionally divided into 3 units: upper, middle and lower Glenn.[1] Each is separated by apparent permeability barriers consisting of interbedded siltstones and shales. In the central portion of the Glenn Pool field the Glenn Sand is present at a depth of approximately 1500 ft., and the thickness varies from 100 to 185 ft. The upper and middle Glenn are the producing intervals in the central portion of the field and the lower Glenn is below the oil-water contact.

Oil from the Glenn Sand has an API gravity of 35.8° to 41.3°. It contains 3.12 to 11.46% paraffin and a sulfur content of 0.3%. Initial reservoir pressure has been estimated in the range of 600 to 700 psi. Current waterflooding injection pressure ranges from 100 to 1100 psi.[1]

From regional studies, the Bartlesville Sandstone is regarded as having been deposited by a fluvial-dominated delta system.[2] In the Glenn Pool field area, the Glenn Sand is predominantly the deposits of delta plain depositional environments. The lower Glenn sandstones are subangular to subrounded, moderately sorted, silty fine- to medium-grained sandstone, with abundant sand-size rock fragments, and thin beds of shale and siltstone.[1] The lower non-porous break consists of interbedded, laminated silty sandstone and shale with localized thin beds of shale, sideritic clay

pebbles and with intervals of carbonate-cemented sandstone.[1] The middle Glenn is subangular to subrounded, and well sorted fine- to very-fine-grained sandstone.[1] It is primarily massively bedded, with portions containing medium-scale crossbedding.[1] The middle Glenn forms the major part of the reservoir.

The upper non-porous break consists of thin silty shale or interbedded laminated, silty sandstone and silty shale.[1] It is an effective permeability barrier but limited lateral extent may result in localized contacts between the upper and middle Glenn. The upper Glenn is in part massively bedded and in part medium-scale crossbedded. It consists of angular to subangular, moderately sorted very-fine to medium-grained sandstones,[1] and contains abundant carbonaceous fragments and a few sand-sized rock fragments. The upper portion of the upper Glenn contains poorly sorted very-fine- to medium-grained sandstones with silty interlaminations, sparse carbonate or silica cement, and visible porosity.

Self Unit

The Self Unit, the area of investigation of Phase I of the project, is a 160 acre tract located in the south-east portion of Glenn Pool oil field in section 21-17N-12E (**Figure 2**). The first well on the lease was put on production on November 6, 1906. In all, 5 wells were put on production in 1906. Out of the three Glenn Sand intervals, the upper and middle are present while the lower Glenn is absent in the Self Unit. ARCO's report by Heath[3] on the Glenn Sand Unit gives a brief history about the performance of the Self Unit.

The original oil in place (OOIP) for the unit has been estimated to be 13.009 MMBO. Primary production during 1906-1945 resulted in the production of 1.809 MMBO representing 13.91% of OOIP. In 1945, gas repressuring began in the unit. This resulted in a recovery of 0.231 MMBO representing 1.8% of OOIP. During 1954-1966 the unit was put on a pilot waterflood resulting in the production of 0.169 MMBO (1.3% of OOIP). The recoveries were higher in the areas surrounding the pilot and the gas injectors. In 1966, waterflooding was extended to the majority of the field. In the initial period of waterflooding, the production increased across the entire Self Unit. The total production during 1966-1978 resulted in production of 0.235 MMBO representing 1.8% of OOIP. The unit was redrilled in 1978 on a ten-acre 5-spot pattern. During 1978-1983, 0.146 MMBO production representing 1.12% of OOIP was obtained. From 1984-1992, production was 0.157 MMBO representing 1.2% of OOIP. Total production obtained to date from the unit is around 20% of the OOIP.

The Self Unit experienced good primary recovery, but response to the subsequent secondary recovery efforts has not been encouraging. A study of the available well logs and core reports

indicates that lithologic heterogeneities and permeability vary throughout the lease. Well logs taken in the 1980's indicate higher water saturations in the middle Glenn portions than in the upper Glenn. Upper Glenn portions could not be swept by waterflooding because, perhaps, of lower permeabilities in these portions and inadequate perforation coverage.

Despite subsequent waterflooding, water injection could not be contained on the lease and water possibly migrated to other parts of the field. Large permeability variations in the upper and middle Glenn also contributed to this inefficient use of water injection. Injection pressures and rates vary throughout the lease; pressures range from 50 to 700 psi, and the rates range from 40 to 2000 barrels of water per day. Current oil production is 25 barrels of oil per day with a 95% water cut.

Data Collection

In total, 81 wells have been drilled on the Self lease. The study required the availability of all well records. Though starting production and abandonment data for most of the wells are available, information with regards to the production history for individual wells could not be traced. The lease-wide production records are not available before the year 1935. Well chronology has been established by analyzing two well maps: well map as of 8/12/55 and well map as of 5/15/81, and the other sparsely available well records. Information pertaining to the number of producing wells each year is available from production documents but information regarding the location or respective number had to be estimated based on the documents mentioned above. The well map depicting all the wells drilled in the Self Unit is shown in **Figure 3.** Initial development occurred along the periphery of the unit; subsequently, development occurred in the interior.

As already mentioned, the unit was put to production in 1906, though no exact date could be found. Heath's report[3] lists the cumulative production through 1946 as 1.809 MMBO. Yearly production information from 1906-1935 was extrapolated based upon the number of wells operating in the respective years and the production information for the years 1935-1946. From 1936-1972, the yearly estimation was carried out on the basis of production information available for one month, three months, or in some cases six months. From 1972 onwards, production data availability is complete and detailed. Annual water injection and production rates are available for the Self Unit and the adjoining Burrows lease combined. Data for individual leases have been obtained based upon their respective oil production fraction. The overall production history based on the above information is summarized in **Figure 4.**

For information related to the petrophysical properties, well logs for the drilled wells after 1978 are available. Permeability data availability for the Self Unit is not that abundant. Though eight core reports are available from the wells operating during the 1940's and 1950's, the logs for those

wells could not be traced and as a result no relationship between the core and well log of the same well could be established. Furthermore, only the existing wells have been logged and there is no core report relevant to these wells.

Well schedule, water injection and production data were summarized based on the 1002-A forms, production reports, PI forms and other miscellaneous documents available from Uplands Resources and Oklahoma Well Log Library.

Based on the available data, a preliminary reservoir description was constructed.[4] Using this description the reservoir performance was simulated followed by the selection of a test well site. The well was drilled in December 1993. The details are provided in the previous annual report. The new data collected from the test well (Self Well No. 82) and the modified geological description based on the new information are discussed in the following section.

Geologic Description
(by Dennis Kerr and Liangmiao Ye)

Executive Summary

In 1994, the geological work for the Glenn Pool project focused on the geological modeling of the Glenn Sand reservoirs in the Self Unit. Through the detailed well log correlation, the Glenn Sand is divided into six discrete genetic intervals (DGIs). As a result of advanced information acquired in the Self Well No. 82, a detailed facies interpretation and reservoir architecture reconstruction have been conducted for each DGI. Petrophysical property measurements of cores were analyzed to evaluate the relationship between petrophysical properties and facies/subfacies and DGIs. The transfer of Phase 1 achievements has begun through presentations and publications.

Data Acquisition

The vertical test well (Self Well No. 82) was drilled for the collection of data using advanced technology, and to evaluate the subsurface mapping completed prior to drilling. The subsurface maps consisted of facies and net-sand isopach maps for each of seven discrete genetic intervals (DGIs).

Core was cut from 1420 to 1575 ft. depth in 3 core runs. The amount of core recovered was 153 ft. with the unrecovered 2 ft. section being from the base of the Glenn Sandstone in core run no. 3. Well site observations noted that oil was bleeding from discrete stratigraphic intervals of 1 to 6 ft. thick in DGI A, C, D, and E. The core was archived and processed at the Amoco Research Lab in Tulsa, Oklahoma.

A detailed core description was made as the core was being processed and prepared for subsampling. The description is stored in a computer graphics software file used by Amoco. The final description includes a hand-drawn lithologic and sedimentary structure profile.

Core plugs were cut using two spacing schemes and different orientations. Because the upper 46 ft. of the core is composed of mudstone and the lower 41 ft. of the core is composed of sandstones largely depleted of hydrocarbons, plugs were cut at about 3 ft. intervals. The upper 46 ft. of the Glenn Sandstone, the interval of greatest interest to the project, was plugged at about 1 ft. intervals. Orientations of plugs in the mudstone interval were horizontal, vertical, and 45 degrees inclined to the core axis; these oriented samples are of particular interest to the geophysical studies. Plugs cut in the sandstones were horizontal and vertical to the core axis at each sampled interval. Core plug measurements include: porosity, permeability, velocity, grain density, and mineralogy. Full results except mineralogy are available.

A microresistivity log (FMI) was successfully acquired in the Self Well No. 82 through the Glenn Sandstone. The data were processed by the Amoco Production Company well log services group in Houston, Texas. The processed log was examined and analyzed with the final core description and photography. The microresistivity was evaluated at Amoco Research Labs in Tulsa, Oklahoma.

Assessment of Pre-Drilling Maps and Correlations

Drilling of the Self Well No. 82 provided an opportunity to assess the predictive quality of the reservoir architecture maps developed prior to drilling. Overall, the expected thicknesses were within the contour interval used in the working facies and net-sand isopach maps (contour interval of 5 ft.) for each discrete genetic interval. The prediction of the presence of DGI B at the location of Self Well No. 82 was not validated by the results of Self Well No. 82; DGI B is markedly truncated by erosion prior to deposition of the channel-fill facies of the overlying DGI A.

Self Well No. 82 well data were integrated with data from the other 41 wells of the Self Unit, resulting in the reevaluation of the Glenn Sand reservoir correlation. It was concluded that the Glenn Sand reservoir is better divided into six DGIs (i.e. descending from A to F) rather than the seven DGIs used in 1993. A sandstone distribution table for each DGI for all wells has been completed, and is the basis for geologic simulation.

Core Description

The whole core collected in the Self Well No. 82 well has been fully documented (**Figure 5**, for example). The documentation includes a detailed sedimentologic description and color photography. Core-plug remnants were used for thin-section cutting. Selected intervals were loaned to the NIPER Lab in Bartlesville, Oklahoma for CTSCAN analysis.

Core observations of sandstones from discrete genetic intervals (DGIs) A and B have bearing on the production potential of the uppermost part of the Glenn Sand. Oil in the sandstone pores appears to be degraded and immobile. Thus, the upper 14 feet of the Glenn Sand is not likely being swept by the present water-flood program, at least in the vicinity of the Self Well No. 82.

Facies/subfacies descriptions for the reservoir sandstones have been refined as a result of the analysis of the Self Well No. 82 core.

Channel-Fill Facies (Encountered in DGIs A, B, and C):

Upward-fining texture. Upward decrease in scale of physical sedimentary structures. Upward increase in proportion of mudstone interbeds. Carbonaceous debris common throughout.

Lower channel-fill subfacies: well to moderately sorted, medium-grained sandstone with medium-scale (2 to 8 in.; 5 to 20 cm.) cross stratification. Mudstone drapes common on cross strata.

Middle channel-fill subfacies: moderately sorted, lower medium-grained to poorly sorted, silty fine-grained sandstones with horizontal to low-angle parallel stratification and ripple lamination. Medium- to very-thin-bedded (1 to 6 in.; 2 to 15 cm.) mudstones to silty mudstones drape lateral accretion surfaces.

Upper channel-fill subfacies: mudstone to silty claystone.

Splay Facies (Encountered in DGIs D and E):

Upward-coarsening texture from fine-grained to medium-grained sandstone. Upward increase in stratal thickness in lower levels only; otherwise, irregular vertical stacking of thick to thin beds (0.4 to 2.5 ft.; 8 to 75 cm.). Ripple lamination and low-angle parallel bedding dominated; medium-scale cross stratification and contorted bedding less common. Thin bedded (0.1 to 0.4 ft.; 3 to 8 cm.) mudstones interstratified with sandstones throughout. DGI D includes more numerous mudstone drapes and thin laminations when compared to DGI E.

Channel-Mouth Bar Facies (Encountered in DGI F):

Channel-mouth bar facies is characterized by well sorted, generally massive, upper medium- to lower coarse-grained sandstone.

Oil staining observed in the Self Well No. 82 core largely correlates with facies/subfacies characteristics (**Figure 6**). In DGI C, actively bleeding oil corresponds to the sandstones between mudstone drapes on lateral accretion surfaces within the middle channel-fill subfacies. By contrast, the cross-stratified sandstones of the lower channel-fill subfacies appear to be flushed. In DGI D, actively bleeding oil was observed from all but one 4 ft. thick sandstone; each interval is divided by interstratified mudstones. Thus, facies/subfacies characteristics appear to be influential in oil saturation of the Glenn Sand.

FMI Analysis

Analysis of the microresistivity imaging log (FMI) collected in the Self Well No. 82 is complete. Efforts have focused on DGIs C, D, and E because these units appear to have the highest potential for additional oil recovery. FMI analysis has constrained the spatial orientation of architectural elements in the vicinity of Self Well No. 82. Using the results from core studies and FMI analysis, a detailed facies architecture has been constructed for the interwell region in the vicinity of Self Well No. 82.

The following list summarizes our conclusions thus far:

Structural dip azimuth averages 153° and dip angle 4°.

DGI C:

Lower channel-fill subfacies cross strata average dip azimuth 121°.

Lateral accretion surface average dip azimuth 150°.

Lateral accretion surface dip azimuth shows progressive upward rotation from 200° to 146°.

Angle of dip azimuth between cross strata and lateral accretion surface indicates a downstream location with increasing amplitude in thalweg sinuosity.

From spatial orientation and vertical spacing, it is expected that 19 lateral accretion mudstone drapes are present between Self Well No. 82 and Self Well No. 81.

DGI D:

Divided into 4 splay units based on orientation patterns and separation by thin mudstone beds.

Relative Level	Dispersal Orientation
highest	southeast
	northwest
	northeast
lowest	southwest

Of the 22 ft. of thickness, only a 4 ft. interval appears to be swept by waterflooding. This is not obvious in a conventional log suite, but was confirmed by the core studies.

DGI E:

Divided into 2 splay units based on orientation patterns.

Relative Level	Dispersal Orientation
higher	south
lower	northeast

The lower of the two splays appears to have a markedly higher water saturation.

Facies Interpretation

Refinements of the facies interpretation and reservoir architecture were achieved through FMI analysis (Self Well No. 82), and core and log facies studies. The results show that DGIs A through E are regarded as delta plain fluvial channel-fill and crevasse splay sandstones and interdistributary mudstones, and F a channel-mouth bar sandstone. At the location of Self Well No. 82, DGI C is dominated by lateral accretion bar deposits, DGI D is divided into 4 splay units and DGI E is divided into 2 splay units.

Facies distribution has very important bearing on the issue of reservoir compartmentalization. Oil in the reservoir can be trapped by the contact surfaces between different facies units and hence bypassed by the waterflooding.

Facies/subfacies distribution for the whole Self Unit and its vicinity has been refined as a result of the detailed correlation and log facies study of all wells in the unit (**Figure 7**, for example).

In DGIs A through E, facies include channel-fill sandstone, splay sandstone and interdistributary mudstone. Throughout the whole unit, DGI F is regarded as channel-mouth bar sandstone.

Detailed Architecture

In light of the findings from the advanced information collected in Self Well No. 82, detailed facies architecture, especially for DGIs C, D, and E, has been constructed for the immediate vicinity of this well. This detail provides an accurate assessment of the level of heterogeneity for each facies/subfacies, which is very useful for developing a reservoir management plan for the Self Unit.

As mentioned before, at the location of Self Well No. 82, DGI C is dominated by lateral accretion bar deposits. Based on the information provided by FMI analysis, it is inferred that Self Well No. 82 is on the downstream side of the accretion, the lateral accretion surface spacing is averaged at 1.08 ft., and the dip angle is averaged at 6°. Based on this information, and with the help of net sand isopach and net/gross ratio map, it is inferred that 19 lateral accretion mudstone drapes are present between Self Well No.'s 82 and 81. The "exact" spatial configuration of lateral accretion surfaces for this point bar deposits is presented in **Figure 8.**

DGIs D and E are composed of splay deposits at the location of Self Well No. 82. They are divided into 4 splay units and 2 splay units respectively (**Figure 9**, for example). FMI analysis indicates dispersal orientations for these six units are, in descending order, 120°, 315°, 70°, 210°, 180°, 30° respectively. With this information and through detailed log correlation among the surrounding wells, the spatial distribution for each unit is exactly located.

For DGIs A and B, at the location of Self Well No. 82, foreset direction is the same as mud drape direction, illustrating that DGIs A and B here do not fall in a lateral accretion bar but channel-fill deposits. DGI F does not show up much orientation information because of its massive structure.

Shale Maps

To delineate the vertical connection between different DGIs, the shale maps constructed in 1993 have been refined as a result of the new correlation scheme, which indicates that DGI's A, B, and C are vertically isolated from each other. There is evidence for vertical connectivity between C and D, D and E, and especially E and F.

The following points summarize the results.

DGIs A and B are totally separated by 3 to 6 ft. thick shale;

DGIs B and C are well separated generally, except at the locations of 4 wells (about 10% in area) where they are directly contacted vertically;

Between DGIs C and D and D and E, the connection becomes more important. For about 10-15% of the Self Unit there is no shale in between them. Both cases have 7 wells with zero shale thickness.

Between DGIs E and F, the connection becomes even more extensive. There are 16 wells (about 40% in area) with zero shale thickness and another 7 wells with only one ft. thick shale.

Structure Maps

High resolution structure maps constructed for the top of the Inola marker and the top of DGI D sandstone show that there are local highs and local lows superimposed on the general southeasterly dip.

High-resolution structure maps for the top of the Inola marker bed and the top of DGI D sandstone were constructed. Both of these two maps show that the Glenn Sand generally dips in a southeasterly direction about 3-5 degrees. Superimposed on this general trend are local highs and local lows.

For example, at the top of DGI D, Self Well No.'s 81, 76, 77, 56, 62 fall in local highs with about 10-15 ft. relief above the general trend, while Self Well No.'s 37, 72, 75, 53, P12 fall in local low areas with 10-20 ft. relief below the general trend (**Figure 10**). This information should be useful for analyzing oil/water distribution

Petrophysical Properties

Analysis of lab core measurements has shown that the porosity and permeability are strongly DGI related. Descending from DGI A to F, porosity increases from about 8 percent to about 22 percent, while permeability increases from less than 0.1 md to more than 300 md (see **Figure 11**).

From the nine cored wells in the Self Unit, the relationship between facies/subfacies and petrophysical properties within a given DGI suggests that splay sandstones may have higher porosity and permeability than channel-fill sandstones (see **Table 1**). However, this difference may not be significant because samples are biased toward high porosity and permeability intervals in wells drilled prior to Self Well No. 82.

Table 1

Comparison Between Channel and Splay Deposits

	Splay Deposits		Channel Deposits	
Unit	Phi(%)	K(md)	Phi(%)	K(md)
DGI C	16.6 (18, 1)	26.7 (18, 1)	15.5 (74, 5)	58.7 (74, 5)
DGI D	17.2 (61, 4)	73.9 (61, 4)	15.6 (90, 5)	51.0 (90, 4)
DGI E	20.7 (35, 3)	148.5(35, 3)	19.3 (125, 6)	126.7 (125, 6)

The numbers in parenthesis are sample size and number of wells, respectively.

Comparison of Geological Models and Geological Simulation Results

Geological models developed to date are being applied to test geological simulation results.

Cell to cell comparison between geological model and geological simulation results is extremely hard to complete based on the current data configuration. But the general image of the geological simulation results is consistent with the geological model.

Transfer of Phase 1 Achievement

A "core party" was held at the Amoco Core Facility on August 18, 1994. Twenty participants from petroleum geology, geophysics and petroleum engineering experts were invited and present. A poster exhibition regarding the achievements and progress of the project was given in late August in the Department of Petroleum Engineering. A presentation entitled "Facies Architecture of Bartlesville Sandstone, Self Unit, Glenn Pool Field" was given to a Venezuelan Petroleum Industry delegation and DOE representatives on October 4, 1994. An update and overview of the Glenn Pool project, as well as other Bartlesville-Bluejacket Sandstone studies, was offered to an informal group (Tulsa Study Group) that included representatives from independent producers on October 8, 1994. Also two papers titled "Characterization of fluvial-dominated deltaic reservoirs in a mature oil field: Glenn Pool field, Northeastern Oklahoma" and "Interdisciplinary analysis of fluvial dominated deltaic reservoirs: Glenn Pool field, Creek County, Oklahoma" were accepted for the AAPG 1995 Annual Meeting in Houston.

Preparation for Phase 2

An expanding study, which aims at understanding the DGI distribution and facies variation of the Bartlesville Sandstone on a larger scale, is being carried out by investigating well log and core data in the area surrounding the Self Unit. This study will link the Self Unit and the Berryhill Unit

which would be the target for this project in the next phase, and will provide a bridge for transforming our experiences and achievements obtained from Self Unit to the new target area.

A survey and compilation of data from outside the Self Unit were undertaken to prepare for the next target area. This included tracts No. 6, 7, 10, 11, 12, 13, 15, 16, and 18 of Glenn Pool field, covering about 1.6 square miles. Log curves and some core data from about 60 wells have been copied. These data are being investigated to look at the lateral variation of the Glenn Sand reservoir over a larger area than the Self Unit.

Geophysical Description
(by Chris Liner and Gokay Bozkurt)

Executive Summary

This year has seen extensive geophysical work on the project. Cross well seismic data was acquired between the new Self Well No. 82 and three surrounding wells. From this data cross well tomograms were computed by groups at the University of Tulsa, Amoco, Memorial University of Newfoundland, and Imperial College, London. Each group used different computational methods in order to determine what level of processing is needed to generate results useful for geological and engineering characterization of the reservoir.

A velocity-porosity relationship was established using wireline log data. The relationship will be useful to map subsurface velocity tomograms into a 2-dimensional porosity distribution image between the survey wells. We are currently extending this technique to include core geophysical measurements.

The following industry partners have contributed substantially to geophysical project activity in 1994.

Amoco Production Company
- Cross well seismic acquisition
- Cross well tomography computation
- VSP acquisition

Conoco Inc.
- Cross well seismic acquisition
- Field processing

Uplands Resources
- Site access for downhole, surface seismic

Opseis

Surface seismic recording system and source

Mercury International Technology

Surface seismic processing

Industrial Vehicles International

Surface seismic and VSP source

Geophysical Interpretation of Full Field Survey

The full cross well survey was completed in early 1994. The preliminary survey, as discussed in the previous annual report, resulted in high quality data, but the second encountered high ambient noise. The noise levels were high enough to prohibit first-arrival picking over in much of the data. Analysis of the data from the second survey shows that tube waves are emanating from the perforated interval in the receiver well. This is interpreted to be fluid flow or circulation noise through the perforations, even though the well was not flowing fluid at the surface.

Since this image plane was important for characterization of the reservoir, the survey was re-shot by reversing sources and receivers in the two wells. The resulting high-quality data indicates that shooting direction can be an important acquisition factor.

In general terms, cross well seismic imaging is a method capable of resolving very thin beds relative to conventional surface seismic methods. The main advantage of cross well seismic over surface seismic methods is the notable difference of frequencies encountered (i.e., 200-2000 Hz vs. 20-80 Hz, respectively) and the corresponding improvement in resolution. Also, the downhole vantage point allows tight integration with other bore hole information. This can lead to inferences concerning reservoir properties such as porosity distribution and bed continuity.

The cross well seismic objective at the Glenn Pool field is to create tomographic image planes to aid in reservoir characterization. Initial tomography results are discussed by Vassiliou, et al. (1994).[5]

For the full cross well work using the Self Well No. 82, acquisition involved Amoco's piezo-source and a proprietary 15-hydrophone receiver string developed by Conoco, Inc. Conoco also generously supplied personnel, on-site data processing and data editing services.

From early in the project the plan had been to use the Vertical Test Well (VTW) (Self Well No. 82) as the cross well seismic source well (see **Figure 12**). This was considered the best plan to minimize risk of loosing the (expensive) source downhole.

The first full survey, 82Æ64, followed this plan and resulted in high-quality data. **Figure 13** shows some features of the 82Æ64 survey including geometry of selected common source (CSG) and common receiver (CRG) gathers. The CSG and CRG data are plotted in **Figure 14**, and clear first breaks with good relief above ambient noise are evident on both.

Fresh from the success of the 82Æ64 survey, the acquisition team shot 82Æ63. This is labeled survey 2 in Figure 12. The survey geometry is nearly identical to that shown in Figure 13, and **Figure 15** shows a CSG and CRG representative of the data. Compared to the 82Æ64 data quality, the high ambient noise in Figure 4 was surprising. It is important to note that in both surveys every precaution was taken to eliminate known sources of noise. Also, all information on wells 63 and 64 indicated that they were nearly identical in drilling, completion and production history.

On the CRG, ambient noise is strong before and after first-arrival times. This noise is incoherent on the CRG, but on the CSG in Figure 15, the noise is coherent and recognizable as tube wave energy. Upgoing tube waves exist above about 1,500 ft. and downgoing ones exist below this level. As suggested by V. D. Cox, we interpret this as fluid flow noise associated with the perforated interval at 1,460 - 1,505 ft. It is curious that such strong tube wave energy should be generated by downhole (circulating?) fluid flow despite there being no fluid flow at the surface.

The ambient noise problem was serious enough that a significant portion of the wide-angle data could not be picked for first arrivals. Since picked first arrivals are the raw data for cross well tomography, and since this image plane was deemed crucial to the characterization effort, it was decided to back-shoot the 82Æ63 survey as 63Æ82.

In an effort to enhance data quality for better characterization of the reservoir, the 82Æ63 survey was re-shot with reversed source and receiver wells. In theory, the fluid flow noise in the source well (63 well) would radiate very little energy into the formation to appear as ambient noise in the receiver well (Self Well No. 82). In this way, the flow noise would be overwhelmed by the source signal.

Figure 16 shows CSG and CRG data over a common interval in the 63Æ82 survey. Comparing with Figure 15, the data quality is greatly improved. The data for this survey could be picked for first arrivals at all vertical offsets.

Shooting direction in a cross well seismic experiment is usually based on operational issues such as bore hole condition and casing size relative to the seismic tools. Beyond these concerns, it is tempting to invoke the principle of reciprocity, i.e., the data will be identical if source and receiver

positions are interchanged. While reciprocity is a powerful principle known to be valid in arbitrarily complicated physical systems, it silently assumes that the medium is passive. If the medium is active, if it contains sources of energy, then reciprocity does not apply. Interchanging source and receiver in this case can give very different results. Our experience with cross well seismic and fluid flow noise is a simple example of this fact.

We have shown that shooting direction can be a first order concern on data quality. Specifically, if a downhole source of noise exists in one well it is best to use this as the source well. Unfortunately, it is often not known before the survey whether such a downhole noise source exists. This work has been published (Liner, et al., 1994).[6]

The next step in working with the Glenn Pool cross well seismic data is tomographic inversion. This requires the data to be picked for first arrival times on all surveys to be inverted. This amounts to about fifty thousand seismic traces. By March, 1994, all data traces for surveys 82Æ64, 63Æ82, and 81Æ82 were picked by A. Vassiliou of Amoco. Survey 82Æ63 was judged too noisy for reliable picking.

These picks were forwarded to the University of Tulsa, Memorial University of Newfoundland, and, late in the year, to Imperial College, London. The four tomography sites are doing complimentary work by processing the data using different levels of complexity as shown in **Table 2.**

Table 2
Processing of Tomography Data

Group	Rays	Anisotropy	Computer Requirement	Public Domain
TU	Straight	No	PC	Yes
Amoco	Curved	Yes- V_v, V_h	Workstation	No
MUN	Curved	Approx- V_v, V_h	Workstation	Consortium Sponsors
Imperial C.	Curved	Yes- V_v, V_{45}, V_h	Workstation	Consortium Sponsors

This multiple-processing exercise will result in information concerning how much effort is required to successfully image cross well data in fluvial-dominated deltaic settings. By comparing the time and the availability of software, we hope to evaluate the economic feasibility of this technology for small operators.

Geophysical Interpretation of Field Survey

Overview and Anisotropy Discussion

When the data (picks) were processed for tomography, it was quickly apparent that the data presented a difficult geophysical problem because of strong P-wave anisotropy present in shaly rocks above the Glenn Sand. This was first recognized by A. Vassiliou of Amoco, and independently discovered by L. Lines of Memorial University. The following discussion is based on ideas originated by A. Vassiliou.

The seismic P-wave anisotropy seen at Glenn Pool is directly indicated by a comparison of sonic log values and cross well seismic common-level gathers. The sonic measurement relies on measuring travel time for a sound wave moving vertically along the bore hole wall for the length of the sonic tool. Thus, sonic is an indication of vertical velocity, V_v, in the vicinity of the bore hole. In a cross well seismic survey, source and receivers are moved to various depth levels as the survey is shot. A subset of the data can be extracted which has energy traveling horizontally between source and receiver at the same depth (common level gather). The nature of a common level gather makes it an indicator of average horizontal velocity, V_h, over the interwell region. At Glenn Pool, the sonic and common level gather disagree by as much as 25%, indicating seismic P-wave anisotropy where V_v and V_h are significantly different. Importantly, this discrepancy is consistent in 3 directions around the Self Well No. 82 as evidenced by the 3 cross well surveys into surrounding wells. Without this redundancy of proof, the anisotropy indications might be misinterpreted as field measurement errors.

The consequences of this anisotropy concern interpretations and processing of both cross well and surface seismic data. Most tomography programs and surface seismic reflection processing programs do not account for anisotropy. This is due to theoretical and algorithm complexity, excessive computation time, and the fact the P-wave anisotropy has until recently been considered relatively unimportant in sedimentary rocks. For our cross well work at Glenn Pool, the anisotropy issue has been very important. It explains much about the failure of the BOMTOM (isotropic) tomography program to create satisfactory interwell images. We have benefited from collaboration with Amoco (A. Vassiliou), Memorial University of Newfoundland (L. Lines), and Imperial College, London (G. Pratt), where researchers have previously developed anisotropic tomography computer programs. The results from these various groups are not fully consistent and this is the subject of a joint research paper currently being drafted.

It is unclear whether the anisotropy is sufficiently strong to require modification of standard surface seismic processing methods. Early surface seismic tests indicate good results without

special processing but further work is needed to clarify this issue. This is important since surface seismic is ubiquitous in the exploration/exploitation of shallow petroleum reservoirs in Northeast Oklahoma and similar regions in the mid-continent.

Velocity anisotropy is usually indirectly indicated. This can be through core plug measurements at frequencies 100 times (or more) greater than surface seismic frequencies, or tomographic results which are highly processed products, or even non-hyperbolic normal moveout curves on surface seismic data. At Glenn Pool we have rare direct evidence of strong P-wave anisotropy.

The first piece of evidence is the sonic log on the interval 1200 - 1600. Sonic logs measure velocity by refracting a high-frequency P-wave pulse vertically along the wall of the bore hole. Thus, sonic measurements indicate V_v. For example at the 1,250 ft. level in Self Well No. 82 the sonic reading is 90 microsecs/ft., corresponding to a V_v of 11,110 ft./sec.

From the cross well data, we can extract traces which have source and receiver at the same level (depth). The pertinent wells at Glenn Pool were surface surveyed to determine relative wellhead location, and a deviation survey was run on each to track subsurface (x, y, z) coordinates of each well bore. From this information, it is possible to construct a constant level gather for each survey. Since the source and receiver for each trace are at the same depth, the direction of energy travel is horizontal and therefore indicates V_h. One way of displaying this information is shown in **Figure 17**. In this figure the combination of horizontal distance and travel time has been combined to provide a V_h Ps-Sonic reading in microsecs/ft. For example, at the 1,250 ft. level in the 82->64 survey, the first arrival energy indicates a V_h Ps-Sonic value of about 71.5 microsecs/ft., corresponding to a *Vv* of 13,990 ft./sec. Note the consistency of this *Vh* Ps-Sonic value at the 1,250 ft. level in all three surveys.

To summarize, the sonic log in Self Well No. 82 gives V_v=11,110 ft./sec. at 1,250 ft. while the cross well data shows that V_h = 13,990 ft./sec. at the same depth. This represents direct evidence for a V_h about 26% greater (26% anisotropy) than V_v in the rocks at this level. Generally, P-wave anisotropy greater than 10% is rare, which makes the level of anisotropy seen at Glenn Pool quite remarkable.

In the next section, progress in computing tomograms at The University of Tulsa and in comparing with tomograms from other workers is discussed. In the last section, core plug data are shown to exhibit a strong correlation between porosity and permeability. These basic results lay the foundation for creating interwell porosity and permeability maps from the velocity tomograms.

The University of Tulsa Processing and Tomogram Comparison

Commonly, a geophysical procedure involves three steps: data acquisition, data processing, and data interpretation. Cross well data from the Glenn Pool field were acquired during 4 days of field work in late January, 1994. The geophysical work between March-June, 1994 involved mainly data processing.

First arrival travel times from "common source gathers" were picked by Amoco. Each pick was recorded with its source-receiver depth. A data set of source-receiver coordinates and travel times were transferred to parties involved in processing. **Table 3** shows the number of travel time picks and acquisition aperture for the three cross well surveys.

Table 3
Travel Time Data Information For Three Survey Well Pairs

Well Pair	Source Coverage (ft.)	Receiver Coverage (ft.)	Number of Travel Times
63-82	1220-1580	1108-1920	17759
82-64	1120-1920	1216-1568	14736
81-82	1220-1576	1084-1920	18898

The tomographic imaging software for data processing was provided by the U.S. Department of the Interior, Bureau of Mines as part of their technology transfer. The program is installed in The University of Tulsa Geosciences Department Apollo workstation network for current research purposes.

BOMTOM (**B**ureau **O**f **M**ines **TOM**ography) is a straight ray tomographic image reconstruction program using a SIRT (Simultaneous Iterative Reconstruction Technique) algorithm. A generalized flowchart of the program is given in **Figure 18.**

All three University of Tulsa tomograms between the survey wells (63-82, 82-64, and 81-82) were created using a 30-iteration BOMTOM run. A constant velocity of 10000 ft./s is used as an initial starting model. Maximum and minimum calculated velocities allowed are 10000 ft./s and 16000 ft./s, respectively. No other constraints are applied. The rest of the program parameters are left as default.

Figure 19 is the velocity tomogram between Wells 63 and 82 created by The University of Tulsa. The tomogram shows strong x-like artifacts that are typical of isotropic inversion applied to anisotropic data. Furthermore, analysis of the sonic log shows that the straight ray assumption is

not valid in this geological setting. Both anisotropy and strong velocity variations make BOMTOM an inappropriate processing tool for the Glenn Pool data.

Cross Well Seismic Data Migration

Seismic data from three of the cross well surveys (63-82, 82-64, 81-82) were migrated using the method of Liner and Lines (1994).[7] The prestack migration which assumes constant velocity distribution provided promising results. A detailed discussion on the method together with synthetic and real data examples can be found in the original paper.

The product from cross well tomography is a distribution of seismic velocities between the survey wells. On the other hand, migration methods image the reflectors by using these velocities. Migration in general is defined as "an inversion operation involving rearrangement of seismic information elements such that reflections and diffractions are plotted at their true locations" (Sheriff, 1991).[8]

Figure 20 shows an overlay of velocity tomogram and migration results for the 81-82 survey. We expect to see seismic reflectors associated with areas of strong vertical velocity gradient. The migrated traces are in close agreement with the velocity tomogram in defining the reflectors. The algorithm used assumes locally constant velocity. We can expect this method to be approximately correct considering the velocity variations indicated by the sonic log and tomography results. Ideally one should use a more sophisticated cross well migration program which incorporates velocity variations. Unfortunately no such program was available to the research team.

Wireline Logs And Synthetic Seismograms

In anticipation of surface seismic data being acquired on the Self Unit, it is important to model the expected seismic response. This involves velocity and density information at every depth level, calculation of travel times and reflection coefficients, and graphical display of the output.

A complete suite of wireline logs from Self Well No. 82 are available in digital format. The data were transferred to The University of Tulsa Department of Geosciences, and a program was written to view any log interval.

The program was primarily designed to generate synthetic seismograms from sonic and density logs. Reflection coefficients are calculated using the relationship

$$RC = \frac{\rho_{i+1}V_{i+1} - \rho_i V_i}{\rho_{i+1}V_{i+1} + \rho_i V_i}$$

where,

ρ = density (gr/cc) from density log
V = P-wave velocity (ft./s) = 1,000,000/slowness (ms/ft.)

These reflection coefficients are then placed along an axis corresponding to vertical two-way travel time. Finally, the reflection coefficients are convovled with a wavelet to generate the synthetic seismogram. **Figure 21** shows an overlay of the Gamma Ray Log, Sonic Log and Synthetic Seismogram on a tomogram velocity plot from Self Well No. 82.

Deviation Survey

A deviation survey for all four wells (82, 63, 64, 81) was completed in the first quarter, 1994. The data are important, since cross well tomography uses source-receiver coordinates in the bore hole to calculate ray paths. Velocities are obtained by inverting travel times which are related to ray paths. Therefore, the deviation may be critical in tomography where the bore hole is curved.

The deviation data consist of the horizontal offset of a subsurface point (northing and easting) with respect to the wellhead coordinates. The values are recorded at a 50 ft. interval along the bore hole. Since the sources and the receivers were moved at 8 ft. intervals for the cross well acquisition, the deviation values were interpolated at The University of Tulsa to a 8 ft. spacing. A separate program was run to transfer those values into a format acceptable by BOMTOM. We anticipate that incorporating well deviation information will not significantly alter the BOMTOM results.

Cross Well Seismic Simulation

A finite difference wavefield propagation code (Bording, 1994)[9] was tested on a horizontally layered velocity model. The code generates a plane wave from the source well and displays snapshots of the propagating wave field at specified time intervals. The code and accompanying Seismic Unix shell programs are under modification for future use. The tomograms will be input as velocity models for forward modeling. In this way synthetic data can be generated for direct comparison with common-level gathers in the field data. If the velocity field (derived by tomography) is consistent with the field data, then modeled first arrivals should coincide with observed first arrivals.

Seismic-To-Rock Property Transform Using Well Logs

It is extremely important for both economic and scientific reasons to understand reservoir velocities in porous rocks. Cross well tomography has become a useful method in determining the subsurface velocities. The next step is to investigate the appropriate relationships between velocities and reservoir properties (i.e., porosity) such that the subsurface velocity distribution is converted to the reservoir properties.

The goal of this study is to develop seismic-to-rock property transform between velocity versus porosity and clay content from well logs.

A conventional approach that relates P-wave velocity to porosity was derived by Wyllie et al. (1958).[10] This relationship is known as the time-average equation (often Wyllie's equation). It is,

$$\frac{1}{V} = \frac{\phi}{V_f} + \frac{1-\phi}{V_m}$$

where,

V = Velocity of saturated rock
ϕ = Porosity
V_f = Velocity of P-waves in pore fluid (water, oil, gas)
V_m = Velocity of P-waves in the matrix (minerals) composing the rock.

Porosity images using this approach simply result in a re-scaled version of a velocity tomogram, since velocities are mapped one-to-one into porosities for every pixel in the image plane. This equation is considered as a "first approximation" in defining a velocity-porosity relationship.

It is known that acoustic velocities are dependent on various other factors such as mineral composition, pore space configuration, grain compaction, temperature and pressure. Effects of clay content on velocity have been investigated on a large number of samples from different geological settings by Han et al. (1986).[11] It has been suggested that a relationship exists between clay content and velocities in reservoir type rocks.

The effect of clay content and porosity on velocities is investigated for the Glenn Pool field, Self Unit, in an attempt to convert velocity tomograms to porosity tomograms.

Wireline logs are used as a source of data. Velocities are derived from the *sonic log*; percent volume of shale from the *gamma ray log*; porosities from a combination of *neutron-density log* (**Figure 22**). Although log data is available from a larger section of the subsurface, the analysis is confined to a 180 ft. interval (1,400 ft. - 1,580 ft.) which covers the reservoir zone and corresponds to the limits of cross well seismic imaging.

Log data includes information for every half foot depth step. The 0.5 ft. sampling interval yields 360 data points for each measurement in the 180 ft. zone of interest.

Transit time (also known as slowness) measured by the sonic log is easily transferred to velocity by a unit conversion. Volume of shale is calculated from the GR Log after two steps. First the gamma ray index (I_{GR}) for a Gamma reading is computed by simple interpolation between clean formation reading (GR_{cl}) and shaly formation reading (Gr_{sh}). GR_{cl} and GR_{sh} readings (25 and 145, respectively) are obtained by analyzing the entire log. Note the high GR kick at 1,455 ft. which goes beyond 200 API. This value is not selected as a shaly formation reading since it is not a representative value for the whole section.

After obtaining the I_{GR}, volume of shale (V_{sh}) is computed using the following formula (Dresser Atlas, 1979),[12]

$$V_{sh} = 0.33 \times \left[2^{2(2 \times I_{GR})} - 1.0\right]$$

where,

V_{sh} = Volume of shale
I_{GR} = Gamma ray index

True porosity is obtained by averaging the neutron and density logs for each depth step after correcting for shaliness. Shaliness correction for neutron and density porosity is done using the following formulas (Schlumberger, 1975),[13]

$$\phi_{N_{corr}} = \phi_N - \left[\left(\frac{\phi_{N_{clay}}}{0.45}\right) \times 0.30 \times V_{sh}\right]$$

$$\phi_{D_{corr}} = \phi_D - \left[\left(\frac{\phi_{D_{clay}}}{0.45}\right) \times 0.30 \times V_{sh}\right]$$

$$\phi_{N-D} = \sqrt{\frac{\left(\phi_{N_{corr}}\right)^2 + \left(\phi_{D_{corr}}\right)^2}{2.0}}$$

SAS (statistical analysis software) was used to establish a relationship between velocity, porosity, and clay content.

Based on the significance of contribution from each regression variable, the following multiple regression model is derived,

$$V = \beta_0 + \beta_1 1\phi + \beta_2 V_{sh} + \beta_3 V_{sh}^{\ 2}$$

where the response and predictor variables are the same as described above.

The following interpretation for the model is done based on **Figure 23**:

Regression for the data set suggests that approximately 74% of the variation in velocity is explained by the fitted model (R-square=0.7411).

From the F-Statistics and corresponding P-value in the "Analysis of Variance" table, the null hypothesis that $\beta_1 = \beta_2 = \beta_3 = 0$ is rejected, since P-value is so small. At least one of the variables has an effect.

Also in the Type III Tests, the null hypothesis of $\beta_1 = 0$ (after accounting for β_0) and null hypothesis of $\beta_2 = 0$ (after accounting for β_0 and β_1) and $\beta_3 = 0$ (after accounting for β_0, β_1 and β_2) are rejected (P-value too small), which confirms the validity of the model.

The proposed model with the explanatory variable coefficient estimates is,

$$= 15950.5 - 18152.7\phi - 1311.5V_{sh} + 347.8V_{sh}^{\ 2}$$

Partial leverage plots are observed for the above model to reveal the potentially obscured effect of one variable by the other. The slope of the fitted regression line on the partial leverage plots show that the explanatory variables have considerable effect in describing velocity. A variable is interpreted to have little or no effect within the model if the slope approaches zero (line is close to horizontal), which is not the case for the model proposed.

The proposed model differs from the conventional Wyllie's equation as it contains additional V_{sh} (volume of shale) terms. To emphasize the necessity of a V_{sh} term in the equation, Wyllie's equation and the proposed model is compared. A SAS output (**Figure 24**) shows Wyllie's approximation.

Recall Wyllie's equation,

$$\frac{1}{V} = \frac{\phi}{V_f} + \frac{1-\phi}{V_m}$$

Which can be modified as,

$$\frac{1}{V} = \beta_0 + \beta_1 \phi$$

The simple linear regression model provides;

$$\frac{1}{V} = 5.463 \times 10^{-5} + 0.0001\phi$$

The residual plot is expected to have a resemblance to the right-opening megaphone example in Weisberg, 1985 (page 132).[14] This is interpreted as an increasing variance as the porosity gets larger. The physical phenomena causing this can be explained as follows: at low porosities factors effecting the velocities are confined to lithology effects only; as porosity gets higher other effects come into play which change the velocity values (slowness in this example) over a larger interval. Pore related effects such as pore space configuration, pore-fluid pressure and type of clay mineral (shale) distribution between pores (laminar, structural, dispersed) may be some causes of such variation.

Wyllie's model explained 62% of the variation in velocity, whereas the suggested model explained 74% of the variation.

Increasing clay content decreases acoustic velocities. The effect of clay content on velocities should not be ignored when a relationship between velocity and porosity is sought.

Surface Seismic Tests

A zero-offset VSP and a 2-D seismic survey were conducted in August, 1994. The goal was to determine the feasibility of shooting a high-resolution 3-D survey on the Self lease. This geophysical field work was a volunteer effort of Opseis and IVI, both based in Tulsa. Amoco's three-component downhole receiver was used for the VSP survey. The data acquisition was of no cost to the project. The data were processed at Mercury International Technologies (MIT). Furthermore, MIT donated their processing software, iXL, to the Geosciences Department at The University of Tulsa. This will facilitate further processing of any seismic data.

This test involved a high-frequency vibrator, which is more commonly used for civil engineering studies. Oil field equipment on the Self lease was not shutdown so that noise effects could be studied. Unfortunately, there were several equipment compatibility problems among the geophysical systems. Despite this, a short 2-D seismic line was acquired. Subsequent review and processing of the data showed it to be of unacceptable data quality. This was interpreted to be due to the weakness of the source signal.

In an effort to improve data quality, another field test was conducted during December by Opseis. The source used was a large (60,000 lb) vibroseis unit. Several 2-D lines and some pseudo-3-D patches were shot. The data is currently being processed by Mercury International Technology. Preliminary indications are that data quality is much better than the first test and should be sufficient for mapping important horizons in the subsurface.

Other Geophysical Activity:

Horizontal, vertical core velocity measurements were received from Amoco. The petrophysical measurements will be useful in refining the velocity-porosity relationship described in this report.

The tomographic processing teams have continued work on improving their results. The MUN and the Amoco tomogram are available. Results from Imperial College are not yet available. We are currently working on understanding the similarities and differences in these results.

Integration of Geological, Geophysical, and Engineering Information (by Asnul Bahar, Leslie G. Thompson, and Mohan Kelkar)

The integration of geological, geophysical, and engineering information in generating the reservoir description of the Self Unit was carried out using three different models, i.e., Deterministic Model, Stochastic Model without tomography information, and Stochastic Model with tomography information. In each model, geological simulation was conducted to replicate the geological

architecture created by the geologist followed by the allocation of petrophysical properties (porosities and permeabilities). The validation of the results from each model was performed using the static information (well cores and logs) as well as the dynamic information (well tests).

Following the reservoir description task, the flow simulation was conducted to match the past performance and also to predict the future production using three different scenarios. Based on the flow simulation results, the economic analysis was conducted as to the most feasible scenario that is applicable to the Self Unit.

Deterministic Model

Geological Simulation

The common problem encountered in generating the reservoir description is how to fill in the information at the unsampled locations, i.e. at the interwell regions. The conventional way of solving this problem is to assume that a certain relationship (correlation between wells and/or based on similarity) exists in these regions, and that there is a unique set of model output data for a given set of inputs. This is known as a deterministic approach. A model that is commonly used in the conventional approach is known as the layer-cake model.

The geologists involved in this project, Kerr and Ye, have established a stratigraphic framework of the Self Unit that divided the Unit into 6 Discrete Genetic Intervals (DGIs). Using each DGI as a layer, a model with 6 sandstone-layers can be developed. From their interpretation, it is observed that at some interval an impermeable layer exists between two consecutive DGIs. To accommodate this fact, the model is modified to contain this layer in between two DGIs.

For the purpose of flow simulation, each layer is divided into several grid blocks. To cover the 160 ac. of the Self Unit, 400 grid blocks (20 × 20 in X and Y directions respectively) are assigned to each layer. Using this configuration, the dimension of each grid block in X and Y directions becomes 132 ft whereas its thickness is determined using bilinear interpolation based on the well data. **Figure 25** shows the interpolation result for North-South cross section. This figure clearly indicates how each layer is stacked against one another.

Figures 26.A and **B** show the thickness comparison of each layer between well data and the model at Wells No. 43 and No. 37 respectively. The data from these wells were not used as an input in the interpolation process. Thus, these comparisons should validate the interpolation used in generating the model. As these figures indicate, the model conforms to the geological architecture as is commonly observed in the conventional method.

Porosity Description

In assigning the porosity value to each grid block, the well data is first superimposed on the geology data, i.e., the porosity of each DGI/layer is separated from the others. An average value is calculated for each layer at each well. Then, the porosity of a grid block at an unsampled location is calculated using bilinear interpolation of the well data that has been averaged previously. The porosity of the impermeable (shale) grid blocks is set as zero. All of the porosity data used in this study were gathered from the log of currently existing wells. No corrections or correlations to core data are made since none of these wells were cored.

Figure 27 shows the porosity distribution of the East-West cross section. It can be observed that the porosity distribution is almost uniform in each layer. Thus, it is clear that this model can not capture the heterogeneity of the reservoir. **Figure 28** presents the porosity at Self Well No. 82 to show the comparison of the estimated value with the field data at a specific well. It can be observed that the porosity value from the model seems to be inconsistent. It overestimates at the top part of the reservoir (DGIs A, B, and C), but overestimates at the bottom part of the reservoir (DGIs E and F).

Permeability Description

The permeability value for each grid block for this model is estimated using a linear relationship assumption between porosity and the logarithm of the permeability. The only source of data for permeability available for this study is from the core measurements of several old wells, i.e. Well No.'s 28, 31, 32, 37, 43, and 47. Unfortunately, the core data from these wells are not available for the whole intervals. Mostly, they are only from the bottom intervals since those were the most productive intervals. This situation creates difficulty in generating the correlation. In fact, there is no data available for DGI-B and only a few points for DGI-A.

Figure 29 shows the permeability distribution of the North-South cross section. As in the porosity distribution, it can be observed that the areal heterogeneity cannot be captured by this model. Observing the average value for each layer, it is found that the permeability of DGI A (k-average = 15.6 md) and DGI B (k-average = 15.5 md) is higher than the permeability of DGI C (k-average = 8.5 md). This is inconsistent with the field data. The reason for this is the poor quality of the data that were used in generating the porosity-permeability relationship for these DGIs. The core study of Self Well No. 82 indicates that the porosity for DGIs A and B is about 12 - 15% with the permeability in the range of 0.1 to 1 md, while the average value from the old core which was used as input data was 17% for porosity and 60 md for permeability. Overestimated distributions resulted for DGIs A and B. **Figure 30** presents the permeability distribution at Self Well No. 82.

In general, the model predicts a very narrow range of permeability. It overestimates at the top intervals but underestimates at the bottom intervals. Again, the heterogeneity of the reservoir is not captured very well.

Figure 31 presents the comparison of the permeability thickness product (kh) between the well test interpretation and the model. In this figure, any point that lies on the 45° line is a perfect match. Since most of the results lie above this line, it indicates that the model overestimates the *kh* value when compared to the well test results. The procedure that was applied in calculating the *kh* for the model is as follows.

1. A radius of investigation is defined as half the distance between adjoining wells.

2. The permeability inside this radius was averaged geometrically. The geometric average was calculated only for layers which are perforated.

3. The *kh* of the model then was calculated as the summation at each of the layers.

The permeability of the model used for comparison with the well test, such as in Figure 31, is the absolute permeability whereas in practice the permeability calculated from the well test is the effective permeability. Considering that most of the field has been flushed with water, especially at the bottom part of the reservoir, and has been produced with 99% water cut, it is reasonable to assume that the flow in the reservoir is approximately single phase. Thus, the use of absolute permeability for this comparison is justifiable.

Flow Simulation

In order to have confidence in predicting the future performance of the reservoir, a reasonable match in the flow simulation of the past performance has to be achieved. The next task after generating the reservoir description is to conduct a flow simulation. All of the flow simulations presented in this report were conducted using ECLIPSE-100 Black Oil Simulator.

The flow simulation was performed to match the past production from November 6, 1906 until January 1, 1994. In this model, the same number of grid blocks used in the reservoir description is used in the flow simulation, i.e., 20 × 20 × 12 = 4800 grid blocks. Therefore, no upscaling process required for this model.

In running the flow simulation, at least one parameter should be available as a control parameter. This parameter could be oil production rate, water production rate, or bottom hole pressure, etc. Using one control parameter, the other parameters can be used as the match parameter, to which

the flow simulation result is compared. The problem that was encountered in running the simulation is the limited information on any of these parameters. Accurate information about the original oil-water contact was not known. Thus, it was quite difficult to determine the initial conditions of the reservoir. The production data were not available for the early times until 1946. The only data that was available was the first 24 hours production, or the initial potential, of a few early wells. It was decided to make trial and error runs in searching for the bottom hole pressure that could produce the initial potentials at those wells. **Figure 32** presents the initial potential comparison between the simulation and field data using uniform bottom hole pressure (BHP) at all wells of 400 psi. Except for Wells No. 1 and 16, the match is considered reasonable. In order to have a better match for these two wells, a lower BHP value should be used, but lowering the BHP would affect the other well matches. Thus, it is decided to use the BHP of 400 psi for the early production time. Using this value as the control parameter, the simulation is continued until the reservoir pressure is depleted to this pressure. When this happens a lower value of bottom hole pressure is used as the control parameter and the simulation resumes. This process is repeated until the year 1946.

The production profile derived from this method is presented in **Figure 33**. In this figure, the results from 4 case studies were presented. These case studies were conducted due to the uncertainty of the relative permeability data and the initial water saturation. The definition of each case study is presented in **Table 4**. From **Figure 33**, it can be seen that at the beginning, the production is optimistic but close to 1946 the production is low compared to the field data. The flow simulation in the period after 1946 was run using water production rate as a first control parameter with a restriction of a maximum value of oil production rate. These water and oil production rates are the yearly field wide data available for the Self Unit. It can be observed that the simulated results match the field data.

Table 4
Case Definition Used in Flow Simulation

Legend	Description
Case 1	Uniform *Kr* (Glenn Pool Data), Uniform *Swi* = *Swr*
Case 2	Uniform *Kr* (Modified - Glenn Pool Data), Variable *Swi*
Case 3	Variable *Kr* (3 zones - Glenn Pool Data), *Swi* = *Swr* (3 zones)
Case 4	*Kr* as measured by BDM-Oklahoma (2 zones), *Swi* = *Swr* (2 zones)

Figure 34 presents the Original Oil In Place (OOIP) calculated using this model. As a comparison, the calculated OOIP as reported by Heath[3] is also presented. The difference that is

observed among the case studies is due to the difference in the initial water saturation that was assumed in each case.

Figure 35 presents the water cut predicted from the simulation. The field presently produces with a water cut of 99%. It can be seen that the simulated water cut does not match the field data very well. This is probably due to the limited information about the oil-water contact as well as the relative permeability as suggested by Case 2 that gives higher water cut compared to the other cases. In this case the bottom interval (DGI F) was assumed to be saturated with water at the initial conditions and a higher water relative permeability (k_{rw}) was used. Overall information about oil-water contact indicates that water may present in part of the F zone. However, due to limited information, no aquifer model has been used.

In order to see the potential for future use, the oil saturation map has to be analyzed. **Figure 36** shows the oil saturation comparison between the simulation and log-derived values at Self Well No. 82 for each case. The comparison is reasonable. In general, the simulation shows an optimistic result. All cases predicted high oil saturation at almost all units except unit F. In this unit, Cases 2 and 3 predict a relatively lower oil saturation value as observed from the log data. The assumption that the formation is flushed by water at this interval can be justified. Thus, based on this model all the units, except unit F, can be considered good candidates with future potential.

Summary

To summarize the findings from this model, a deterministic model was developed for the Self Unit using available log and core data as well as the geological interpretation. The overall results based on the deterministic model are optimistic when compared to the field data. The *kh* values from the well tests are lower than predicted by the model. In general, variability of the properties observed in the field data is not preserved when using a deterministic model. In the next two sections, the comparison of this model with the stochastic approach will be presented.

Stochastic Model without Tomography Information

Geological Simulation

The name Stochastic Model used in this section represents the reservoir description model generated using the conditional simulation technique. This technique is part of the geostatistical methodology. The word stochastic is used since the process is represented by random variables, whereas the conditional simulation technique means that the technique simulates or predicts several

equiprobable descriptions of the reservoir properties which are conditioned to the data at the sampled locations.

The approach used in this model is a parallel approach where people from various disciplines (geology, geophysics, engineering, management) work simultaneously on a single reservoir; i.e., the Self Unit. Using this approach the reservoir description generated will be consistent with alternative views imposed by various disciplines.

The other factors used in developing this model that can improve the drawback of the deterministic model presented previously are the inclusion of the scale effect and uncertainties. The inclusion of the scale effect is very important, especially in numerical simulators where the grid block properties are not only dependent on the relative location but also on the block's size. The uncertainties in the future performance are important since there are uncertainties involved in the reservoir description process. Knowing the uncertainties in the future performance will provide us with a better judgment with respect to economic assessments of the reservoir. The source of data used in this model is mainly from the core and well logs. The inclusion of tomography data will be presented in the next section.

The program used in generating the reservoir description in this model is the Gaussian Truncated Field Simulation of Lithofacies (GTSIM).[15] The basic principle of this program is to truncate a Gaussian field by threshold values to generate a conditional simulation of the lithofacies. The Gaussian field can be modeled from the variance-weighted or some other weighted average of the pdf-type indicator covariances. Meanwhile the threshold can be determined either from the local lithofacies proportions, also called proportion curves, that can be input to the program by the user or calculated from a pdf (probability density function) type indicator kriging. The first option is the recommended option since it allows the input of prior geological knowledge. Details about this program can be found elsewhere.[15]

The implementation of the GTSIM program in generating the reservoir description of the Self Unit follows the following procedures.

1. Transformation of geological data into categorical variables.

2. Determination of spatial relationship or variogram.

3. Determination of proportion curve.

4. Simulation for several realizations.

A categorical variable is a code use to represent a geological facies, in this model it is a DGI, at a particular location. Every DGI is assigned one variable with the value either 1, to indicate the presence, or 0, to indicate the absence, of the corresponding DGI at that location. To account for the shale in the model, a variable is also assigned to it. Thus, all together there are 7 types of categorical variables in the model, named consecutively from 1 to 6 for DGIs A through F and 7 for shale.

The relationship of one variable from one location to another location is known as the spatial relationship. One way to measure this relationship is through the variogram. **Figures 37.A** and **B** show the typical variogram of the DGIs in the vertical and horizontal directions.

One important piece of information that can be inferred from the variogram calculation is the continuity of one variable in a certain direction, i.e., whether the continuity is isotropic or anisotropic. It has been observed that based on the variogram analysis there is no certain anisotropy angle in the horizontal direction in any of the DGIs (including shale unit). On the other hand, the isopach maps shows that the channel-fill trends in a certain direction, especially in DGIs A, C, and D with major directions at 110°, 45°, and 45° respectively. Using this fact as the soft information, the simulation can be run and the result can be compared with the isotropic case as inferred from the variogram analysis.

The proportion curve can be determined by calculating the probability of each categorical variable (DGI) to exist at a certain depth. This proportionality curve controls how much of each DGI should present at a particular depth. **Figure 38** shows the input proportion curve as provided by the geologist. The program honors this proportion curve and internally transforms it into the suitable threshold curves.

Provided with the categorical variables, the variogram, and the proportion curve, the simulation is ready to be run for as many realizations as required. In this report, five such realizations are presented. The results will be used to predict the uncertainties. The number of grid blocks used in the simulation is 256,000 (40 × 40 × 160) with dimension of 33 ft. × 33 ft. × 1 ft. in x, y and z directions respectively. Using this configuration, the simulation requires about 5 - 10 minutes depending on the load of the computer.

Before the results are analyzed and validated, the statistical aspect of the input and output distribution will be discussed. The comparison of the input and the output variogram is presented in Figures 37.A and B. It can be observed that the match is good. Even though it is not shown here, the other variogram comparisons are also good. The second input-output comparison is the

proportion curve. The input proportion curve has been presented previously in Figure 38. As the comparison, **Figure 39** presents the output proportion curve. Again, it can be observed that the match is also good.

Figure 40 shows the horizontal cross section at 25 ft. below marker from 5 different realizations conducted. In general, a similar structure can be observed from these figures even though variations can be noticed among them. The cross section at 25 ft. below marker mainly consists of DGI A (with a probability of about 70%), as can be observed from Figure 40, with no other DGIs present except shale. Thus the isopach map of DGI A may be used as a shape comparison between the simulation and the geological model. The light color in Figure 40 represents the DGI A, either channel-fill or splay. It can be observed that a good match is obtained. The two most similar results are obtained from realizations no. 1 and no. 5, whereas realization no. 3 gives the most dissimilar result.

Figure 41 shows the North-South vertical cross sections using realizations no. 1 and no. 3. This figure shows the lateral continuity of each DGI from the two realizations. Realization no. 1 shows that all units are almost continuous from North to South except that DGIs A and B are cut at the South and in the middle portion of the field. On the other hand, realization no. 3 predicts a continuity of DGI A and the presence of a shale barrier in DGI F at the middle of the field.

To further validate the simulation, the results were compared with the core data of Wells No. 28, 31, 32, 37, 43, 47, and 82. The data from these wells were never used in the conditioning data. Thus, the comparison should give a good cross validation. The matches are good. Two examples of these matches are shown in **Figures 42A** and **B**. These figures also present the result from the deterministic model. In general both methods give similar results, even though the deterministic model predicts a slightly thicker layer. The fact that the well spacing is relatively small (about 300 ft.) provides the deterministic model with a good result.

Porosity Description

The generation of the porosity description in this model is conducted using the simulated annealing method as described by Perez.[16] The procedure is as follows.

1. The calculation of variogram for each DGI.

2. Simulation for each DGI.

3. Filtering process to superimpose the geology data.

To superimpose the geology the filtering process is implemented. Before this process is performed, the simulation is run for each of the DGIs by assuming that the entire reservoir contained that DGI only. That is, for six DGI's (excluding shale) there are six porosity descriptions. These descriptions are then filtered, where for every grid block the type of the DGI was checked and the porosity corresponding to that DGI was assigned to that grid block. A value of zero was assigned to the grid block of shale. By using this filtering process the porosity value at every grid block location is consistent with the underlying geological description.

Figure 43 presents the porosity cross section for 5 different realizations. These figures clearly show the heterogeneity of the reservoir. The porosity cross sections at several depth below marker using the realization no. 1 is presented in **Figure 44**. It can be observed that the porosity increases with depth as was found from the field data.

The validation of this description is performed by comparing the porosity generated from the simulation and the porosity from the core data of the Self Well No. 82. The porosity of the Self Well No. 82 was not used in the conditioning data. This comparison is presented in **Figure 45**. It can be seen that simulation matches the field data very well. This comparison also shows that the model captures the vertical heterogeneity very well. This also presents the comparison between the results of stochastic and deterministic models. It can be observed that the stochastic model gives a better result and preserves the heterogeneity of the reservoir.

Permeability Description

One of the difficulties encountered in the reservoir description process in this study is the limited permeability data. The assumption of a linear relationship between porosity and log of permeability as was used in the deterministic model was not really a good one.

To overcome this problem, a method of conditional distribution was used. In this method the permeability was assigned to a grid block conditioned both to the type of the DGI and to the porosity value of that grid block. The procedure of this method is as follows.

1. The first step is to plot the relation between porosity and permeability for each of the DGIs (A through F) without trying to fit the data for a specific model.

2. The second step is to divide each of these plots into several porosity classes.

3. For each of these porosity classes, the cumulative conditional distribution for permeability is calculated.

4. The last step is to assign a permeability value to a grid block. This is done by first selecting a suitable CDF Plot which corresponds to the type of the DGI and the value of the porosity. Knowing the CDF for that grid block, a random permeability value within that class is assigned.

Figure 46 shows the permeability distribution of a North-South cross section derived from the realizations no. 1 and no. 3. This figure shows that the permeability distribution, developed using this method, is consistent with the field observation, i.e., it increases with depth and there is areal heterogeneity with respect to permeability in the reservoir. It can also be shown that the two realizations are consistent with this observation.

Figure 47 presents the comparison between the permeability values of the simulation and the core data of Self Well No. 82 for both stochastic and deterministic models. As with porosity, the matches can be considered very good. Again, it can be noted that the stochastic model predicts a better result than the deterministic model and follows the heterogeneity of the reservoir.

To cross validate the result, the porosity-thickness product (kh) value from the model with the well test is compared. The comparison is shown in **Figure 48**. Except for Well No. 61, where an anomaly was observed during the test, this figure clearly indicates that the stochastic model does a good job. The overestimated prediction of the deterministic model can be observed from the comparison presented in this figure.

Upscaling of Petrophysical Properties

The reservoir description generated in this model used 256,000 (40 × 40 × 160) grid blocks. This huge number of grid blocks can not be used in the flow simulation due to hardware (memory) limitations. The common number of simulator grid blocks used in the industry is in the range of 15,000 - 30,000 grid blocks. Unfortunately, the facility that is currently available for this study can handle only up to about 6,400 grid blocks. Thus, an upscaling process of the petrophysical properties is required before the simulation can be run. To get the total 6,400 grid blocks the configuration is reduced to 20 × 20 × 16. This means that every 4 blocks in the horizontal plane have to become 1 super block, while for the vertical direction average, every 10 blocks have to become 1 super block. All together, 40 blocks have to become 1 super block.

The upscaling of porosity is performed using a simple arithmetic average while the permeability is upscaled using the combination of arithmetic and harmonic average as follows.

1. Permeability average in either X or Y direction (Kx or Ky).

•The permeability generated by the simulation was assumed to be the permeability in the horizontal direction ($Kx = Ky = Ksimulation$).

•For blocks in the horizontal plane:

-Two harmonic averages (kh_1 and kh_2) were calculated for 2 pair blocks in the direction of flow, as follows :

$$kh_i = \frac{2\,kx_1\,kx_2}{kx_1 + kx_2}$$

-The super block average is calculated as the arithmetic average of kh_1 and kh_2, as follows:

$$k_x = k_y = \frac{kh_1 + kh_2}{2}$$

-The arithmetic average is used to calculate the average for vertical blocks.

2. Permeability Average in Z direction (Kz)

•Kz is assumed to be some percentage of Kx.

•Harmonic average kh_i was calculated for blocks in the direction of flow (vertical direction).

•The super block average for Kz is calculated as the arithmetic average of the 4-neighbor horizontal blocks.

Flow Simulation

The number of grid blocks to be used for the flow simulation as mentioned in the previous section is 6,400 (20 × 20 × 16) blocks. The dimension of each grid block in the horizontal directions (Δx and Δy) is chosen to be fixed at 132 ft. Several cases were run in the beginning of this study using a uniform size in z direction with Δz = 10 ft. It was observed that the results were not satisfactory. Thus, it was decided to run the simulation using a variable size in the vertical direction. This size is determined by observing the significant changes in the formation as given by the well log. The resulted size is as follows: 15, 15, 10, 5, 5, 5, 5, 5, 5, 5, 5, 10, 10, 20, 20, 20 ft. All of the simulation results presented below use this configuration.

The first result presented is the comparison of the initial potential of the reservoir between the simulation and the field data as shown in **Figure 49**. The bottom hole pressure used in this model is not a uniform value as was used in the deterministic model, but rather a variable value that is unique for each well. The result was derived using realization no. 1 of the reservoir description generated. It can be seen that the match is good.

Figure 50 presents the field oil production rate for Case 4 using realizations no. 3 and no. 5, and the deterministic model. It can be seen that with respect to the different realizations, there are no significant differences in the results. The two realizations consistently predict the same result. Compared to the deterministic model, the stochastic model gives a better result at the early period. This may be partly due to the variable bottom hole pressure (BHP) used in the stochastic model.

Figure 51 shows the results of OOIP and cumulative production at 1946 for different realizations and the deterministic model using Case 4. The three realizations show a consistent result, even though some uncertainties can be observed. The mean value from these realizations is 11.77 MSTB which is less than what is estimated by the deterministic model. Thus, this result shows that the deterministic model is more optimistic compared to stochastic models.

Figure 52 shows the field water cut predicted by the simulation for different realizations. As in the deterministic model, the simulation does not match the field conditions very well. The comparison presented in Figure 52 once again supports the argument about the optimistic result of the deterministic model. Its water cut prediction is much lower (thus, the oil cut is much higher) than the ones that are predicted by the stochastic model.

The comparison of the simulation result with respect to the log data of Well No. 82 is presented in **Figure 53**. From this figure it can observed that the heterogeneity of the reservoir was not really captured very well. This is may be related to the grid resolution (number of grid blocks and its size at a particular location) that is very difficult to solve at the present condition.

Summary

The stochastic model performs a very good job of capturing the reservoir description. It replicates the geological architecture very well. It matches the porosity as well as the permeability data at wells not used as conditional data and performs a reasonable job of matching the historical production performance.

Stochastic Model with Tomography Information

Porosity Description

This section presents the integration of the seismic data into reservoir description based on the stochastic model presented previously. The same geological model will be used in this model but the porosity simulation contains extra information. Since the permeability description is related to the porosity distribution then the permeability distribution will also contain extra information. The term seismic in the above statement refers to the tomogram as interpreted from a series of cross well seismic field test surveys that were performed in the Self Unit between Wells No. 82 - 63, 82 - 64, and 82 - 81 in January, 1994. Three tomogram panels are available for this study. The inversion of seismic data into velocity distributions at each panel was conducted by Liner et al. The discussion presented here started from the assumption of known velocity distributions in each tomogram panel.

The use of velocity data in the reservoir description is related to the porosity distribution as given by the Wyllie Equation where the porosity is linearly related to the reciprocal of velocity which is known as transit time. The main advantage of having these data is to get a better spatial relationship (variogram) in the interwell region which is missing from the usage of log or core data alone. It is expected that the tomogram data will improve the variogram model with respect to the range of the model.

To superimpose the geology, the data are separated according to the type of the DGI at each location. In this case, the separation is not a straight forward process due to the differences in the grid block configuration. The velocity distribution has poor vertical resolution but better horizontal resolution compared to the simulated geological model. Horizontally, the changes of geology are known for every 66 ft. whereas the changes of velocity are known for every 13 ft. Since the simulation of porosity follows the grid block configuration of the geological model, it was decided to take the average of 5 velocity data values before the conversion is done. On the other hand, in the vertical direction the geology is known on a one foot interval whereas the velocity is only known for every 12 ft. For this case, no averaging process is required.

Figures 54.A through **C** present the porosity distribution at each tomogram panels after applying the correlation between porosity and transit time. It can be observed that the layer of highest porosity occurs at the middle of the formation (DGI D). This result does not match with the observed field data where porosity increases with depth. There are two reasons that can be suggested for this result. The first one is related to the velocity distribution itself. The velocity distribution indicates that a layer of low velocity (high porosity) exists in the middle of the Glenn

Sand. The other reason may be that the correlation used in transforming the velocity into the porosity is not accurate. In spite of this concern, we decided to use this distribution since we wanted to preserve the information in the original form as much as possible.

The variograms for each DGI generated using the porosity distribution in each panel are shown in **Figures 55.A** and **B.** The separation of porosity of DGIs B and D from the other DGIs is due to the difference in the sill value in each DGI. It can be observed that in all DGIs the variogram of the conditional data can be represented by the spherical model. This observation can be used as the first important conclusion, i.e., the spherical model that was assumed previously in generating the stochastic distribution is justified.

The second conclusion that can be drawn from the variograms generated is related to the range parameter. It can be observed that the range of the porosity spatial relationship is at least the distance between two wells, i.e., about 300 ft. Thus, the assumption of using a range equal to the distance of the closest well pair can also be justified. This assumption was used for DGIs B, E and F. The porosity variogram for DGIs A, C, D was modeled previously using soft geological information where the range is assumed to be a number that is greater than the distance between the wells and is related to length of the channel-fill in each DGI. Thus, this assumption can also be justified.

The simulation of the porosity distribution as before is conducted using the simulated annealing method. The only difference between this distribution and the previous one is in the conditioning data. The variogram models are the same since the assumptions used previously are justified.

The comparison of the porosity at Self Well No. 82 is presented in **Figure 56.** In general the match of porosity at Self Well No. 82 from this model can be considered good except in the zone of DGI D where two peaks occur. This discrepancy may be due to the high velocity region in the D zone found from the velocity distribution.

Permeability Description

Following the same method used previously, the permeability distribution is generated using the conditional distribution method where it is calculated using the distribution function of the permeability in a porosity class.

The comparison of the permeability at Self Well No. 82 is presented in **Figure 57.** This figure shows that the model with tomogram data performed a better job than the model without the tomogram data. This statement can be verified by observing the top and bottom zones. In the top

zone, the previous model (no tomogram) tends to give a higher value whereas the present model (with tomogram data) remains in the range 0.1 to 1 md. The core data show a very low value. At the bottom interval, the present model follows the core data consistently whereas the previous model predicted a layer with a lower permeability value. At the middle of the formation, both models give the same result.

The validation of the permeability distribution generated using this model is done by comparing the product of permeability and thickness (kh) as was done for each model. This comparison is presented in **Figure 58**. This figure clearly indicates that the tomogram model performs an excellent job. The matches are good for all wells including the result of Well No. 61 where a kh value of 1,530 md-ft. was calculated from the well test and the model predicted 1,405 md-ft. This figure is an important illustration of the principle that addition of different information reduces uncertainty in the reservoir description.

Flow Simulation

Figure 59 presents the field oil production rate predicted by the simulation. For the early period, the tomogram model shows a slightly higher production rate compared to the non-tomogram model. The higher production rate for the same relative permeability curve may be due to the higher initial oil in place which means a higher pore volume generated from the reservoir description. To see if this is the case, **Figure 60** compares the original oil in place calculated using several models. It can be seen that the tomogram model estimated the most optimistic original oil in place.

Figure 61 compares the field water cut predicted using this model with respect to the other models. It can be seen that the two stochastic models give about the same prediction of water cut during the life of the reservoir even though it does not match very well with the field data. The deterministic model remains the optimistic model since it predicts the lowest water cut while the field was operated with a very high water cut.

Finally, the comparison between the simulated and the measured oil saturation at Self Well No. 82 is presented in **Figure 62**. As it is shown in this figure, there is no significant difference among the models with respect to the oil saturation at Self Well No. 82. The three models do not follow very well the heterogeneity of the oil saturation profile. This is mainly due to the resolution of the grid blocks configuration.

Summary

To summarize the findings in this model, the tomogram data can be incorporated into the reservoir description through velocity porosity transformations. The main use of the tomogram data in this model is to estimate the variogram models used in the previous model. It is found that the spherical model was adequate for the modeling purposes and the range of the porosity is not less than the distance between two wells. In general, the results are in good agreement with the other stochastic model except for the permeability distribution where the model with tomogram data performs much a better job. Especially, the dynamic reproduction of the well test permeability data is much improved after incorporating the tomogram data. This indicates that additional information can improve the reservoir description.

Reservoir Management

The overall goal of the study is to improve the secondary recovery performance through the use of a better reservoir description and better reservoir management. This section presents the analysis that led to the reservoir management plan of the Self Unit for future production. The analysis starts with the discussion of the future production forecast using three different scenarios for three reservoir description models discussed in the previous chapters, i.e., the deterministic model, the stochastic-model without tomography information, and the stochastic model with tomography information. The three scenarios are:

1. Drilling no additional wells,

2. Drilling a horizontal well, and

3. Drilling new vertical production wells.

Each scenario is related to the well completion and the water injection rate. To cover several possibilities of this configuration, several sub-scenarios are defined within each scenario. The flow simulation is run for each sub-scenario until the year 2000 and the increase of production (if any) is compared with the base case which is the simulation with current field conditions (based on 1993 data).

Following the flow simulation, an economic analysis is performed for several selected sub-scenarios that would give the best increase of production. The analysis is based on the data provided by Uplands Resources Inc. Conservative estimates are used for the cost of production to avoid over optimistic forecasts of the profits. The best scenario is determined by the rate of return

and the pay-out time as criteria based on a constant oil price at the current level of $17.00 per barrel.

Future Production Forecast

The definition of each sub-scenario (presented in **Table 5**) is determined based on the following two reasons: the Self Unit has not been completed very well at the middle to the bottom interval (DGIs D and E), and it is feasible to increase the injection rate. Since the deterministic model predicted relatively high permeability and high oil saturation in DGIs A and B then these two DGIs cannot be ignored for this model. Thus, for the deterministic model the future forecast will also include DGIs A and B in addition to DGIs D and E whereas for the stochastic model only DGIs D and E are to be considered for recompletion. The exclusion of DGI C is due to the relatively low permeability (in both models) and the fact that it has been opened within most of the Unit. The DGI F has been excluded from any sub-scenario since it has been flushed by water as observed on the flow simulation runs.

The possibility of increasing the injection rate was based on the data from 1992 and 1993 where the production increased 38% (from 21 BOPD to 29 BOPD) when the field was flooded with a 125% higher injection rate. This fact suggests that the field gives a reasonable response to an increase in the amount of water injected. We expect that, in the future, by increasing the water injection ratio, we can increase the oil production.

Scenario 1: Drilling No Additional Wells / Current Field Configuration

From Table 5, there are 5 sub-scenarios defined for Scenario 1, i.e., Scenario 1A through 1E. For each of these sub-scenarios, the results of the 4 case studies (defined in Table 4) of the stochastic model without the tomogram data will be presented. For the purpose of comparison and also to evaluate the uncertainty of the result, Case 4 will be run using Scenario 1D for other models, i.e., deterministic, stochastic description without tomogram for 3 realizations, and stochastic description with tomogram data. The result is presented at the end of this section.

Figures 63.A through **E** present the result of Scenario 1A through 1E respectively. The result of Scenario 1A shows that there will be no increase of production if this scenario is applied in the Unit. Thus this scenario can be ignored. Figure 63.B shows that the range of additional oil production that can be expected by implementing Scenario 1B is between 10 to 16 barrels of oil per day. In this scenario, Case 4 shows almost a steady performance whereas the other cases seem to decline faster. In Scenario 1C the first three cases predicted almost the same result, but Case 4 is very pessimistic. A contrasting performance can be observed by comparing the result of Case 4

between Scenarios 1B and 1C. This result indicates that Case 4 is more sensitive to the opening of new intervals (Scenario 1B) than to increasing the injection rate (Scenario 1C).

Table 5
Definition Of Sub-Scenario Used In Future Production Forecast

Name	Description
Scenario - 1A	Open Well 82 As Producer Convert Well 81 As Producer
Scenario - 1B	Reopen DGIs* At All Wells Base Injection Rate
Scenario - 1C	Current Perforation Double Injection Rate
Scenario - 1D	Reopen DGIs* At All Wells Double Injection Rate
Scenario - 1E	Reopen DGIs* At All Wells Triple Injection Rate
Scenario - 2A	Horizontal Injection Well With Injection Rate Of 1000 BWPD, Reopen DGIs*, Double Rate At Old Wells
Scenario - 2B	Horizontal Injection Well With Injection Rate Of 2000 BWPD, Reopen DGIs*, Double Rate At Old Wells
Scenario - 2C	Horizontal Injection Well With Injection Rate Of 3000 BWPD, Reopen DGIs*, Double Rate At Old Wells
Scenario - 2D	Horizontal Injection Well With Injection Rate Of 3000 BWPD, Reopen DGIs*, Base Rate At Old Wells
Scenario - 2E	Horizontal Producer Well Reopen DGIs*, Base Rate At Old Wells
Scenario - 3A	4 New Vertical Wells (Producer) Base Rate At Old Wells
Scenario - 3B	4 New Vertical Wells (Producer) Double Rate At Old Wells

*Reopen DGIs means: Reopen DGIs A, B, D, and E for deterministic model and DGIs D and E for stochastic model

The result of Scenario 1D, which is the combination of Scenarios 1B and 1C, shows the combined effect of the previous two scenarios. It can be seen that more additional production can be

expected from this scenario. Thus, by simultaneously opening DGIs D and E and increasing the injection rate, a better result will be achieved. Scenario 1E shows the effect of higher injection rate. Intuitively, the result should be better and this is proved from Figure 63.E. Overall, it can be concluded that significant increase of oil production can be obtained if the formation is reopened at DGIs D and E and simultaneously the water injection rate is increased.

The comparison of the simulated future production for different models using Scenario 1D - Case 4 is presented in **Figure 64**. There are two important points that can be concluded from this figure. First, the stochastic model demonstrates its capability of giving an estimation of the uncertainty (for a given set of information) of the future production whereas the deterministic model predicts only one value. The increase of oil production from the stochastic model ranges from 18 - 21 barrels of oil per day in 1995 whereas from the deterministic model this value is 21 barrels of oil per day. Secondly, the deterministic model is more optimistic. It can be seen that at any time in future the deterministic model always provides a higher prediction.

Scenario 2: Drilling Horizontal Well

The purpose of this scenario is to explore the feasibility of drilling a horizontal well in the Self Unit. This prediction is very critical since the cost of drilling a horizontal well is very high (cost ~ $400,000). We would investigate the effect of three sub-scenarios as defined in Table 5. The first one is related to the amount of injection rate either in the horizontal well or at other wells if this horizontal well is to be used as the injector. The second one is to see the effect of recompleting other old wells. The last one is to see whether the horizontal well should be an injector or producer.

The horizontal well investigated in this study is located in the vicinity of the Self Well No. 82. The simulation has been run for 3 different areal locations and 6 different vertical positions, but no significant difference in the results is observed. **Figures 65.A** through **E** present the results of Scenario 2A through 2E respectively. Figures 65.A through C show the effect of injection rate in the horizontal well on the production performance. It can be observed that only a slight increase of additional production can be obtained. Figure 65.D shows the effect of injection rate at the old wells. It can be observed that the result of Case 4 almost remains the same. This result is also observed in Scenario 1, where Case 4 is more sensitive to reopening DGIs than increasing the injection rate. In addition, this result also shows the importance of opening DGIs simultaneously with increasing the injection rate. Finally, Figure 65.E shows that an injector horizontal well is preferable to a producer horizontal well.

Overall, excluding Scenarios 2D and 2E, the additional oil production from this scenario ranges between 21 - 41 BOPD whereas the range for the first scenario is 16 - 39 BOPD. It is evident that drilling horizontal well does not provide significantly better performance compared to the first scenario. Intuitively, this additional oil production will not be able to cover the cost of drilling a horizontal well at the current level of oil price.

Scenario 3: Drilling New Vertical Production Wells

An additional 4 vertical wells are used in this simulation. The locations were determined based on the oil saturation map and also by considering the vacant space that exists in the Self Unit. **Figures 66.A** and **B** show the simulation for this scenario. The conclusion about the importance of increasing injection rate as found from the previous scenarios can also be observed from this scenario by comparing the results of Scenarios 3A and 3B. From Figure 66.A it can be observed that the overall additional oil production using this scenario is about the same as for the previous scenarios, which ranges from 18 to 37 BOPD. Thus, there is no significant increase in oil production after implementing this scenario. Comparing the results of the three scenarios, it can be concluded that the best alternative from an economic standpoint is Scenario 1 since there are no drilling costs associated with this scenario.

Economic Analysis

As mentioned previously, the criteria used in the economic analysis are the rate of return and the pay out time. These parameters will be calculated using the first scenario (except Scenario 1A) which is found to be the only scenario that is feasible for the Self Unit. Before this calculation is performed, the simulations were rerun for another 4 years so that a 10 year projection can be made. The revenue is calculated using the constant oil price of $17.00 per barrel. The capital and operating costs are provided by Uplands Resources Inc. The capital cost includes the cost to improve the water injection system that is capable of doubling or tripling the injection rate and the cost that is related to opening new intervals (perforation, stimulation, etc.). The fixed cost to improve the water injection system is $87,495, whereas the cost to reperforate DGIs D and E is predicted as $61,600. The fixed cost provided is applicable to tripling the injection rate.

The operating cost is mainly due to chemical treatment of water, electrical, and maintenance costs. This cost varies significantly for the Self Unit. It ranged between $6 per bbl of oil to $9 per bbl of oil during 1993-1994. The value of $9.50 per barrel of the produced oil is considered to be a conservative estimate under current conditions. In this study, this value is used for the condition where no increase of injection rate is applied (Scenario 1B). For the scenario where the injection rate is to be doubled (Scenario 1C and 1D), the operating cost of $10.50 per barrel of produced oil

is used. For Scenario 1E (tripled injection rate) the operating cost is assumed as $11.50 per barrel of produced oil.

Figure 67 presents the different rates of return (ROR) estimated for the 4 case studies using 4 different scenarios (1B through 1E). The ROR shown in Figure 67 is the rate of return for the period where the production is still profitable (non negative cash flow). **Figure 68** presents the result of pay out time predictions for the cases investigated.

As Figure 67 indicates, the highest ROR is indicated from Scenario 1B. This is mainly due to the lowest capital costs (equal to the cost of reopening DGIs D and E only). But the uncertainty among the four cases in this scenario is significant. To further examine the effect of the operating cost, a sensitivity study is conducted by increasing the operating cost by $1.00, so that it becomes $10.50 / $11.50 / $12.50 for no increase in injection rate, double injection rate, and triple injection rate respectively. The result is shown in **Figure 69**. It can be seen that Scenario 1B is not very stable (negative ROR for Case 2 and 3) and very sensitive to the operating cost. **Figure 70** presents the effect of oil price on the ROR prediction. It can be seen that in order for this scenario to work the oil price can not be lower than $15.00 per barrel.

Figure 71 presents the comparison of the ROR and pay out time estimated from the different models using Scenario 1D of Case 4. This figure shows one of the advantages of the stochastic model whereby it provides the estimation of uncertainty. In this case, the predicted ROR ranges from 10 to 22 percent and the pay out time varies between varies 4 to 6 years, whereas the deterministic model predicted one single value of 31% for ROR and 3 years for pay out time. This figure also confirms the optimistic nature of the deterministic model.

Summary

The flow simulation to forecast the future production has been conducted. It is found that the additional oil production that can be expected from the Self Unit is in the range of 16 - 41 barrels per day depending on the specific scenario applied to the unit. The drilling of any extra wells, either one horizontal well or several vertical wells, is not feasible for the Self Unit at the current level of oil price since the increase of oil production can not justify the cost that is required to drill those wells. The scenario of reopening DGIs D and E and simultaneously increasing the injection rate was found to be the most feasible. The economic analysis has been done for this scenario. A rate of return in the range of 10 - 25% can be expected by applying this scenario. The deterministic model consistently predicts optimistic results compared to the stochastic model.

References

1. Kuykendall, M. D., and Matson, T. E.: "Glenn Pool Oil Field, Northeast Oklahoma Platform," *American Association of Petroleum Geology - Treatise of Petroleum Geology Atlas of Oil and Gas Fields: Stratigraphic Traps III* (1992) pp 155-188.

2. Visher, G. S., Saitta, B. S., and Phares, R. S.: "Pennsylvanian Delta Patterns and Petroleum occurrences in Eastern Oklahoma," *American Association of Petroleum Geology Bulletin,* Volume 55, pp 916-926.

3. Heath, E. S.: "Evaluation of the William B. Self and T. R. Burrows Leases, Glenn Pool Field," ARCO Reservoir Engineering Report (April 4, 1984).

4. Kelkar, M., Liner, C. and Kerr, D.: "Integrated Approach Towards the Application of Horizontal Wells to Improve Waterflooding Performance," Annual Report, DOE/BC/14951-5(DE94000137), Bartlesville Project Office, USDOE, OK (June 1994).

5. Vassiliou, A.A., Savage, C.W., Liner, C.L., Bozkurt, G.B., and Lines, L.R.: "Glenn Pool Project: Initial Tomographic Results," 64th Annual International Meeting, Society of Exploration Geophysicists (1994) pp 302.

6. Liner, C.L., Bozkurt, G., and Cox, D.V.: "Shooting Direction and Cross Well Seismic Data Acquisition," 64th Annual International Meeting, Society of Exploration Geophysicists (1994) pp 32-36.

7. Liner, C.L. and Lines, L.R.: "Simple Prestack Migration of Cross Well Seismic Data," *Journal of Seismic Exploration,* 3, (1994) pp 101-112.

8. Sheriff, R.E.: *Encyclopedic Dictionary of Exploration Geophysics: Geophysical Reference Series 1,* Third Edition (1991).

9. Bording, R. P.: "A Finite Difference Wave Field Propagation Computer Algorithm," Personal Communication (1994).

10. Wyllie, M.R.J., Gregory, A.R. and Gardner, L.W.: "Elastic Wave Velocities in Heterogenous and Porous Media," *Geophysics,* 21, (1956) pp 41-70.

11. Han, D., Nur, A. and Morgan, D.: "Effects of Porosity and Clay Content on Wave Velocities in Sandstones," *Geophysics,* 51, 11, (1986) pp 2093-2107.

12. *Dresser Atlas: Log Interpretation Charts,* Houston, Dresser Industries Inc. (1979) pp 107.

13. *Schlumberger: A Guide to Well Site Interpretation of the Gulf Coast,* Houston, Schlumberger Well Services Inc. (1975).

14. Weisberg, S.: *Applied Linear Regression,* Second Edition, Wiley Series in Probability and Mathematical Statistics, John Wiley & Sons Inc. (1985).

15. Xu, Wenlong and Journel A. G.: "GTSIM: Gaussian Truncated Simulations of Lithofacies," Report-6 Stanford Center For Reservoir Forecasting (May, 1993).

16. Perez, G. : "Stochastic Conditional Simulation for Description of Reservoir Properties", Ph.D. Dissertation, The University of Tulsa, Tulsa, Oklahoma (1991).

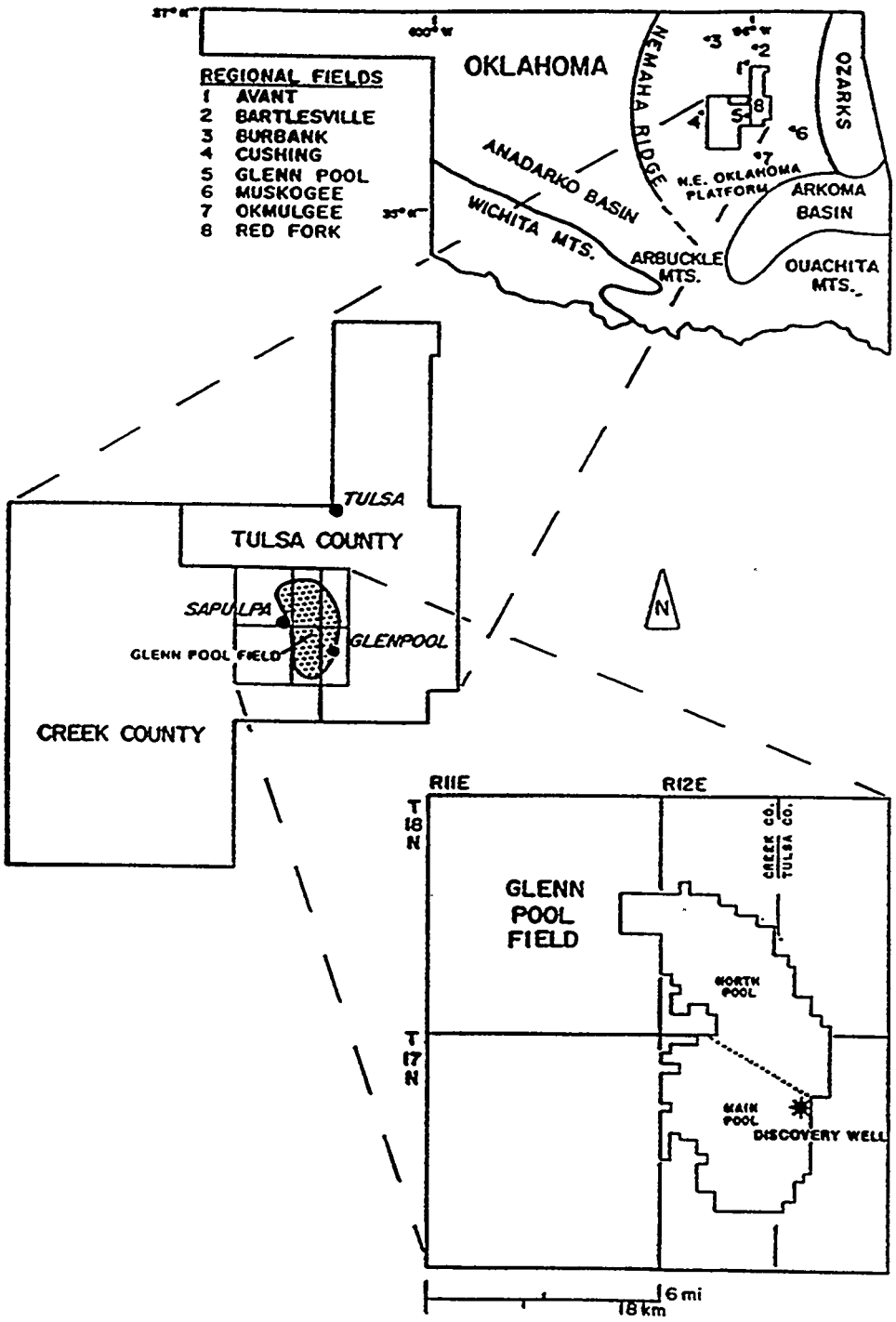

Figure 1

Location Of Glenn Pool Oil Field (Kuykendall And Matson[1])

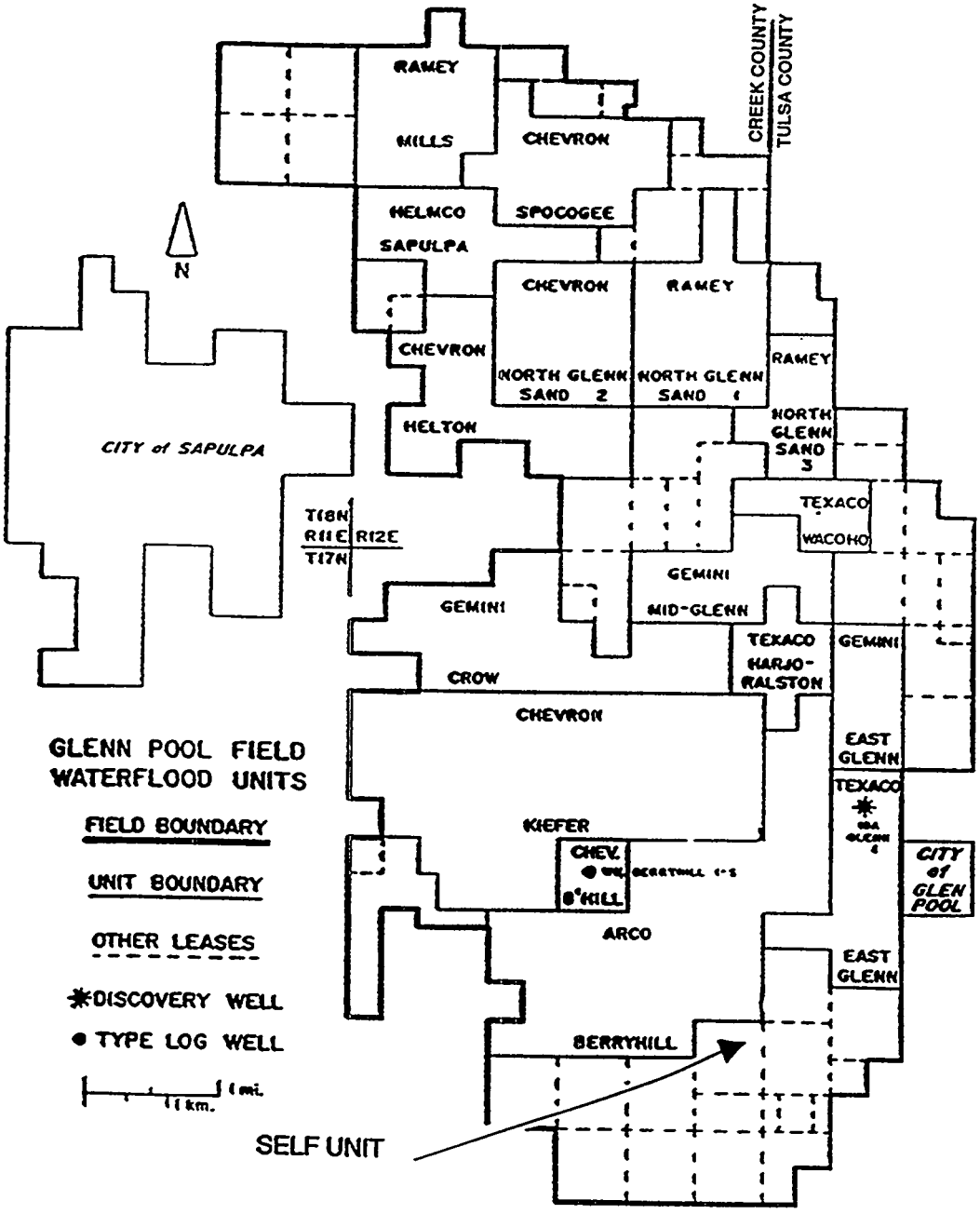

Figure 2

Self Unit Location (Kuykendall And Matson[1])

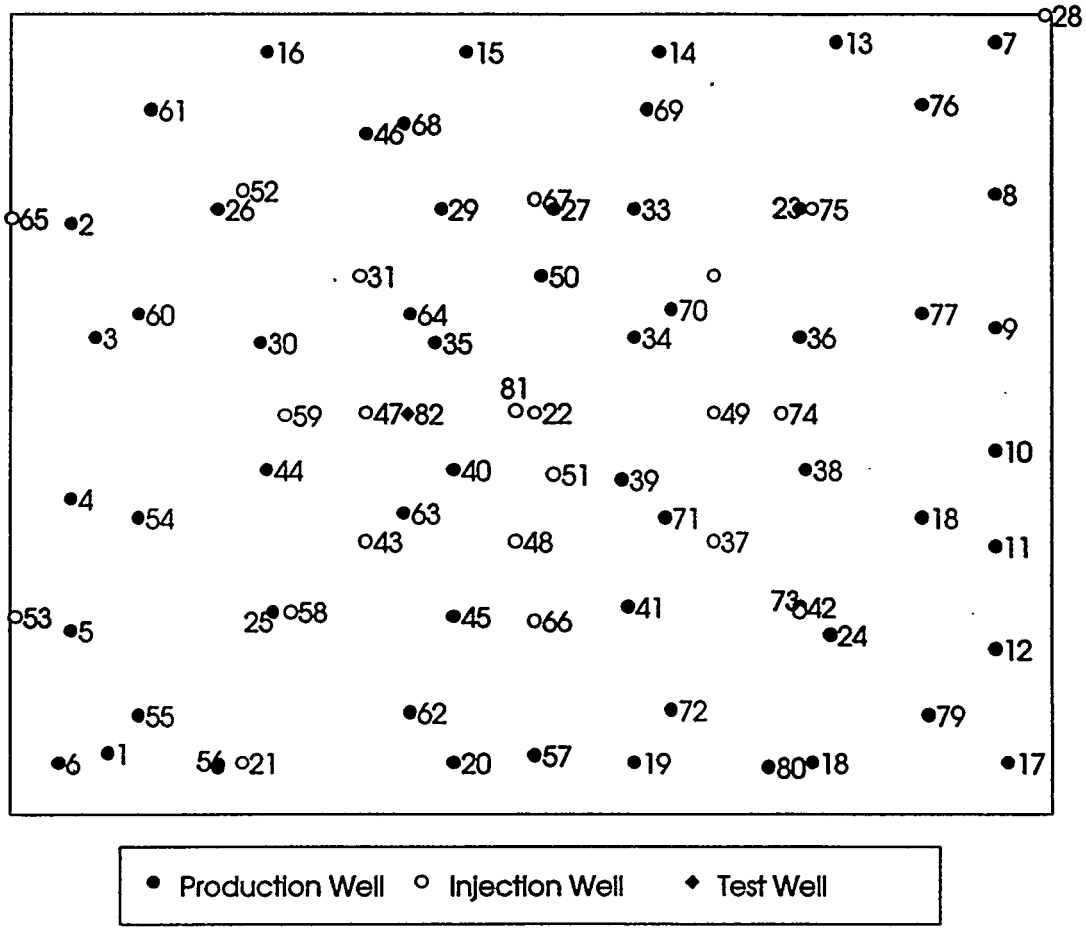

Figure 3
Well Locations

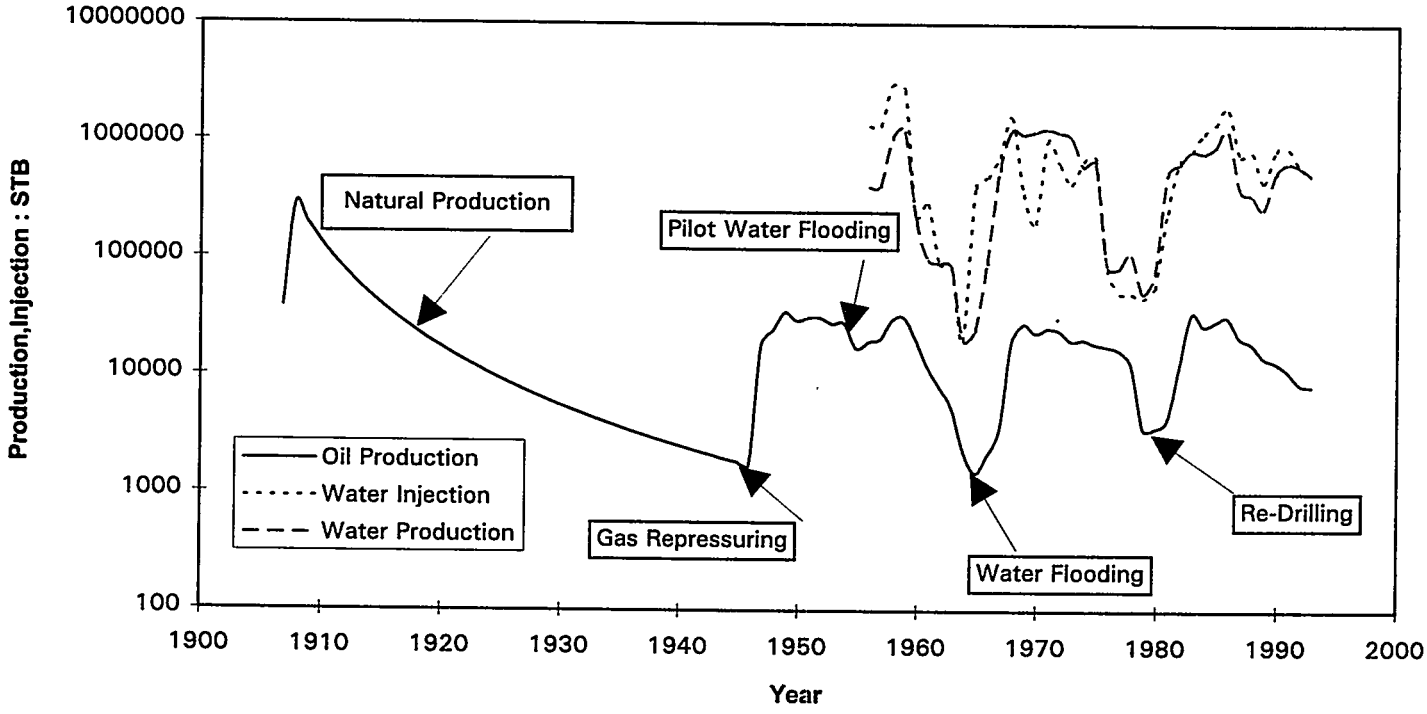

Figure 4
Self Unit History

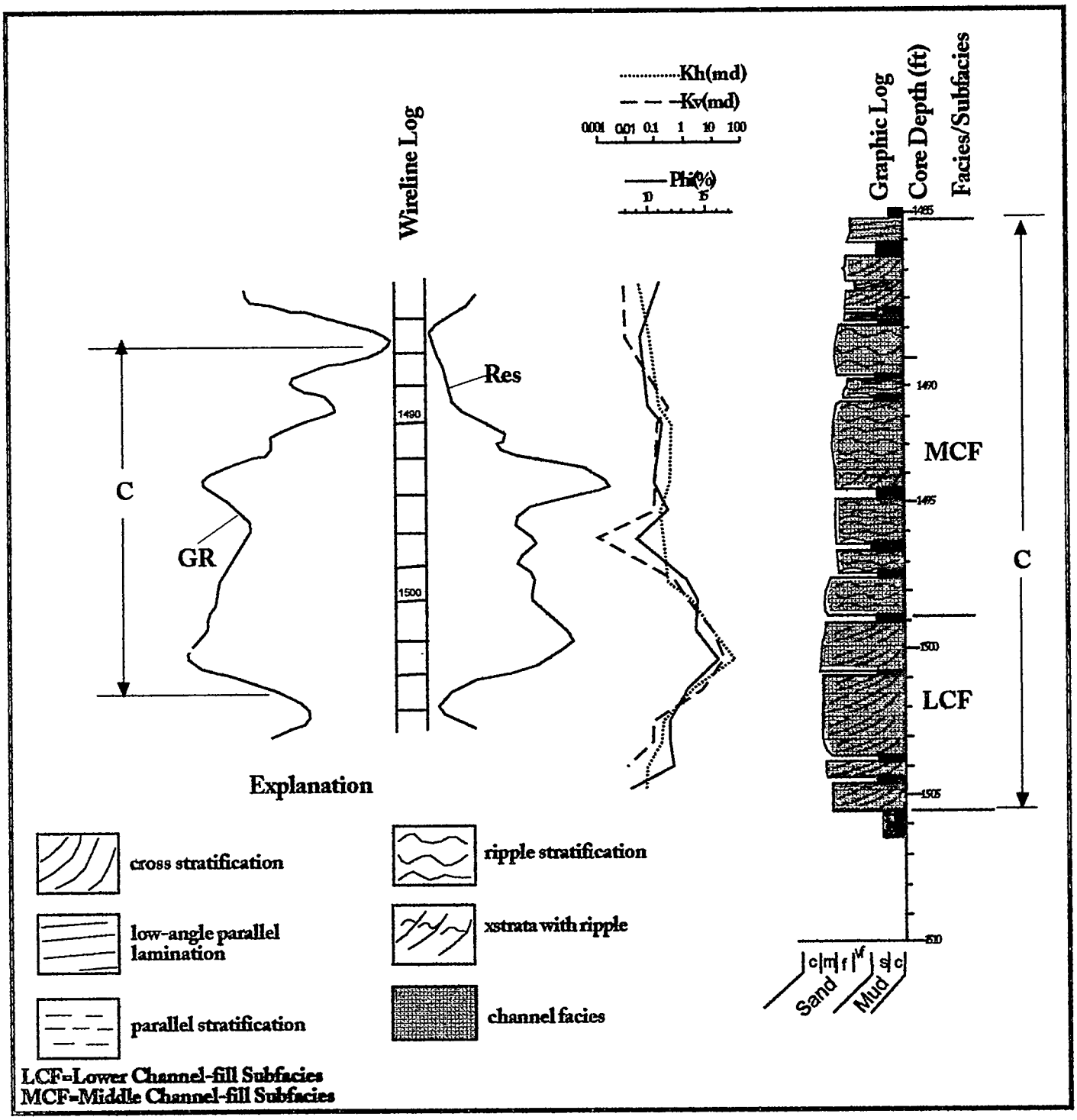

Figure 5

Glenn Pool Field, Uplands Resources, Self No. 82, Discrete Genetic Interval C.

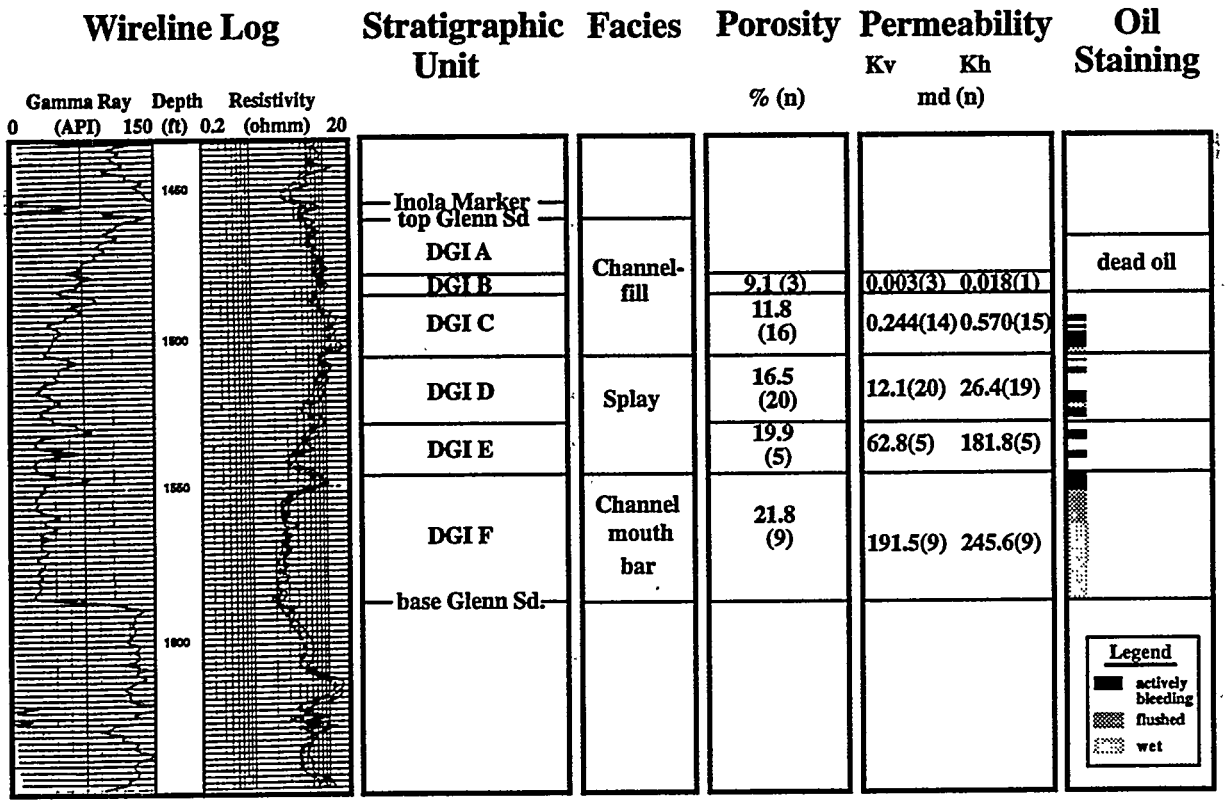

Figure 6

Uplands Self No. 82 Well Summary. Stratigraphic Units Include The Stratigraphic Marker Bed (Inola) And The Discrete Genetic Intervals (DGI) That Make Up The Glenn Sand. Permeability Values Are Geometric Means For Each DGI Sampled (n = Number Of Samples) With Reference To Air Through Conventional Core Plugs.

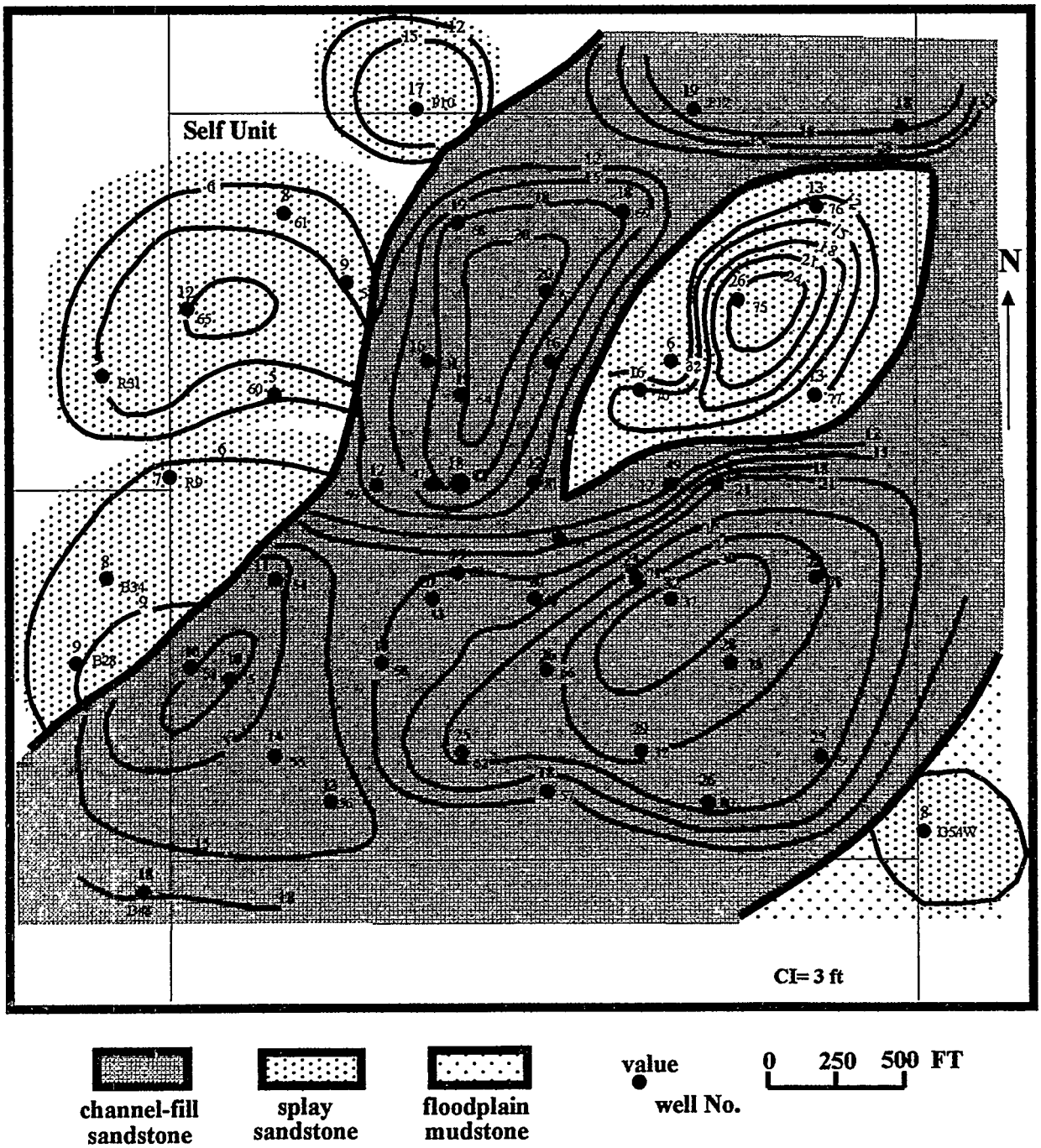

Figure 7

Glenn Sand - Unit C, Net Sand Isopach And Facies Map (Self Unit And Vicinity)

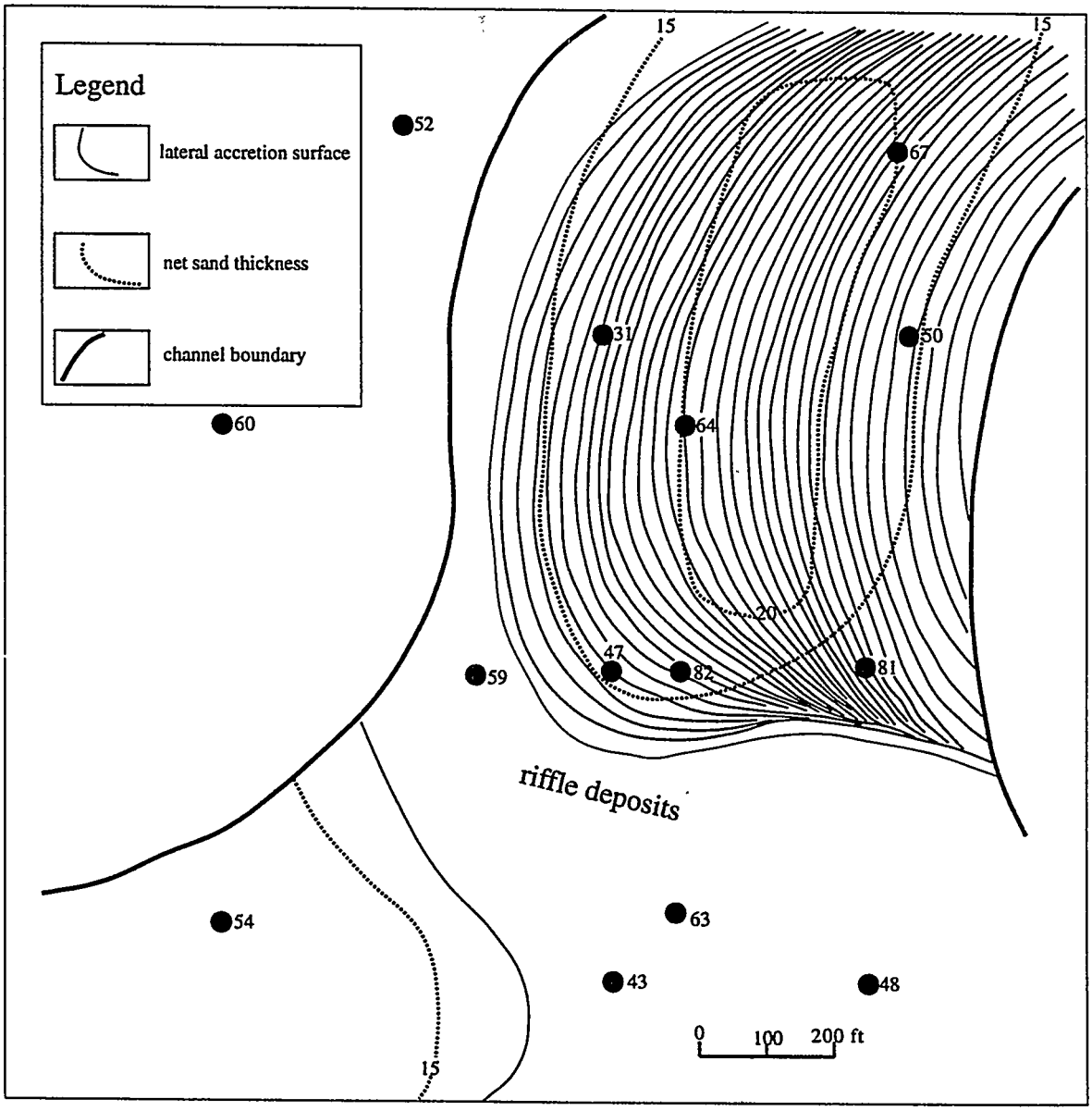

Figure 8

Detailed Reservoir Architecture For A Point Bar Deposits In The Vicinity Of Self Well No. 82, Unit C

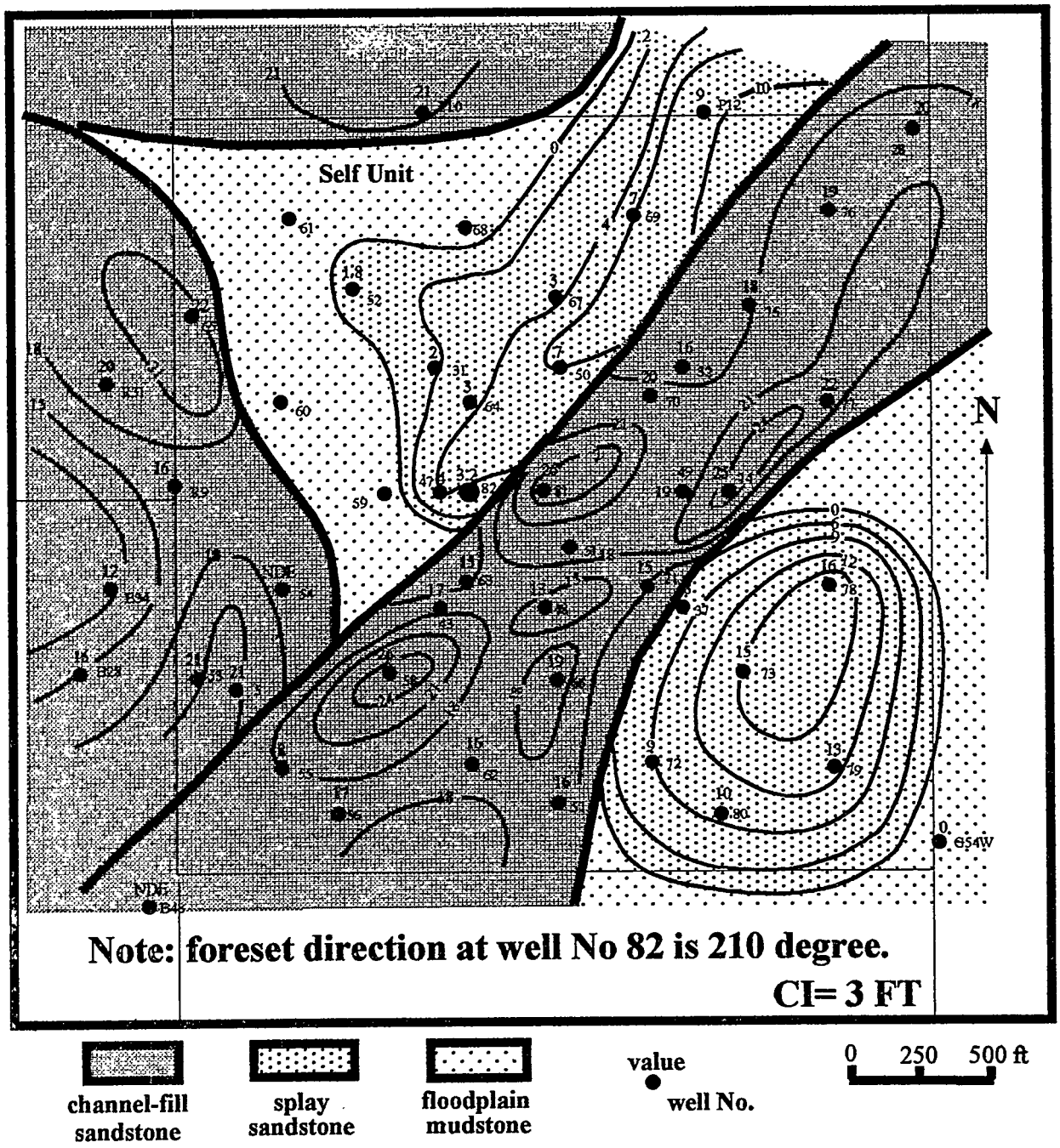

Figure 9

Unit D No. 1 Splay In The Vicinity Of Self No. 82

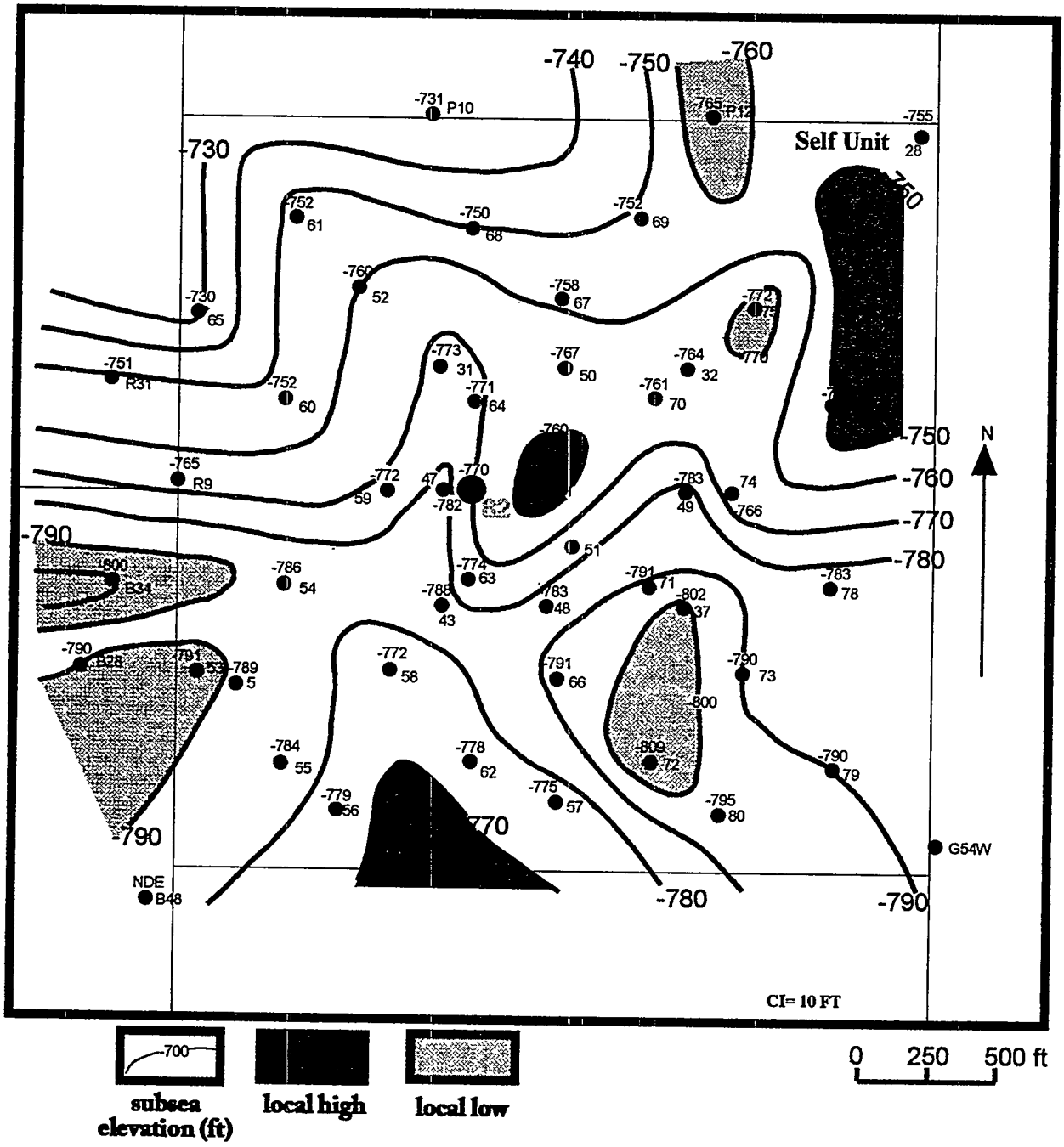

Figure 10

Structure Map To Unit D Sandstone

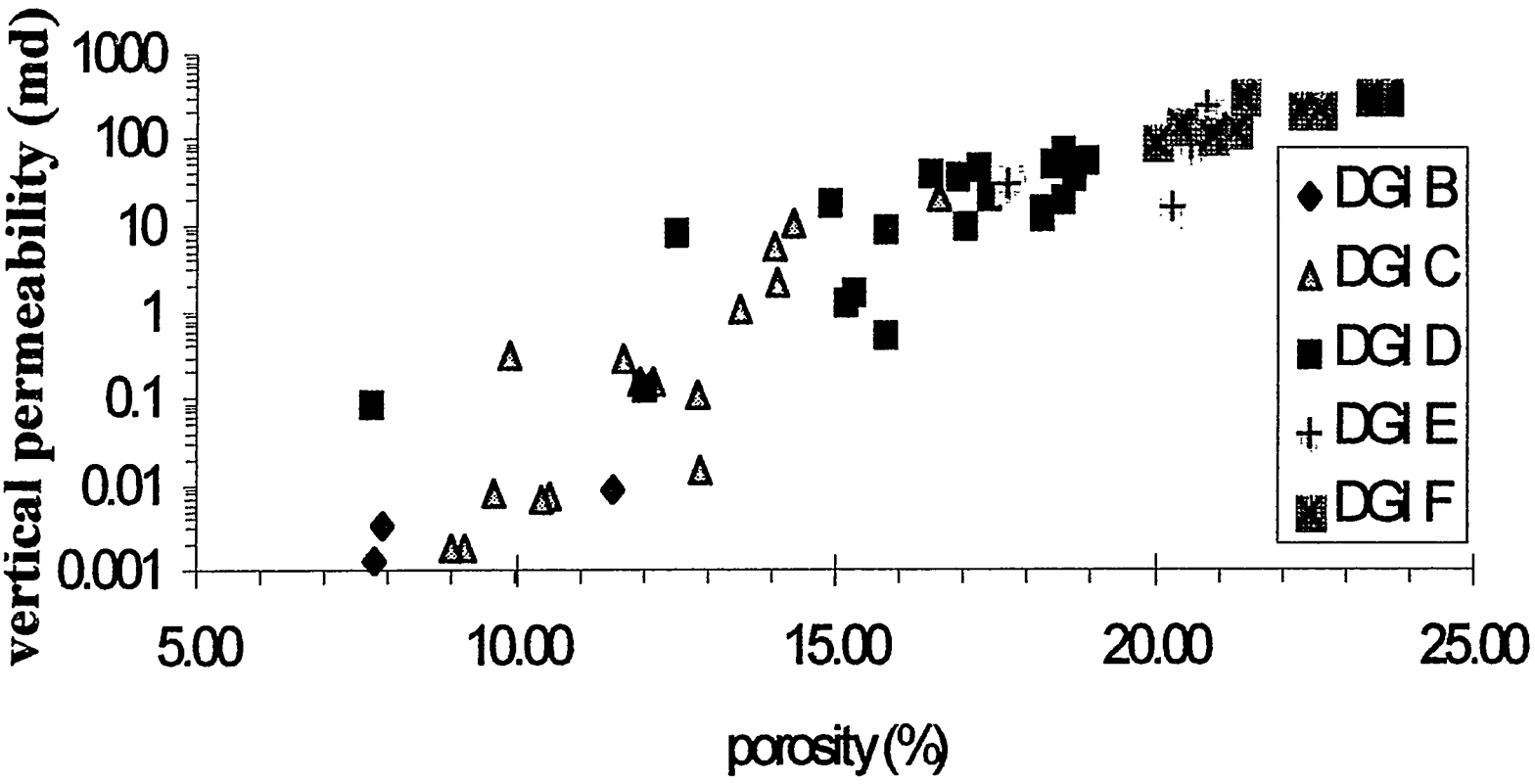

Figure 11

Porosity Versus Vertical Permeability For Difference DGI's

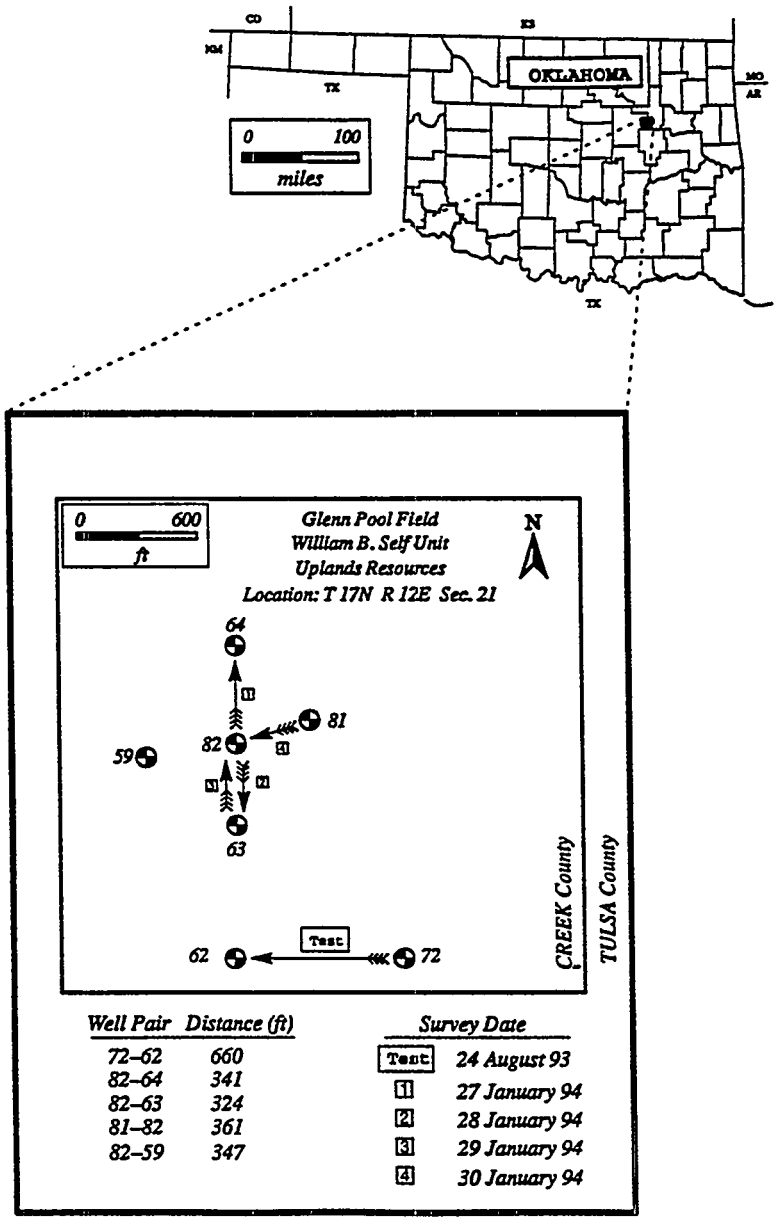

Figure 12

Glenn Pool Project Location And Site Map. Only Those Wells Involved In The Crosswell Seismic Work Are Shown. Arrows Indicate Crosswell Shooting Direction By Pointing At The Receiver Well.

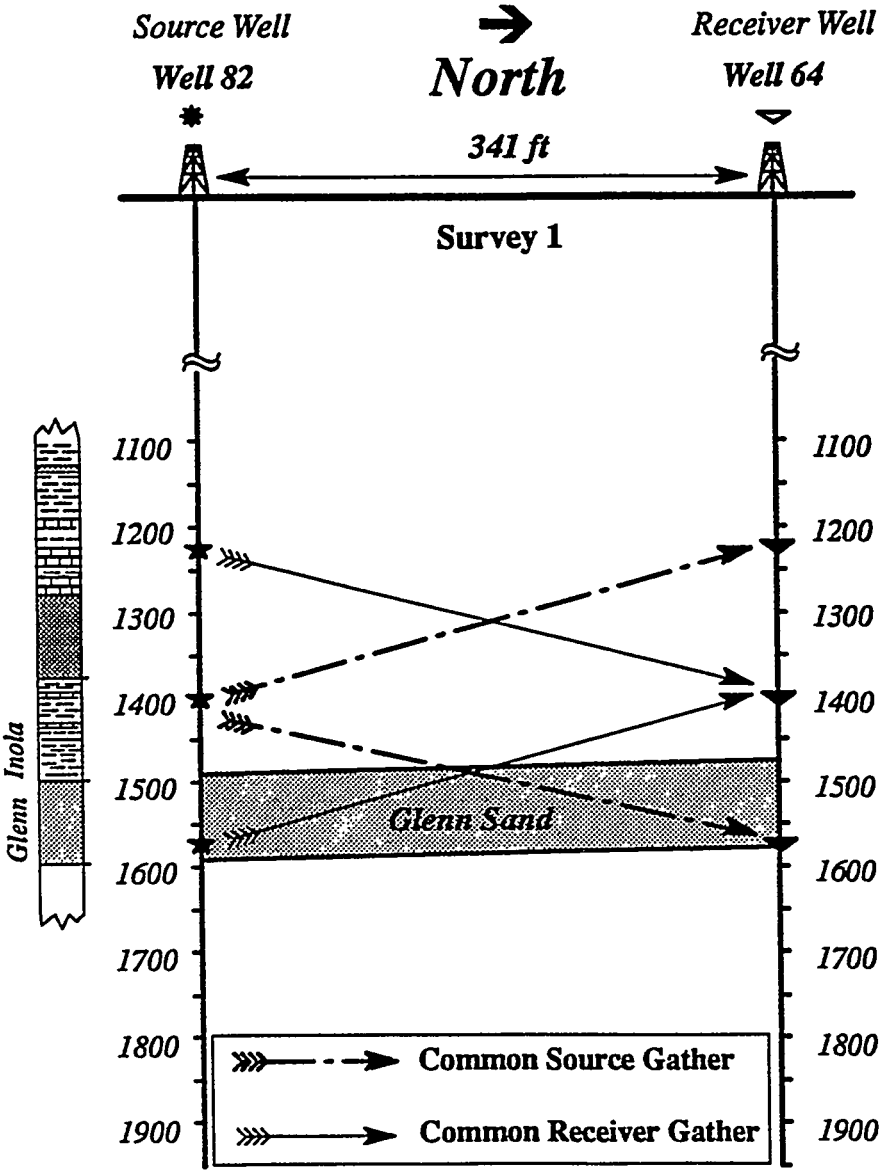

Figure 13

Some Features Of The 82-64 Survey Including Generalized Stratigraphic Column And Reservoir (Glenn Sand). Also Included Are Representative Common Source (CSG) and Common Receiver Gathers (CRG.

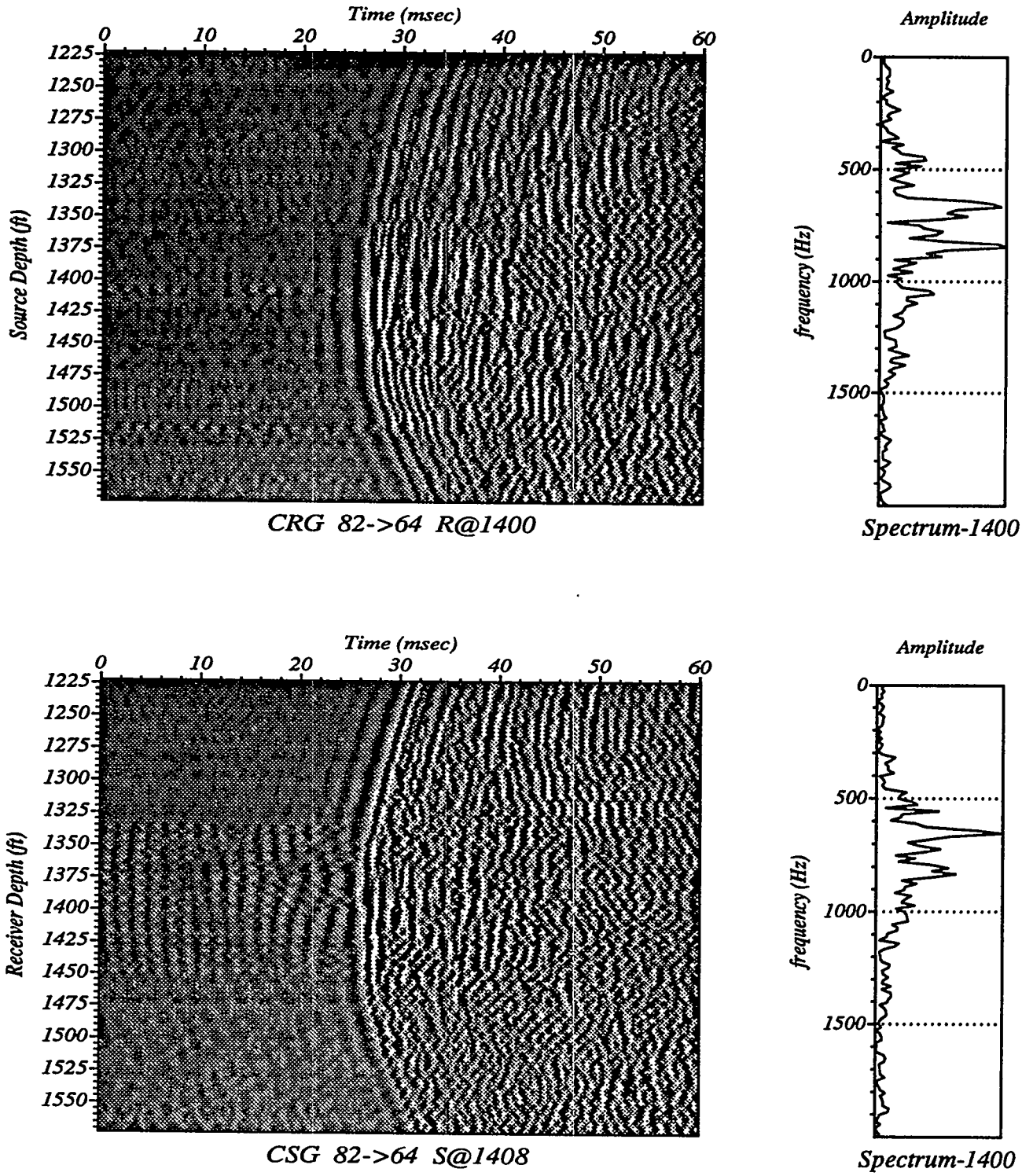

Figure 14

Selected CRG and CSG Data From The 82-64 Survey. Beside Each Gather Is A Frequency Spectrum For A Trace Near The Center Of The Gather. The Data Quality Here Is High and First Arrivals Stand Out Well Above Ambient Noise Levels. The Receiver Well (64) Is Perforated On The Interval 1452-1473.

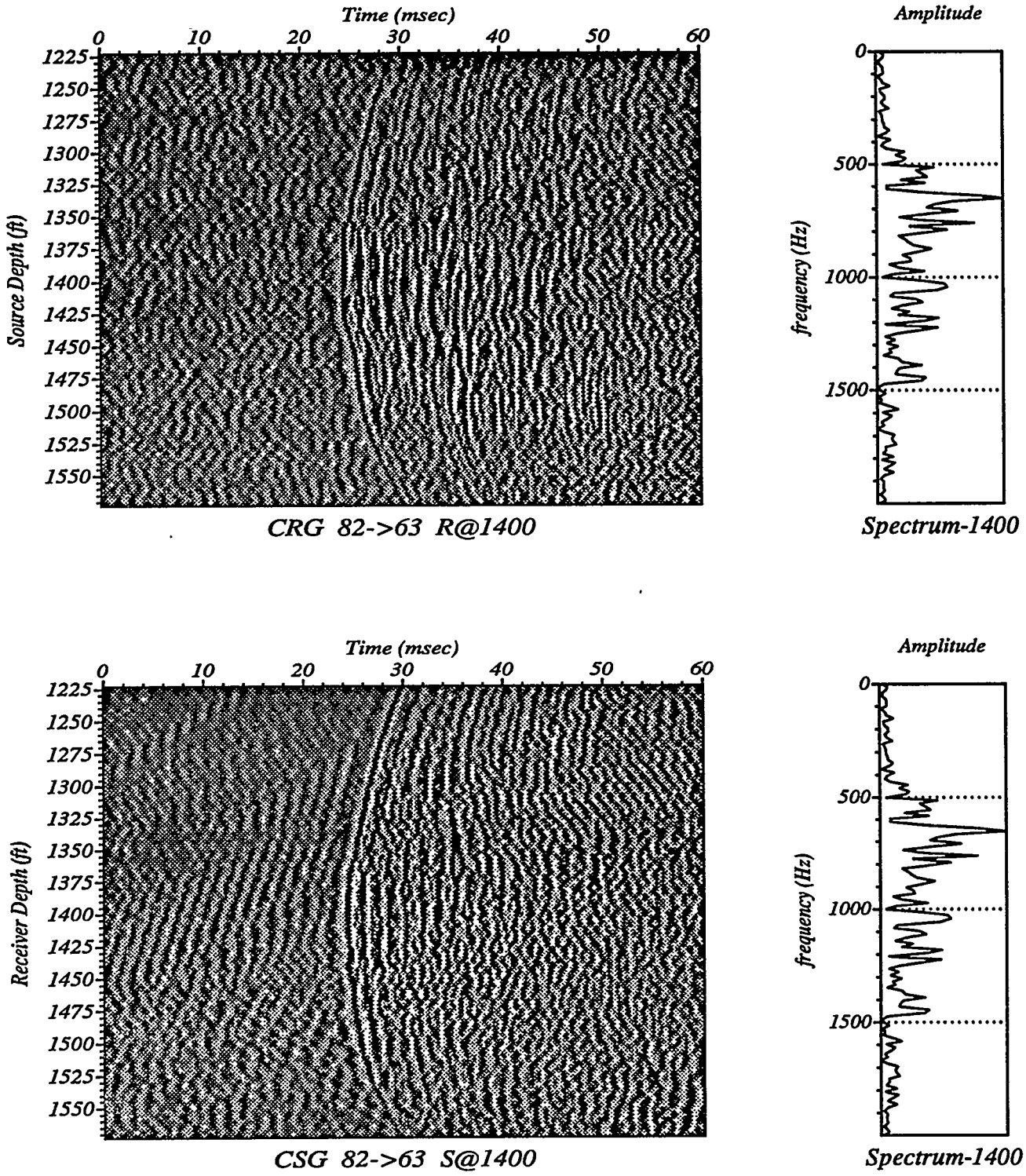

Figure 15

CRG And CSG Data From The 82-63 Survey. Note Strong Ambient, Pre-First-Arrival Noise In The Data. The CGS Data Shows The Noise To Be Coherent Tube Waves In The Receiver Well (63). The 63 Well Is Perforated On The Interval 1460-1505. It Is Interpreted That Tube Waves Were Generated By Fluid Flow In The Perforated Interval.

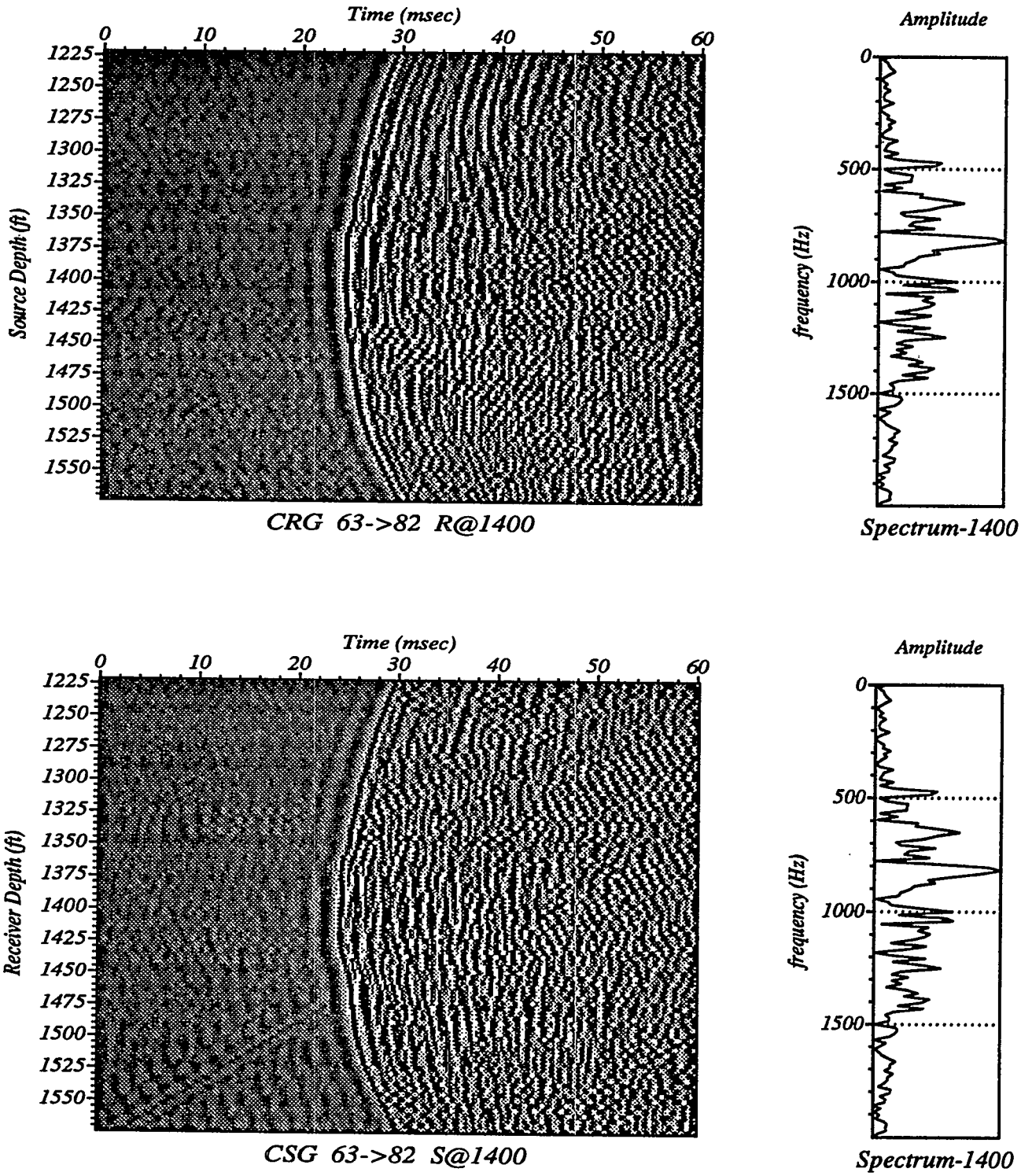

Figure 16

Data From The 64-82 Survey Over The Same Range As Shown In Figure 15. By Simply Reversing The Shooting Direction, High Quality Data Has Been Acquired.

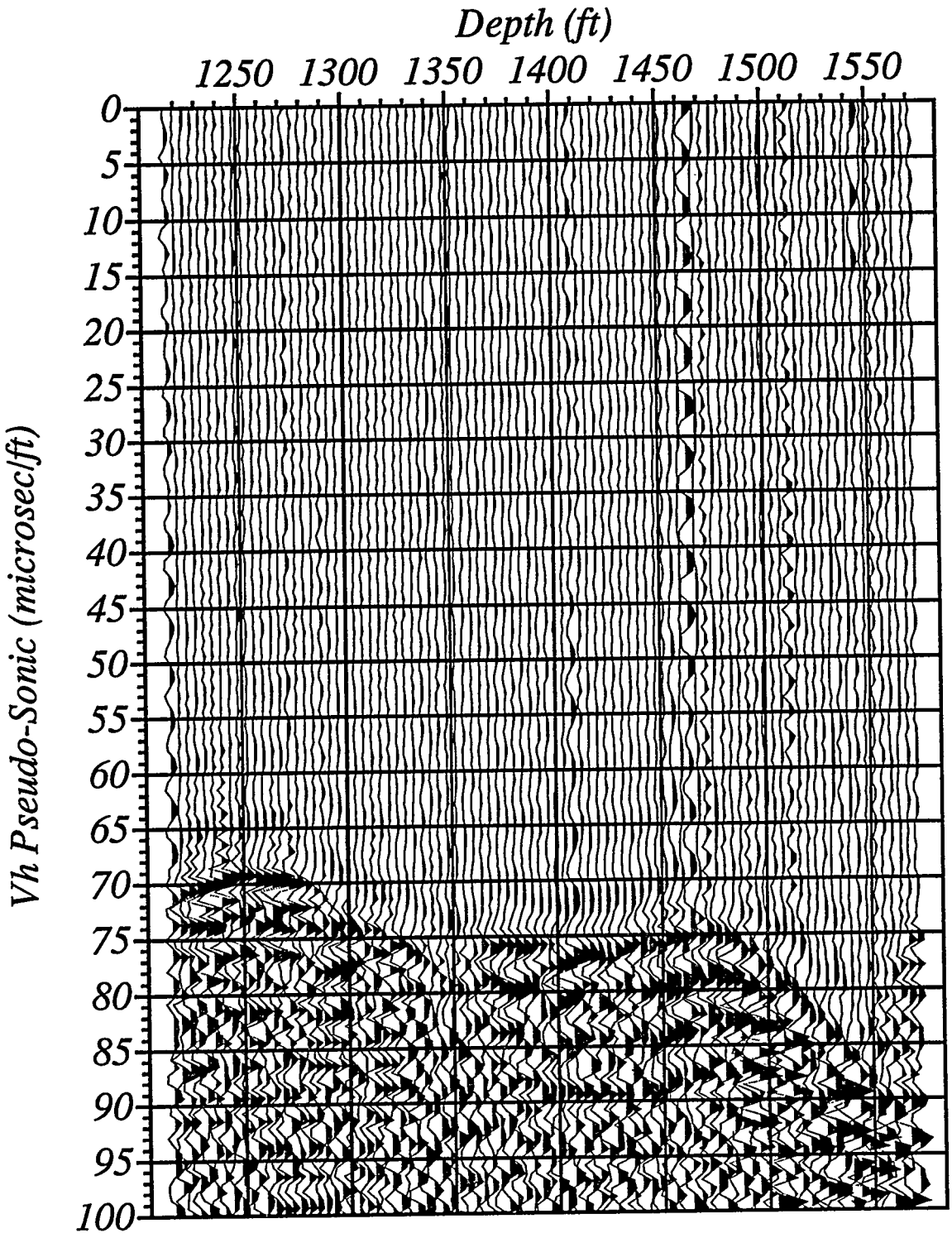

Figure 17

82>64 Constant Level Gather ($x = 350$)

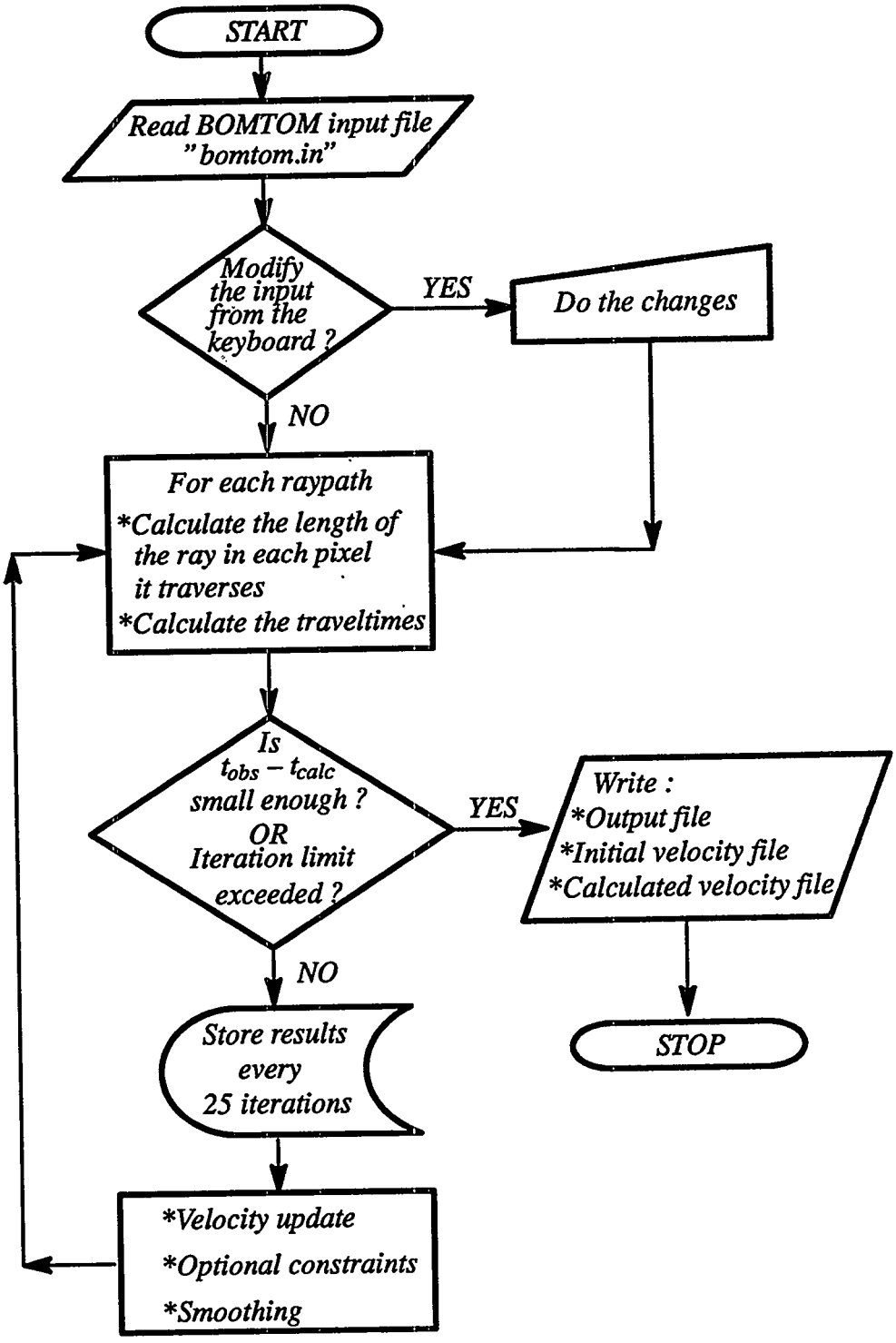

Figure 18

A Generalized Flowchart Of BOMTOM

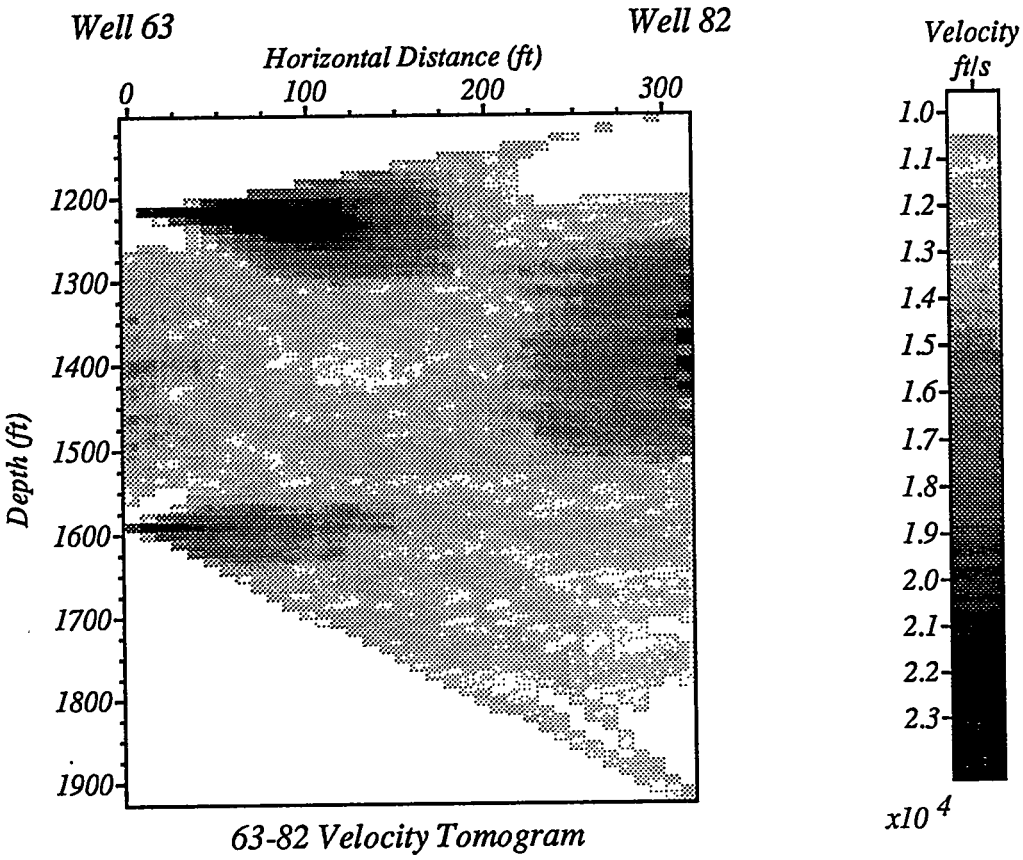

Figure 19

TU Velocity Tomograph Between Wells 63 And 82

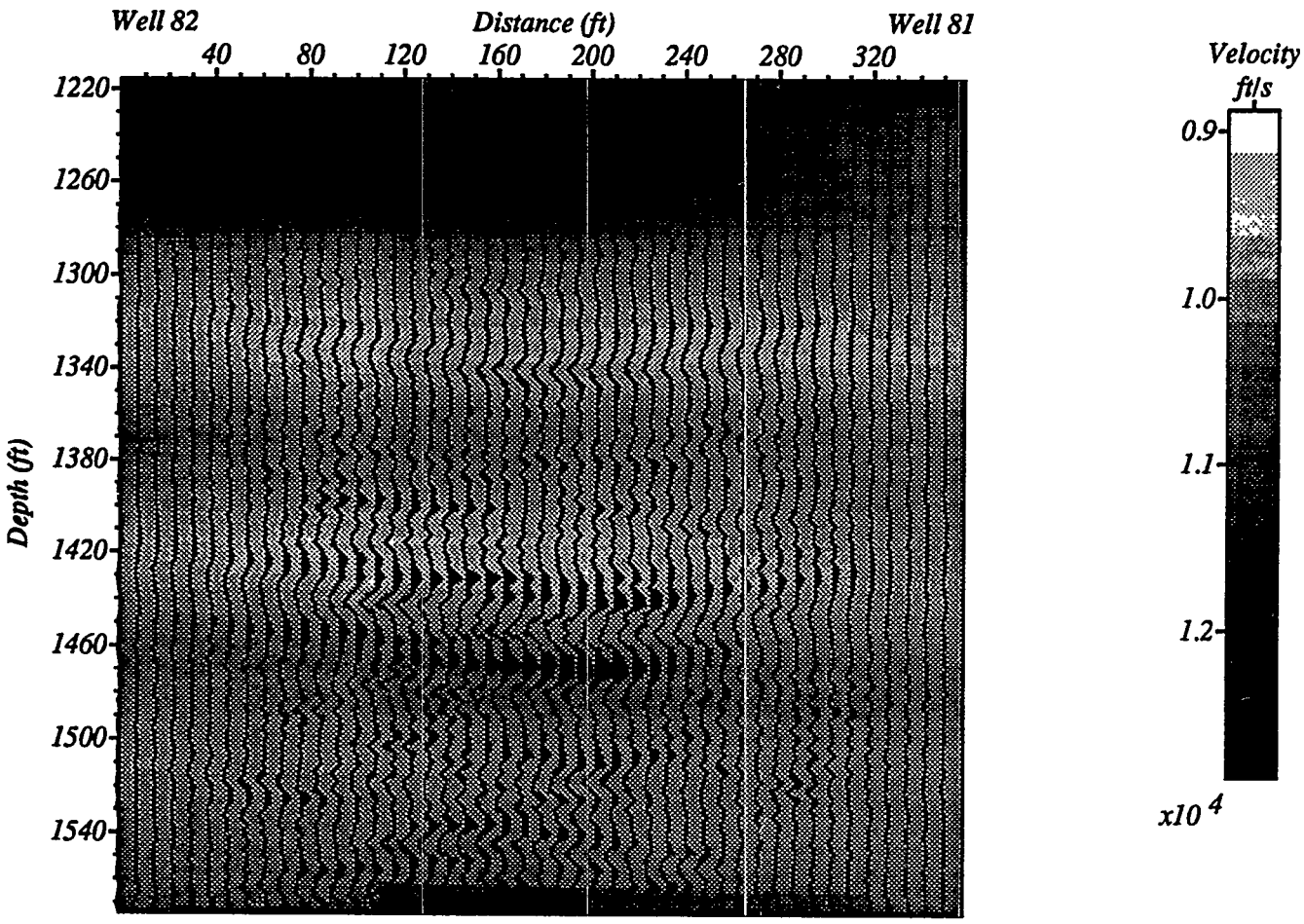

Figure 20

82_81 Survey: Velocity + Migration Overlay

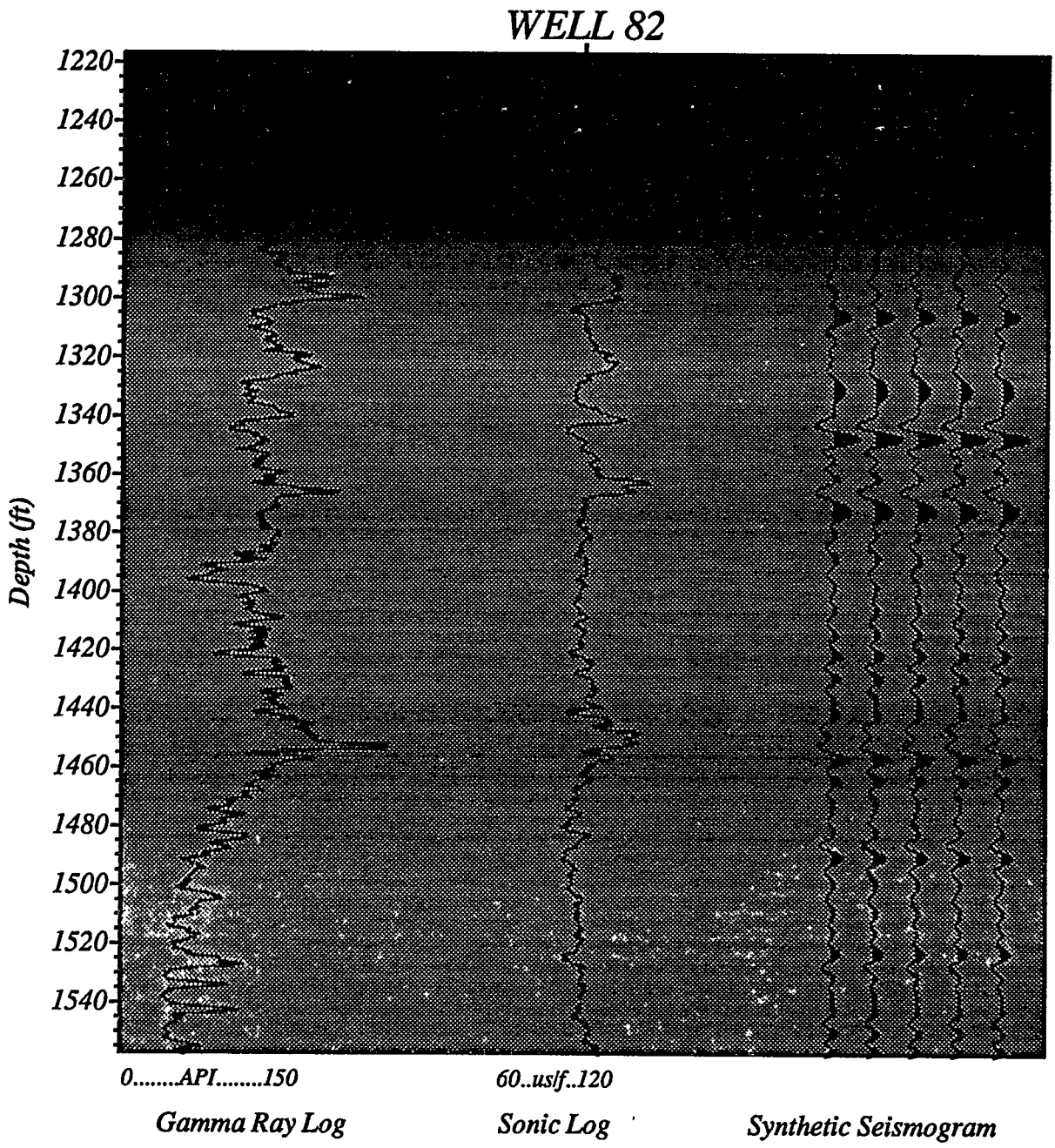

Figure 21

Well 82: P-Wave Velocity + Well Log Overlay

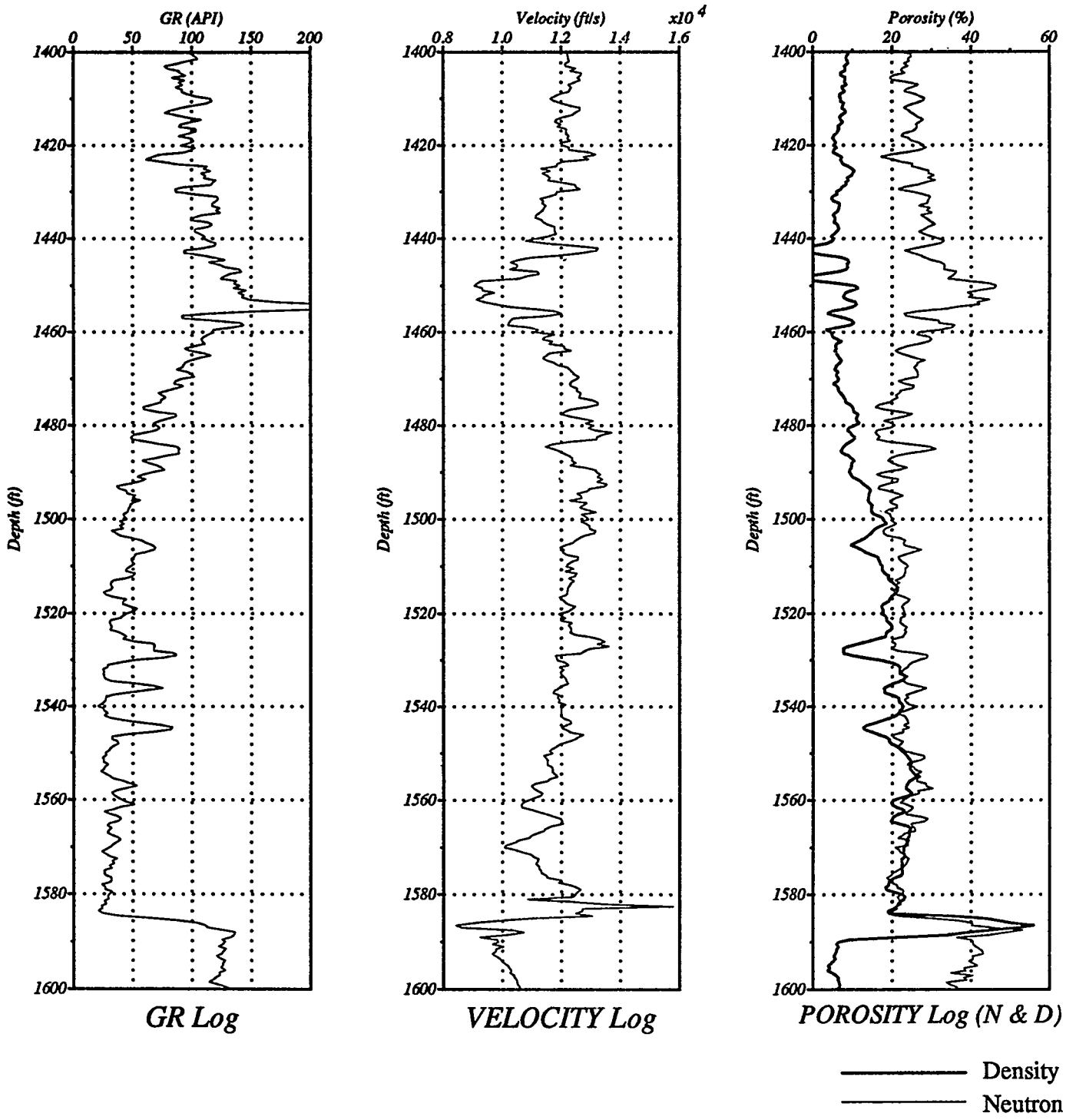

Figure 22

Well Logs Used In This Study

V = PHI VSH VSH*VSH
Response Distribution: Normal
Link Function: Identity

Summary of Fit			
Mean of Response	11942.2863	R-Square	0.7411
Root MSE	426.9700	Adj R-Sq	0.7389

Analysis of Variance					
Source	DF	Sum of Squares	Mean Square	F Stat	Prob > F
Model	3	186318286	62106095.4	340.6743	0.0001
Error	357	65082317.3	182303.410		
C Total	360	251400604			

Type I Tests					
Source	DF	Sum of Squares	Mean Square	F Stat	Prob > F
PHI	1	159512338	159512338	874.9827	0.0001
VSH	1	18742759.7	18742759.7	102.8108	0.0001
VSH*VSH	1	8063188.64	8063188.64	44.2295	0.0001

Type III Tests					
Source	DF	Sum of Squares	Mean Square	F Stat	Prob > F
PHI	1	135807077	135807077	744.9508	0.0001
VSH	1	22788440.8	22788440.8	125.0028	0.0001
VSH*VSH	1	8063188.64	8063188.64	44.2295	0.0001

.Parameter Estimates							
Variable	DF	Estimate	Std Error	T Stat	Prob >|T|	Tolerance	Var Inflation
INTERCEPT	1	15950.5157	138.0539	115.5383	0.0001	.	0
PHI	1	-18152.729	665.0865	-27.2938	0.0001	0.9317	1.0733
VSH	1	-1311.4621	117.2994	-11.1805	0.0001	0.2969	3.3681
VSH*VSH	1	347.7552	52.2899	6.6505	0.0001	0.2908	3.4391

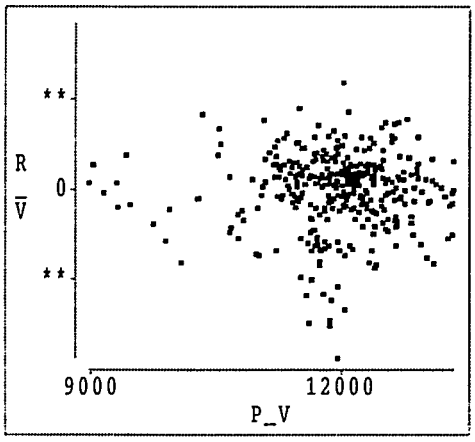

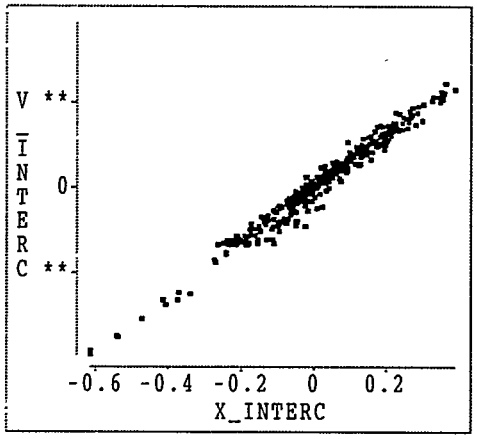

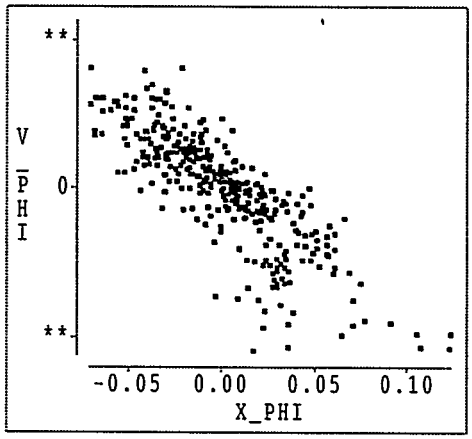

Figure 23

Velocity - Porosity - Volume Of Shale Relationship

D_V	=	PHI
Response Distribution:		Normal
Link Function:		Identity

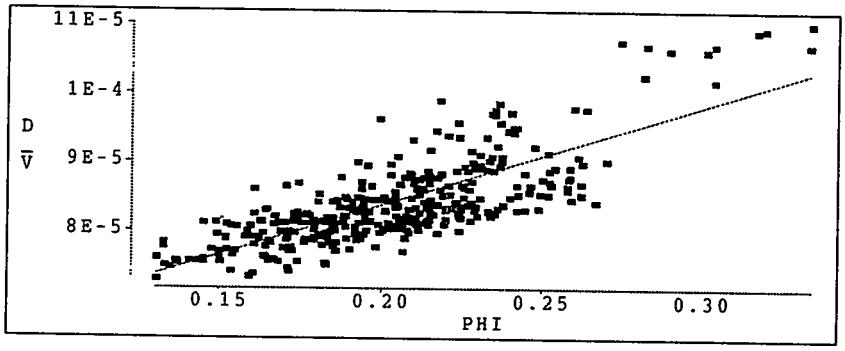

Parametric Regression Fit

	Model		Error				
Type	DF	Mean Square	DF	Mean Square	R-Square	F Stat	Prob > F
Line	1	9.32874E-9	359	1.5619E-11	0.6246	597.2561	0.0001

Summary of Fit

Mean of Response	8.418E-05	R-Square	0.6246
Root MSE	3.952E-06	Adj R-Sq	0.6235

Analysis of Variance

Source	DF	Sum of Squares	Mean Square	F Stat	Prob > F
Model	1	9.32874E-9	9.32874E-9	597.2561	0.0001
Error	359	5.60734E-9	1.5619E-11		
C Total	360	1.494E-08			

Type I Tests

Source	DF	Sum of Squares	Mean Square	F Stat	Prob > F
PHI	1	9.32874E-9	9.32874E-9	597.2561	0.0001

Type III Tests

Source	DF	Sum of Squares	Mean Square	F Stat	Prob > F
PHI	1	9.32874E-9	9.32874E-9	597.2561	0.0001

Parameter Estimates

Variable	DF	Estimate	Std Error	T Stat	Prob >|T|	Tolerance	Var Inflation
INTERCEPT	1	5.463E-05	1.227E-06	44.5186	0.0001	.	0
PHI	1	0.0001	5.942E-06	24.4388	0.0001	1.0000	1.0000

95% C.I. for Parameters

Variable	Estimate	Lower	Upper
INTERCEPT	5.463E-05	5.221E-05	5.704E-05
PHI	0.0001	0.0001	0.0002

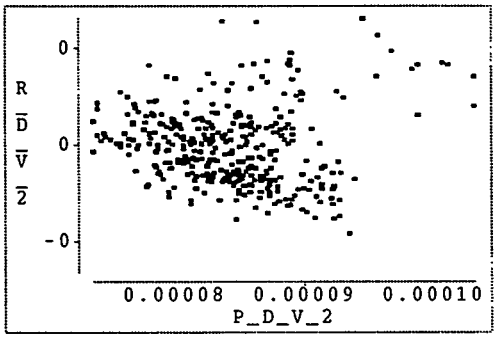

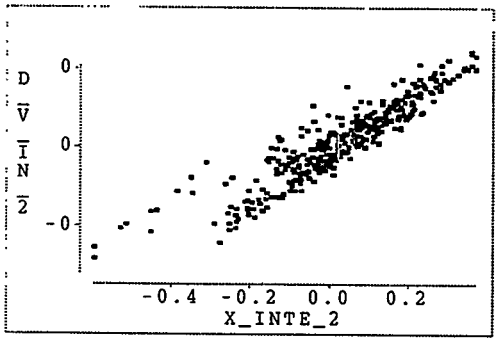

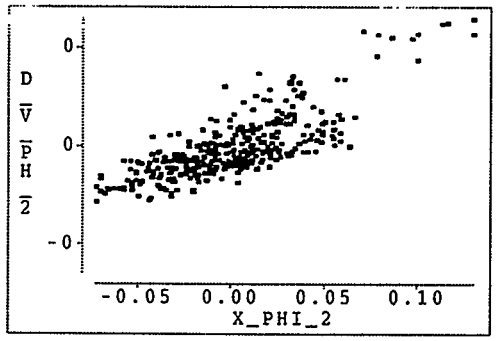

Figure 24

Velocity - Porosity - Volume of Shale Relationship (Wyllie's Equation)

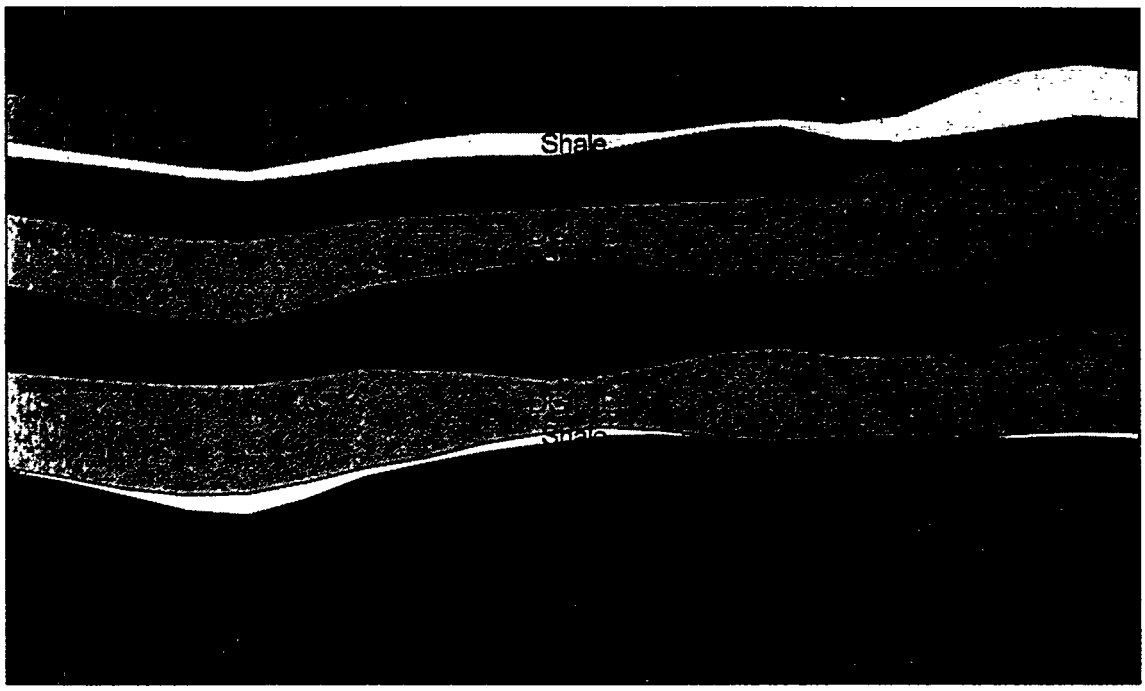

Figure 25.A
Layer Cake Model: North-South Cross Section

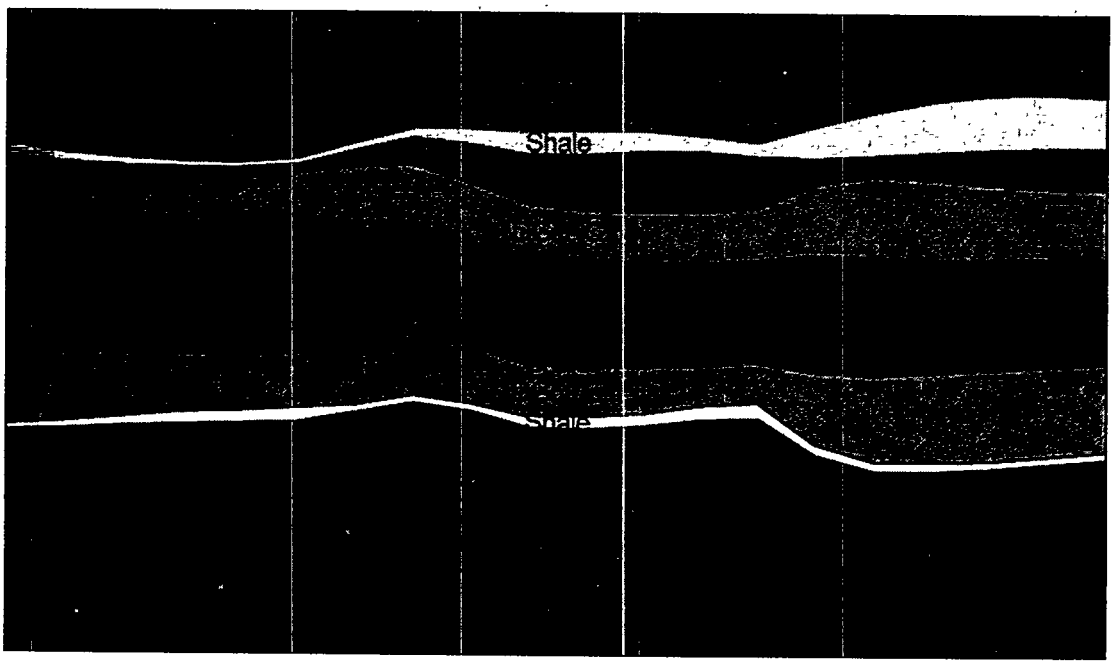

Figure 25.B
Layer Cake Model: East-West Cross Section

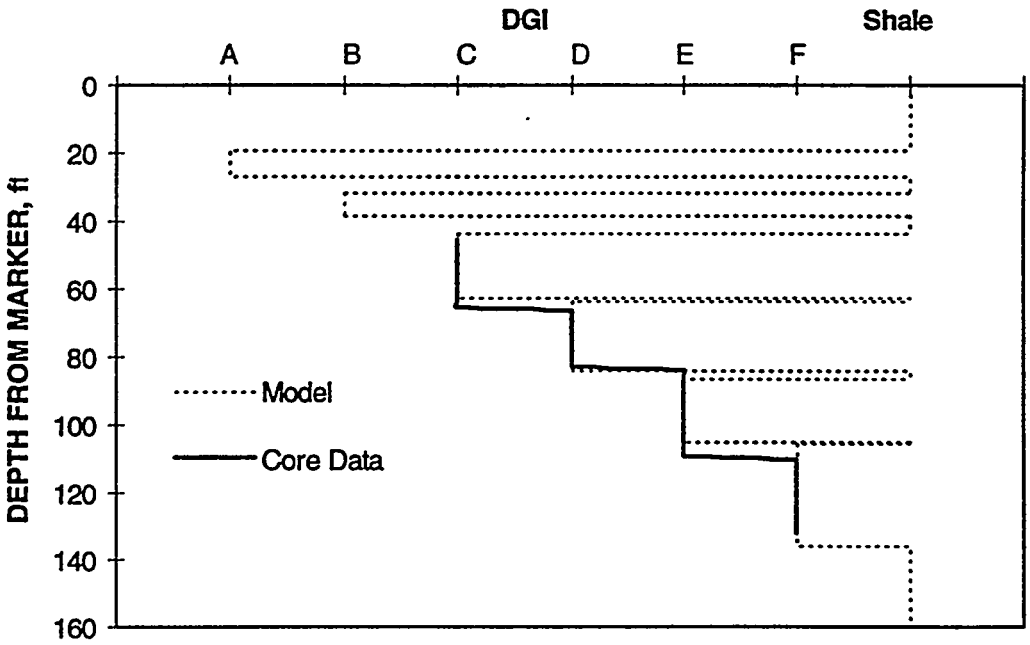

Figure 26.A

Layer Thickness Comparison At Well No. 43 - Deterministic Model

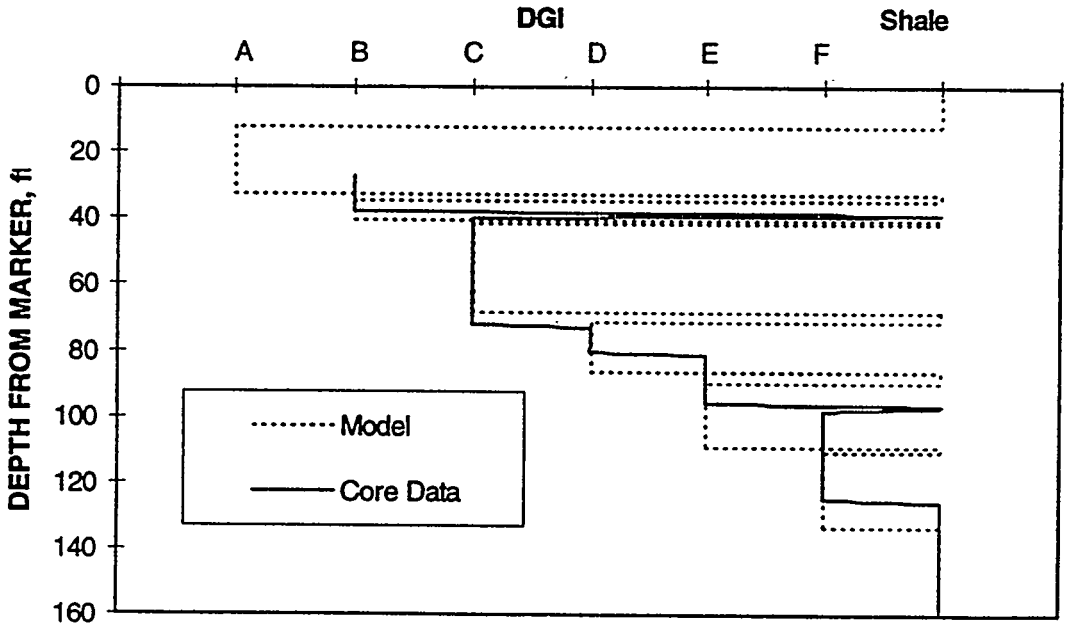

Figure 26.B

Layer Thickness Comparison At Well No. 43 - Deterministic Model

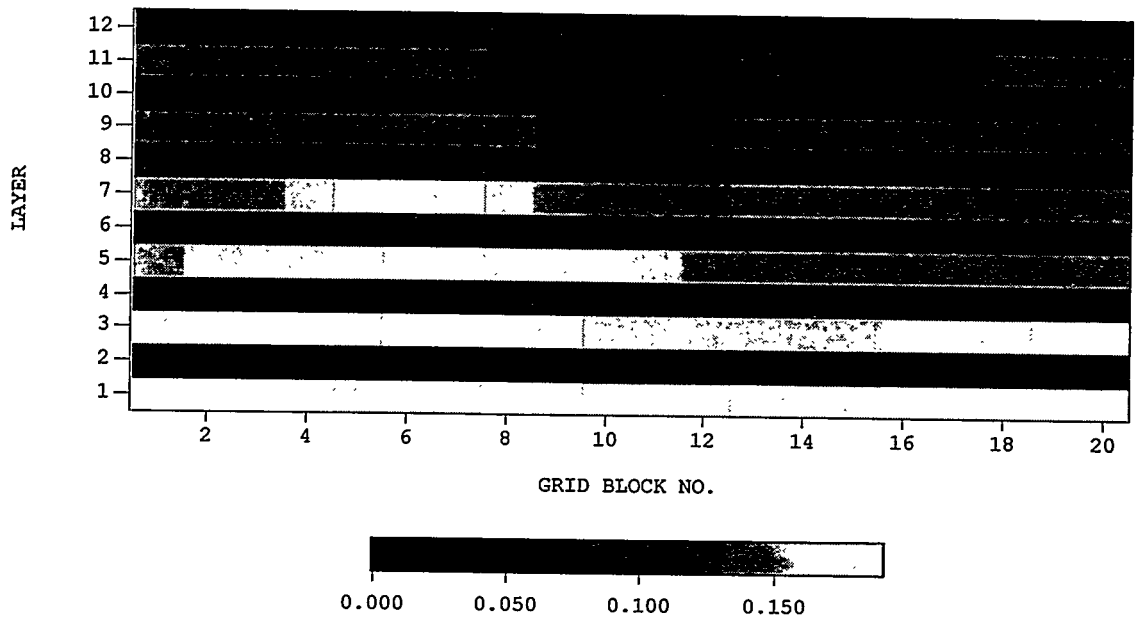

Figure 27

East West Porosity Cross Section - Deterministic Model

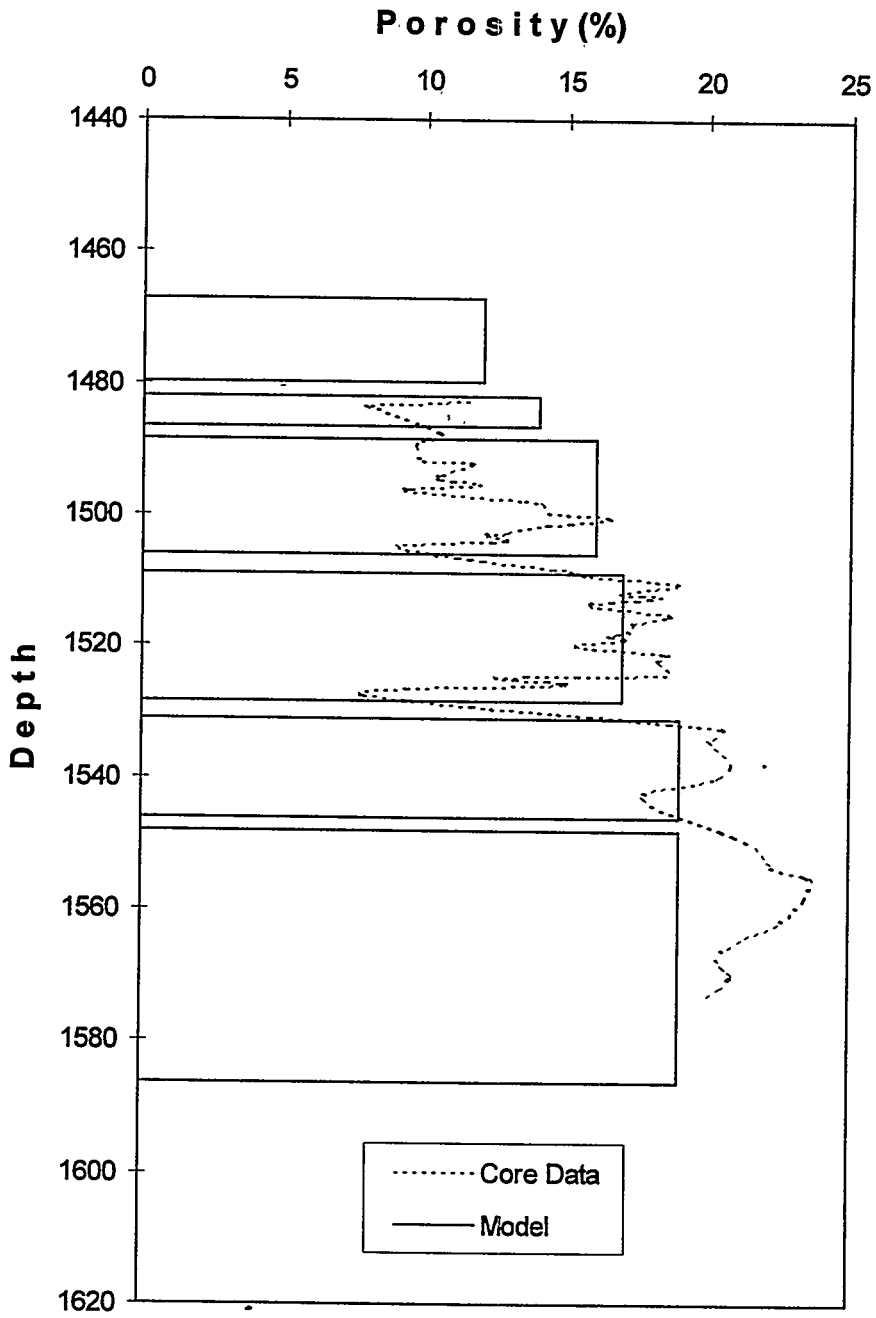

Figure 28

Porosity Comparison At Self Well No. 82

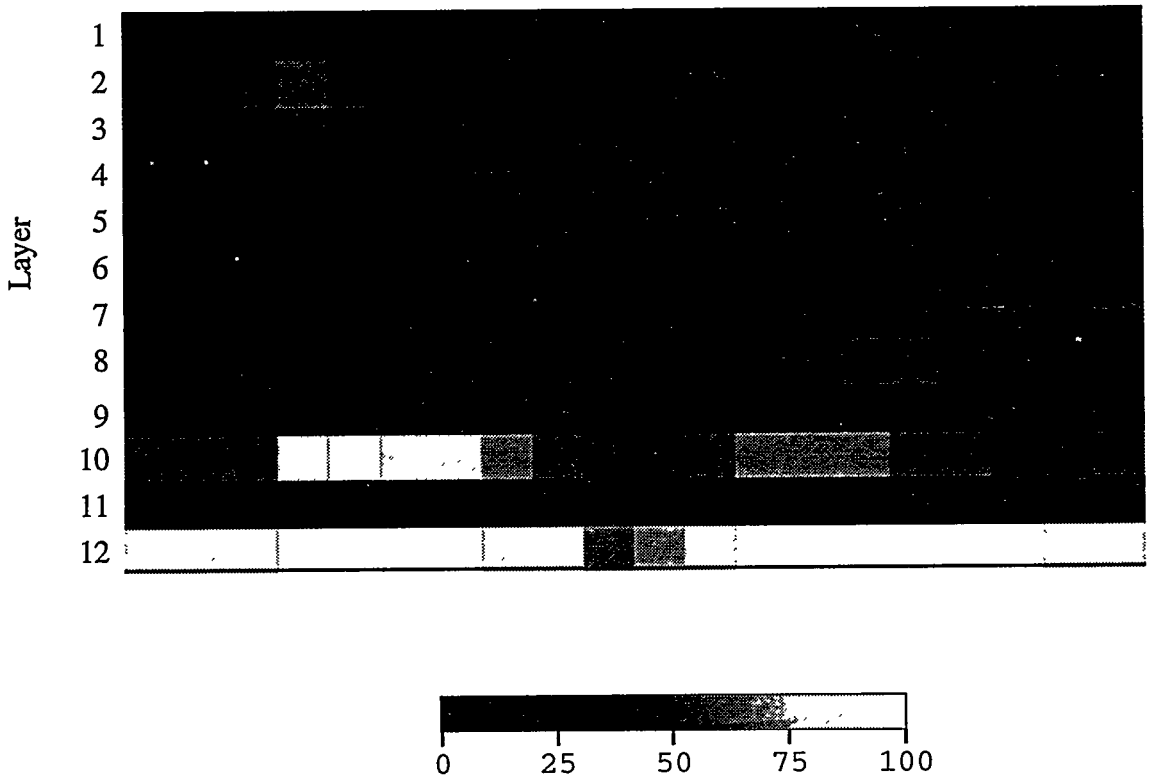

Figure 29

North-South Permeability Cross Section - Deterministic Model

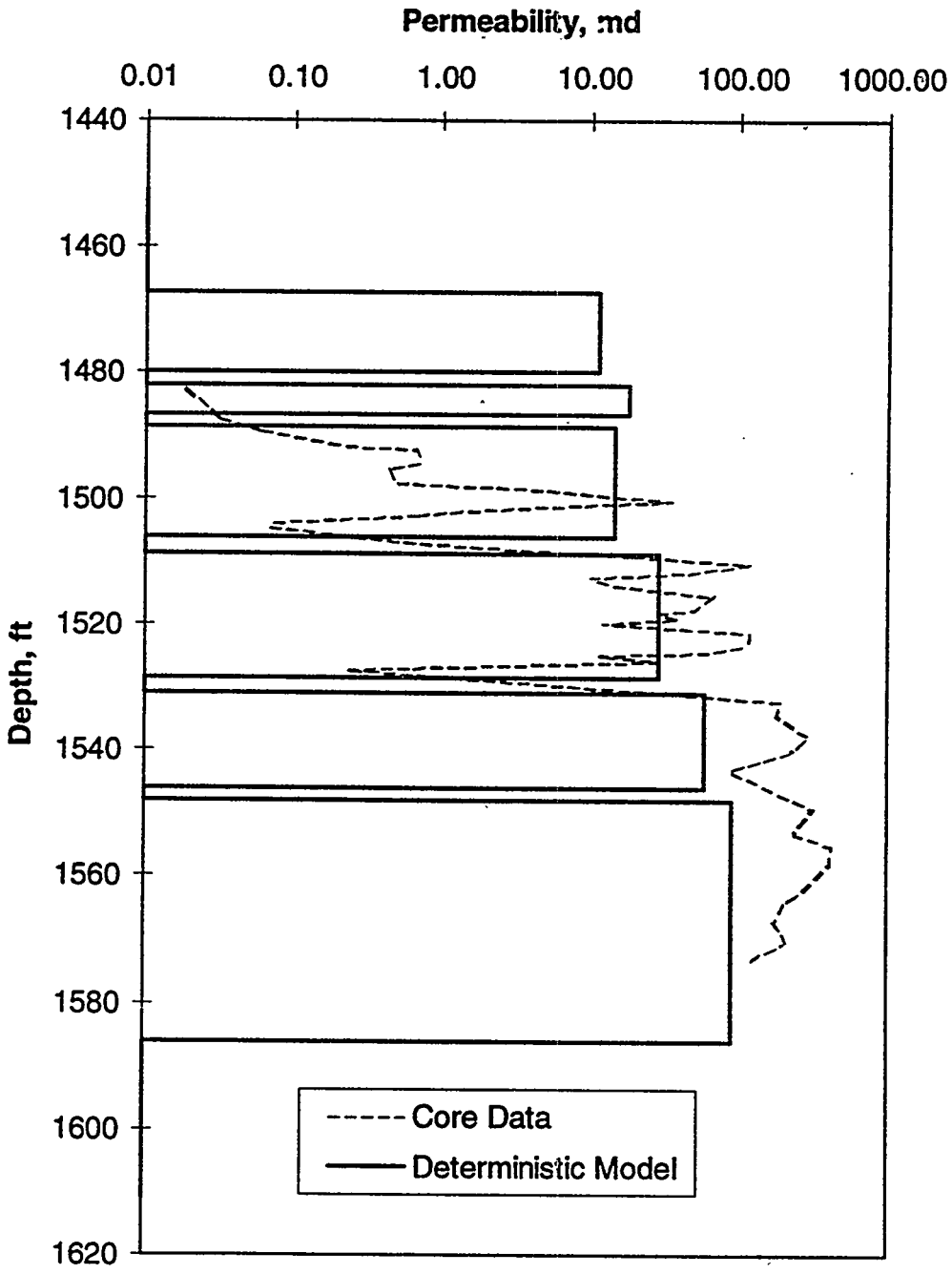

Figure 30

Permeability Comparison At Self Well No. 82 - Deterministic Model

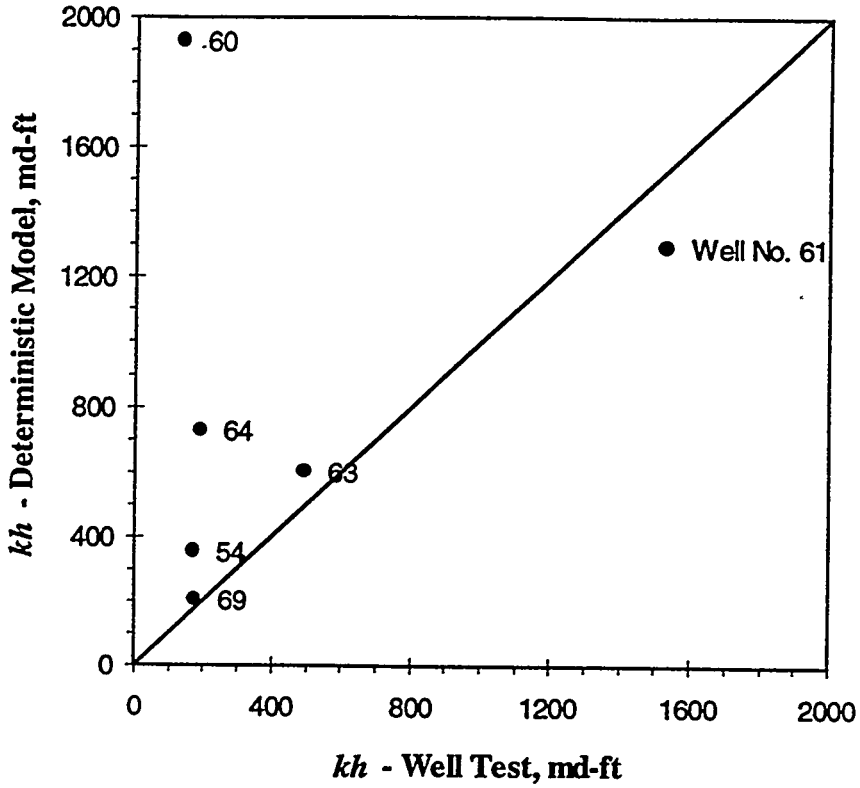

Figure 31
Permeability-Thickness Product (kh) Comparison - Deterministic Model

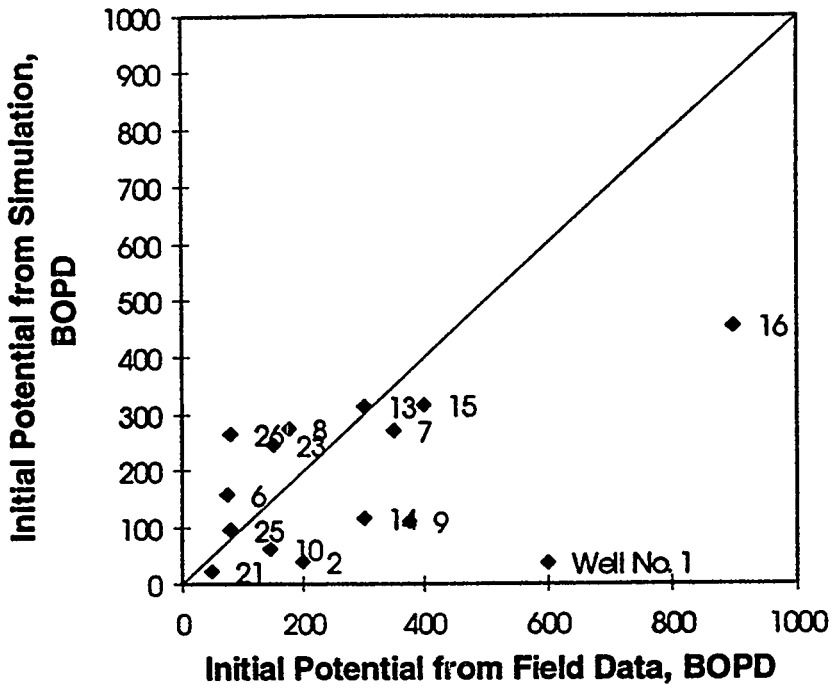

Figure 32

Initial Potential Comparison - Deterministic Model

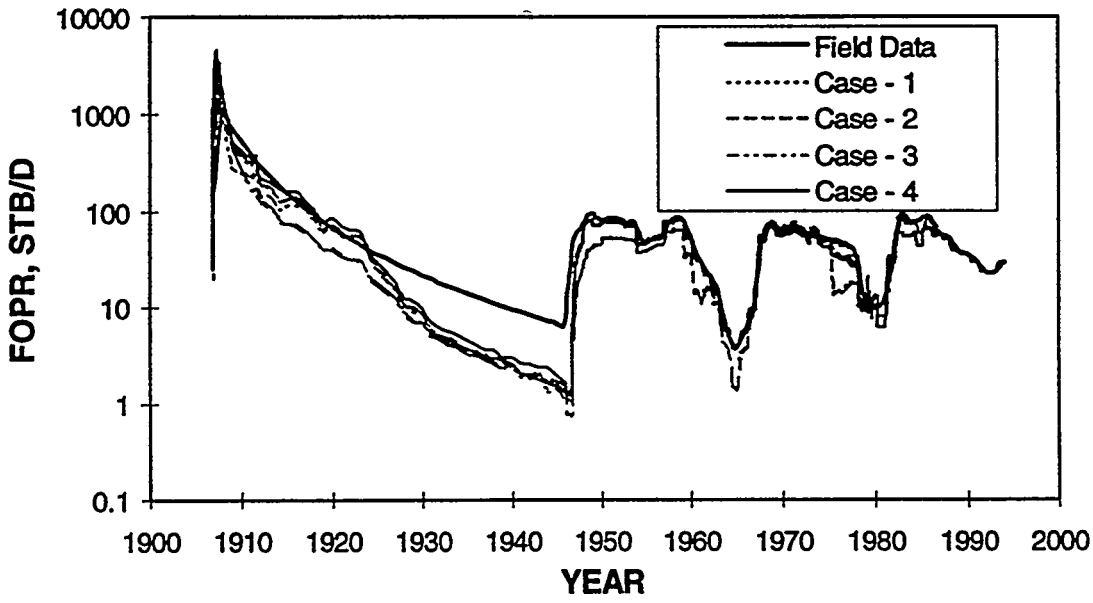

Figure 33

Field Oil Production Rate (FOPR) - Deterministic Model

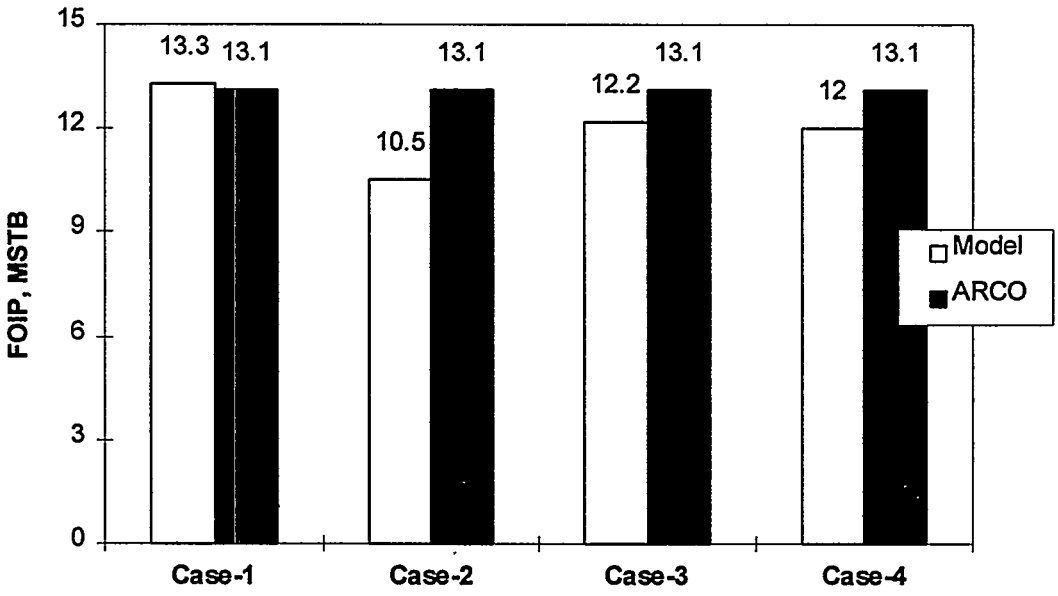

Figure 34
Original Oil In Place Estimation - Deterministic Model

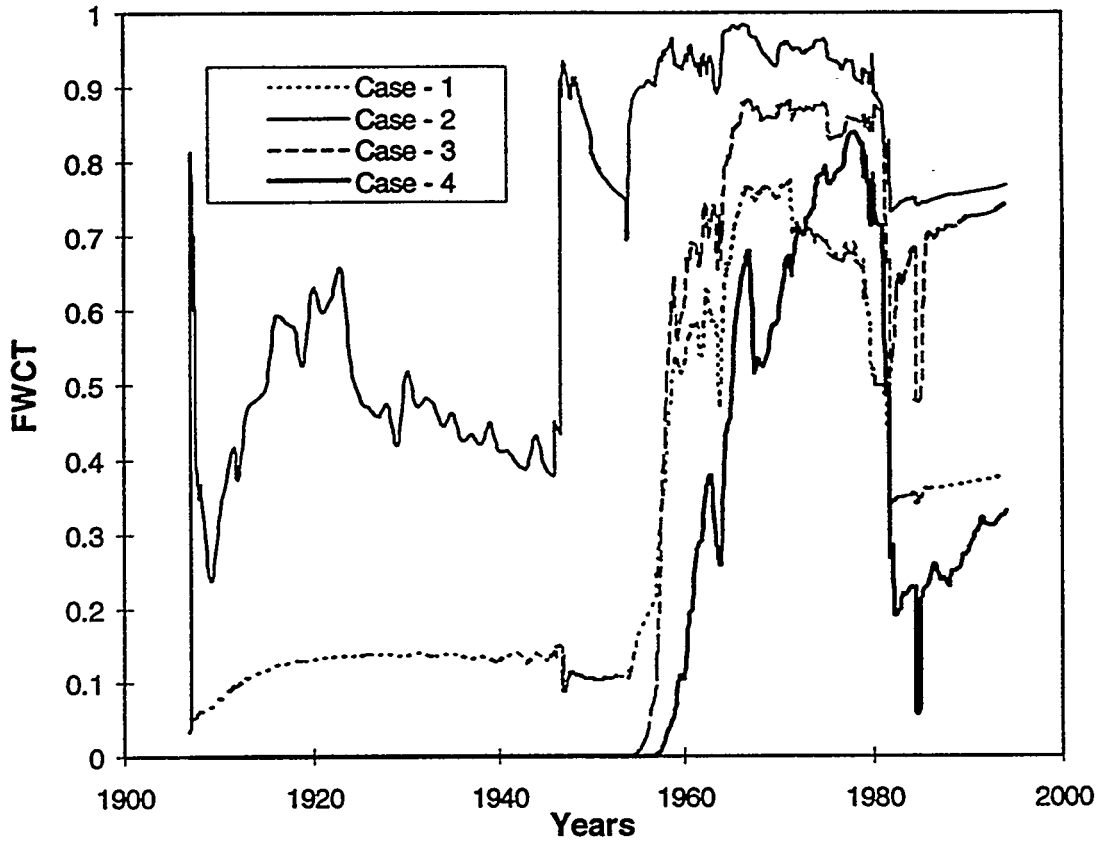

Figure 35

Simulated Field Water Cut - Deterministic Model

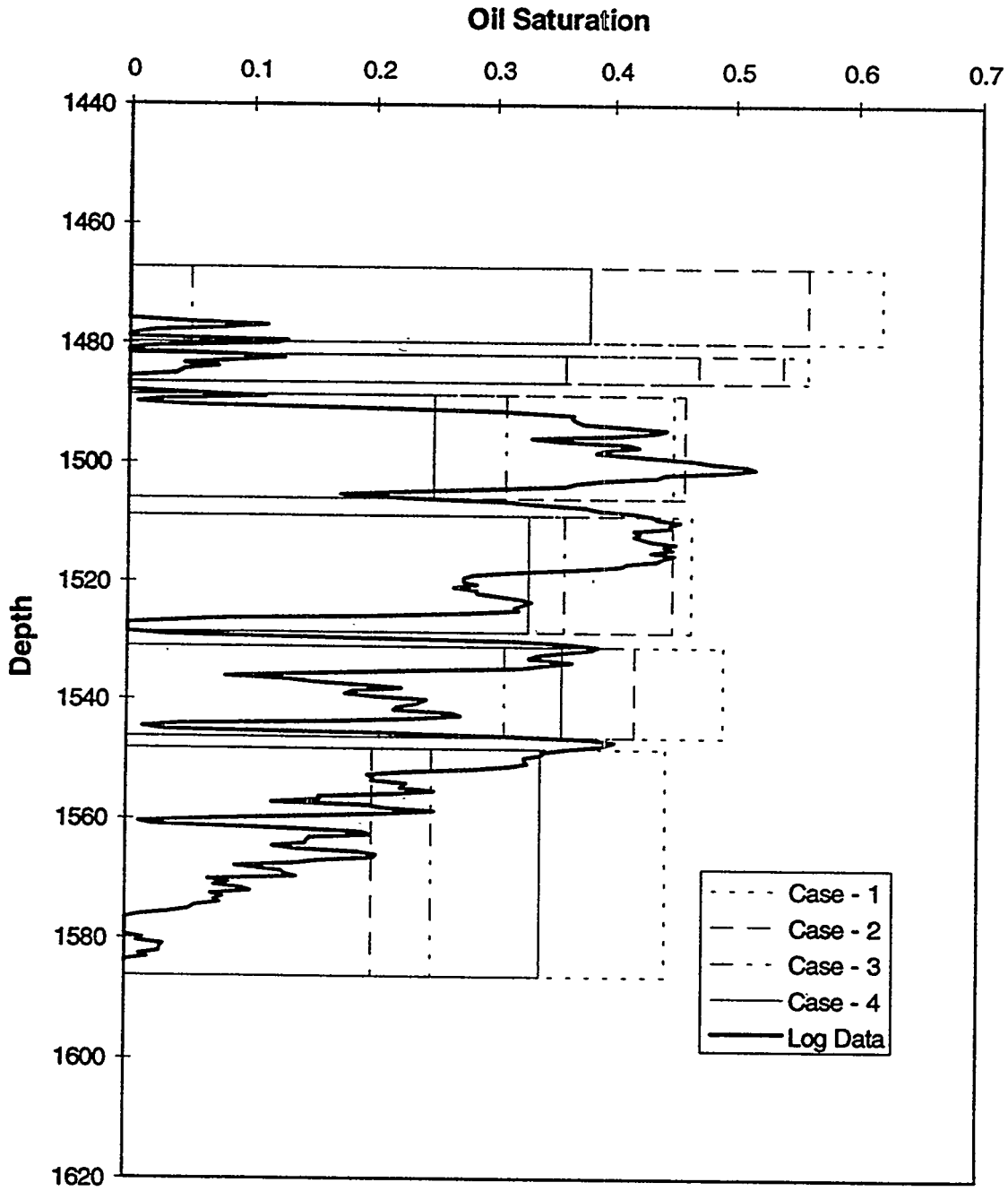

Figure 36

Oil Saturation Comparison At Self Well No. 82 - Deterministic Model

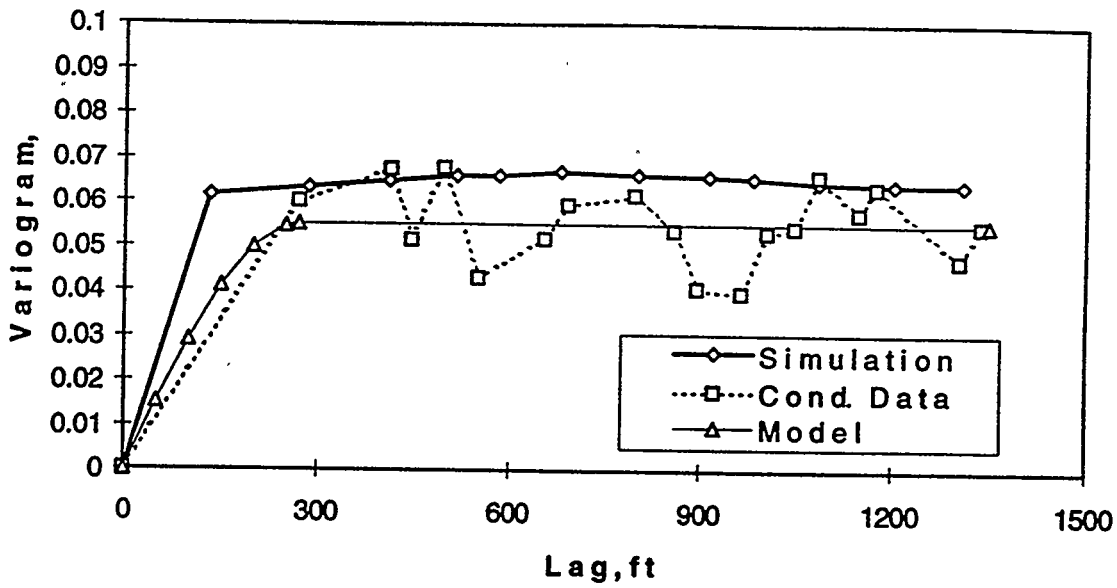

Figure 37A

Horizontal Variogram of DGI-A

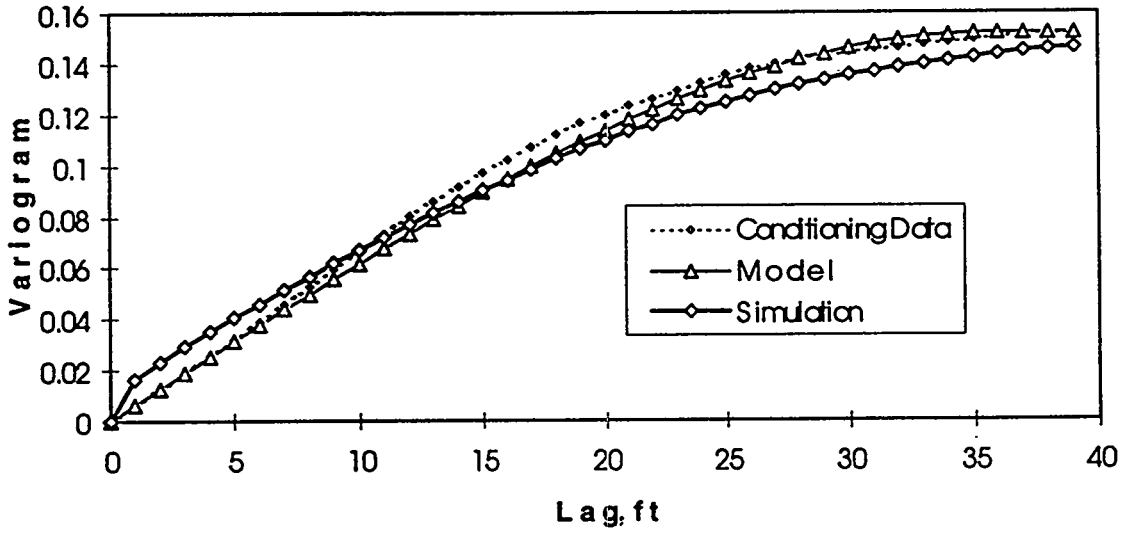

Figure 37B
Vertical Variogram of DGI-C

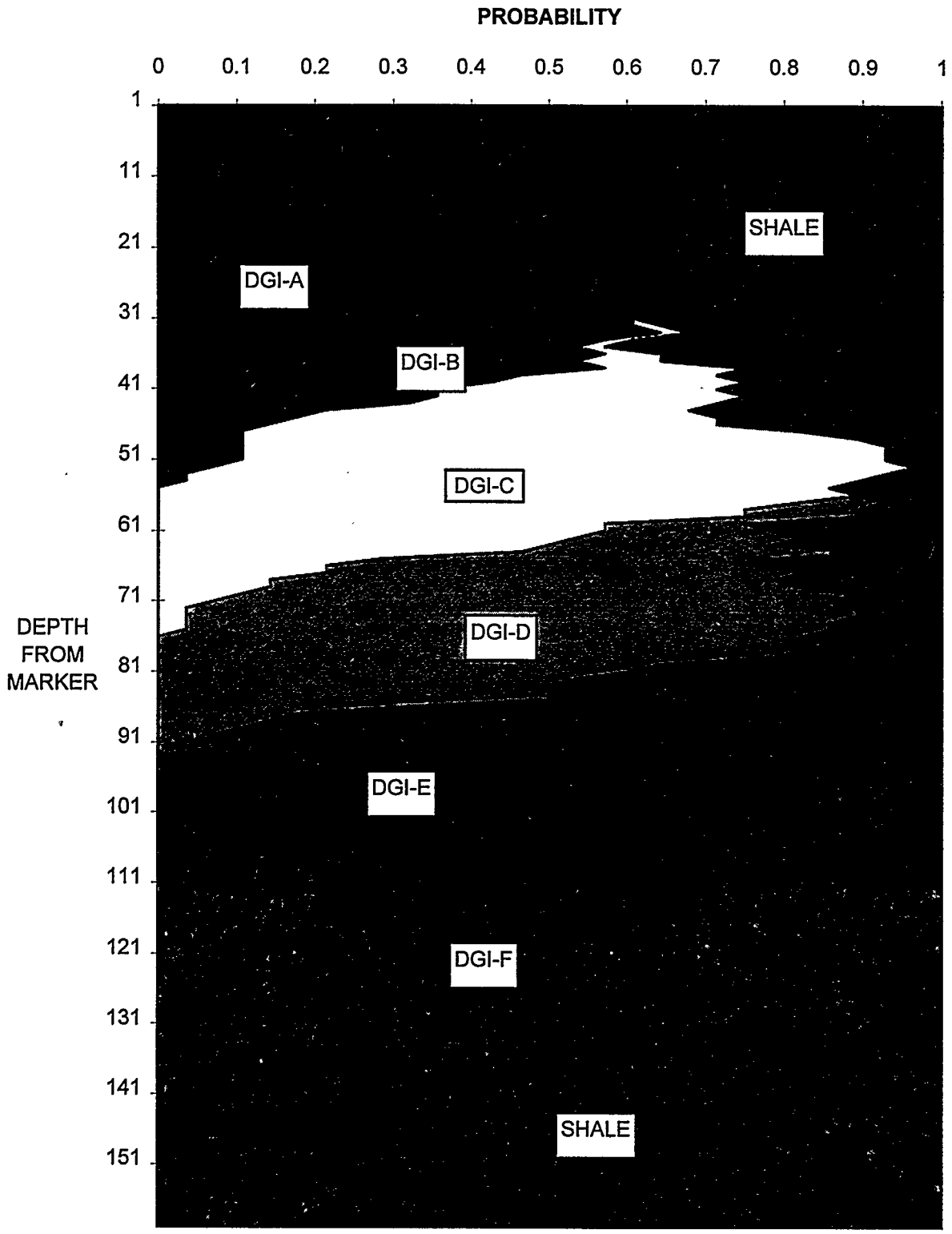

Figure 38
Input Proportion Curve

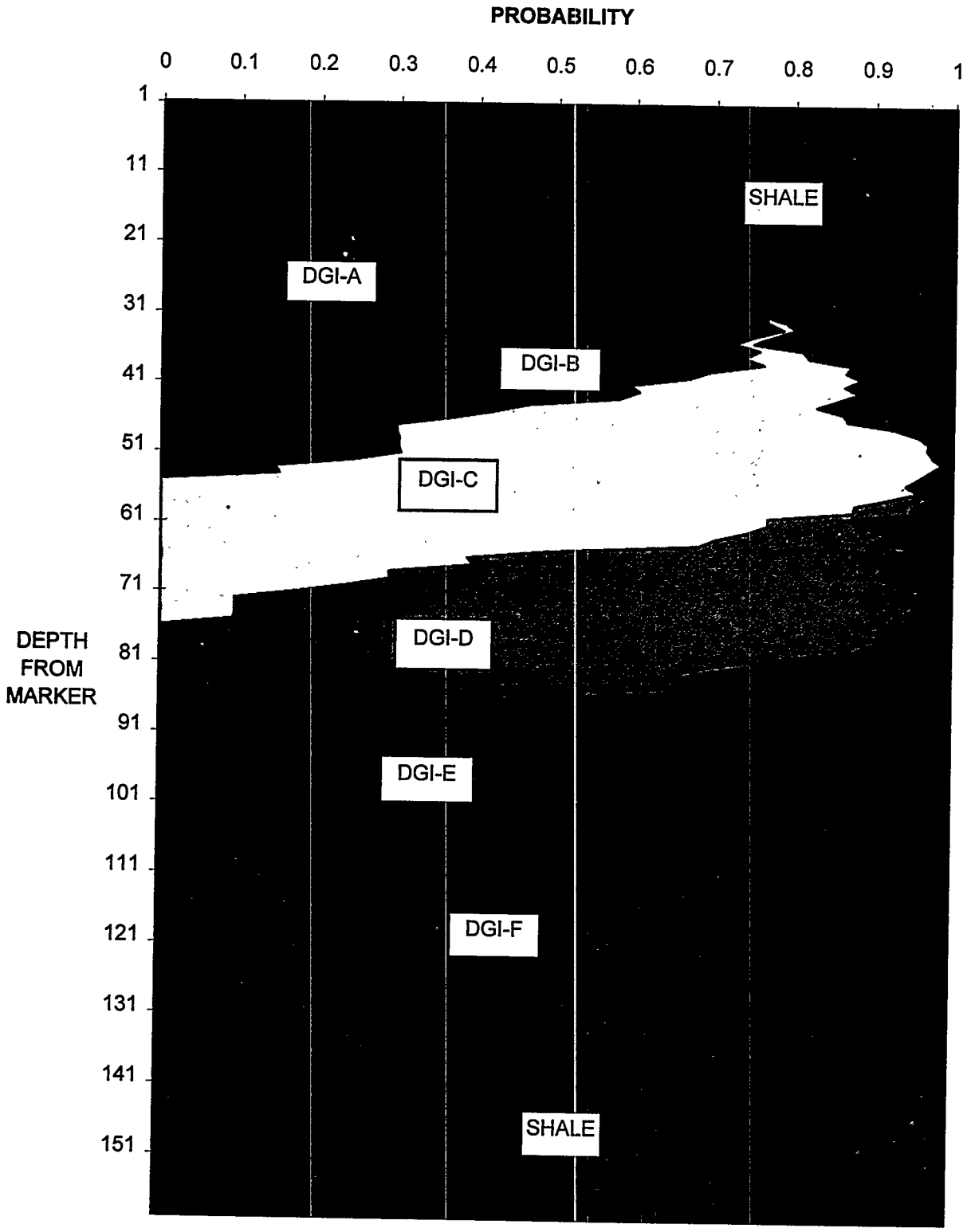

Figure 39
Output Proportion Curve

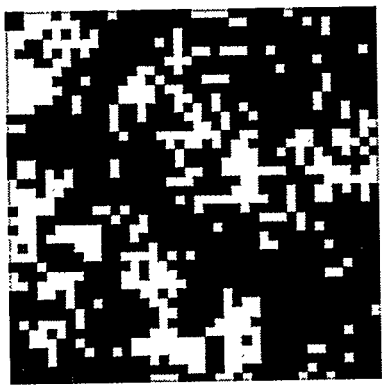

Real. # 1

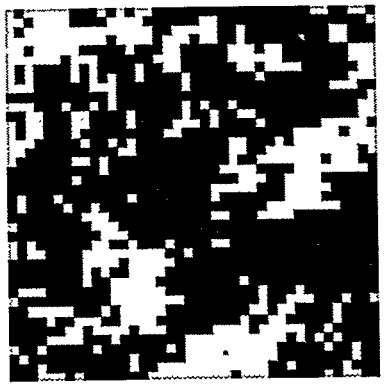

Real. # 2

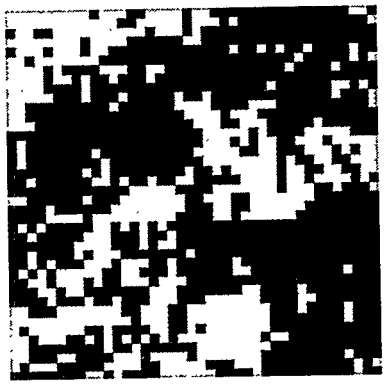

Real. # 3

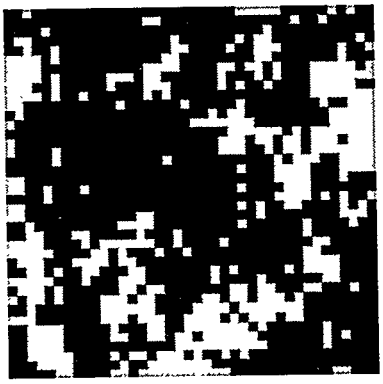

Real. # 4

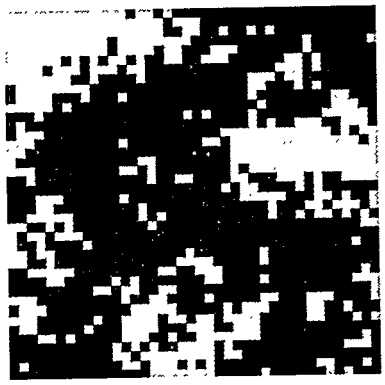

Real. # 5

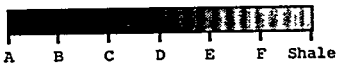

Figure 40

Horizontal DGI Cross Section At 25 Ft. Below Marker For Different Realizations - Stochastic Model

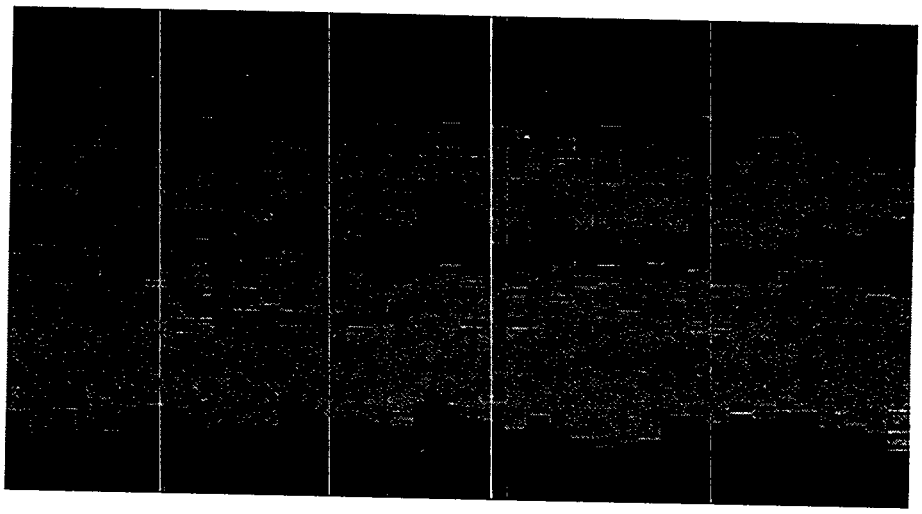

Real. No. 1

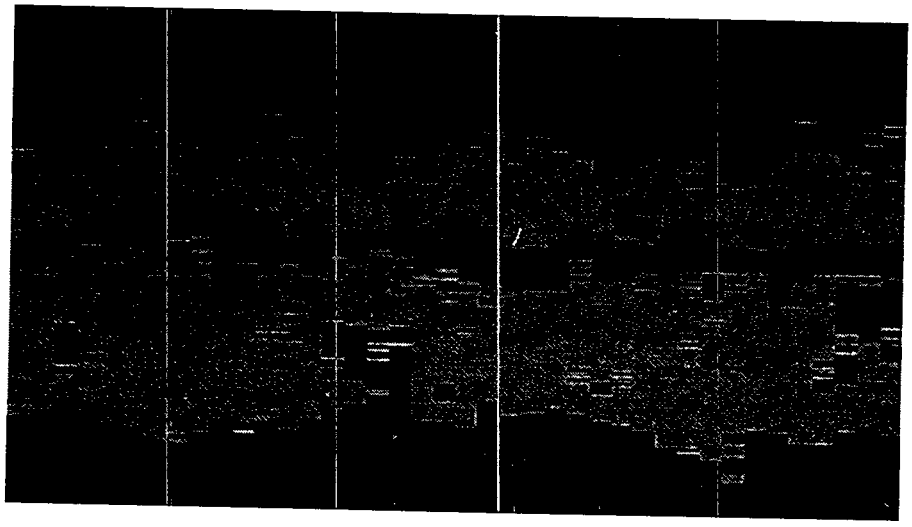

Real. No. 3

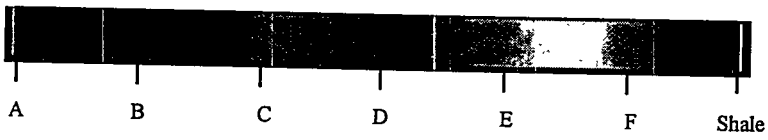

Figure 41

Simulated DGI Distribution - North-South Vertical Cross Section Stochastic Model

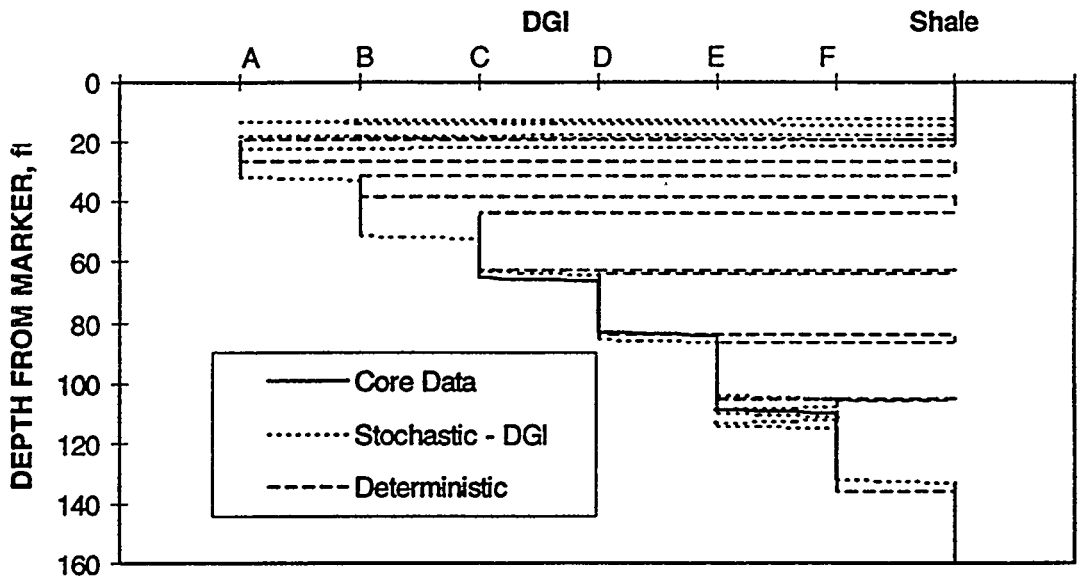

Figure 42.A

DGI Comparison At Well No. 43 - Stochastic Model

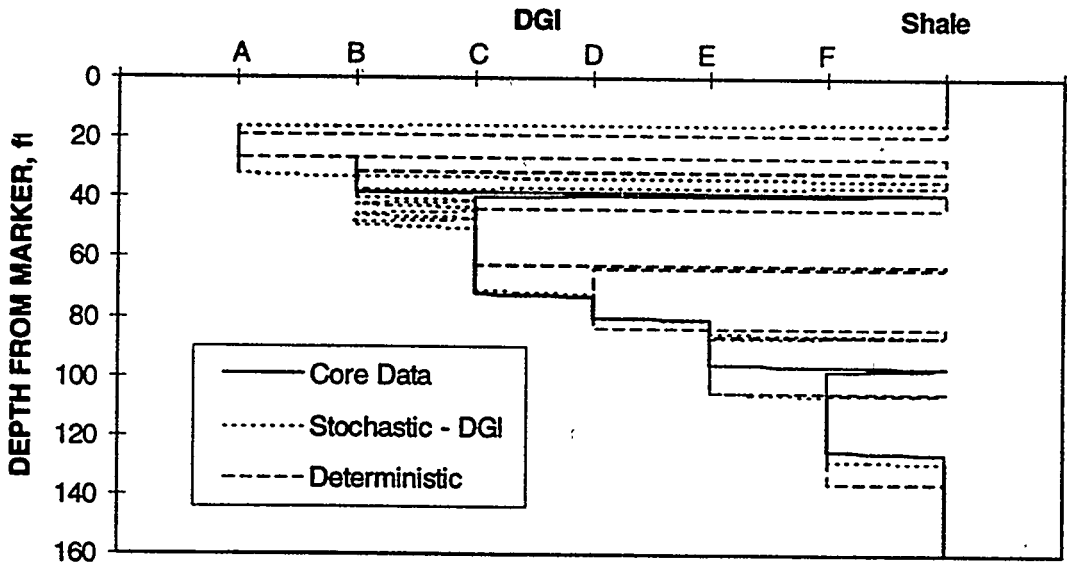

Figure 42.B

DGI Comparison At Well No. 37 - Stochastic Model

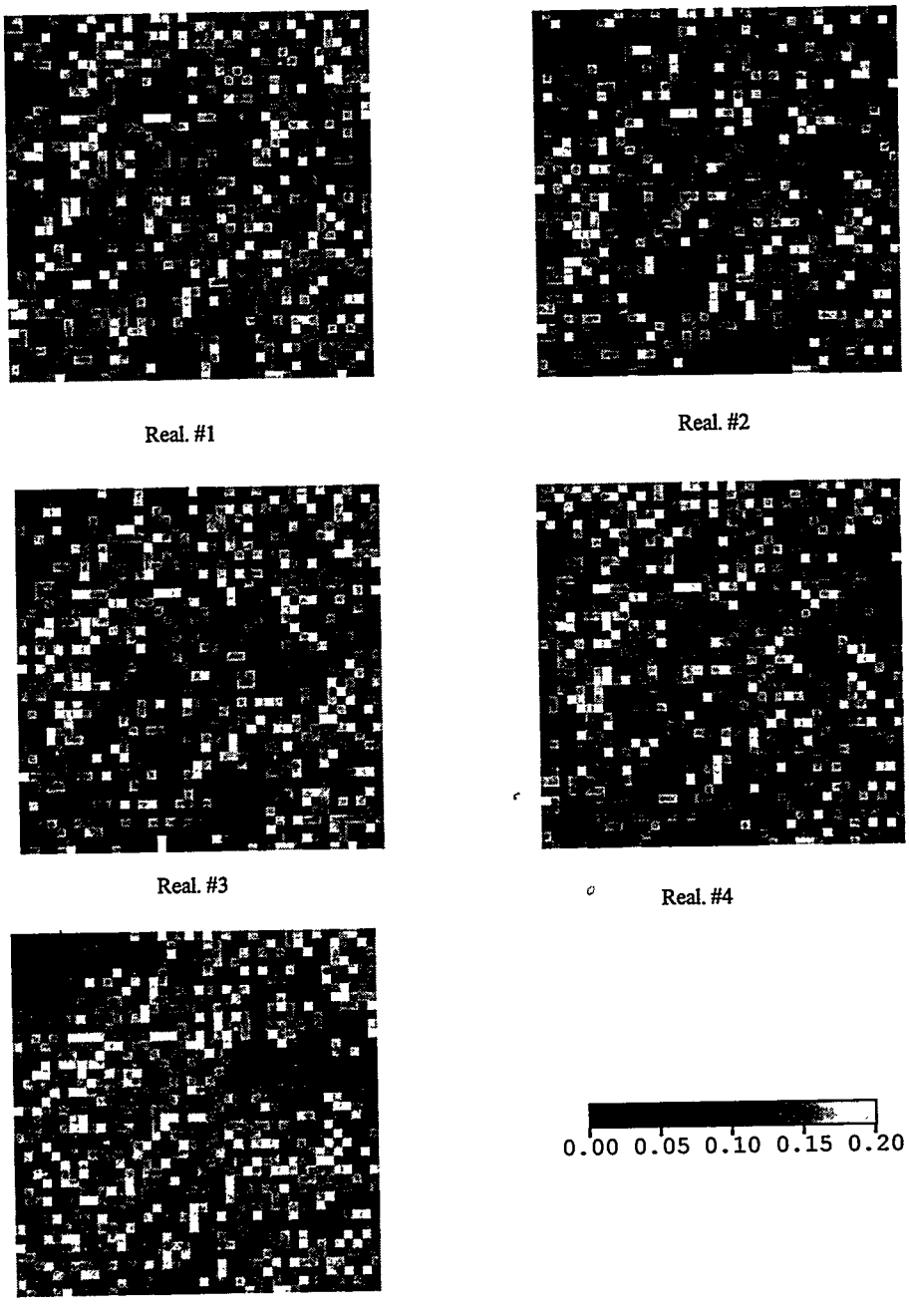

Figure 43

Porosity Distribution - Horizontal Cross Section At 25 Ft. Below Marker For 5 Different Realizations - Stochastic Model

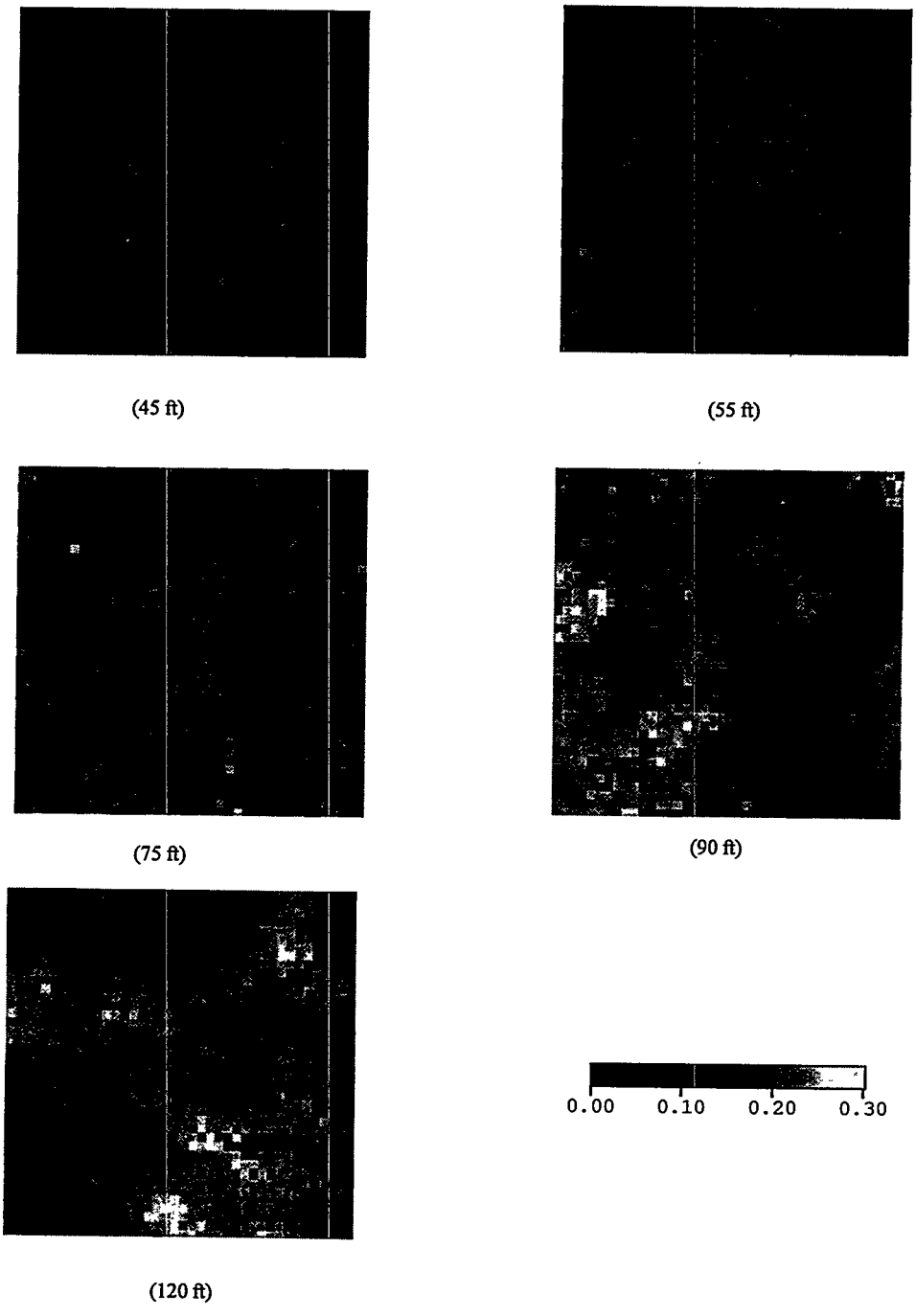

Figure 44

Porosity Distribution - Horizontal Cross Section At Several Depth Below Marker - Stochastic Model

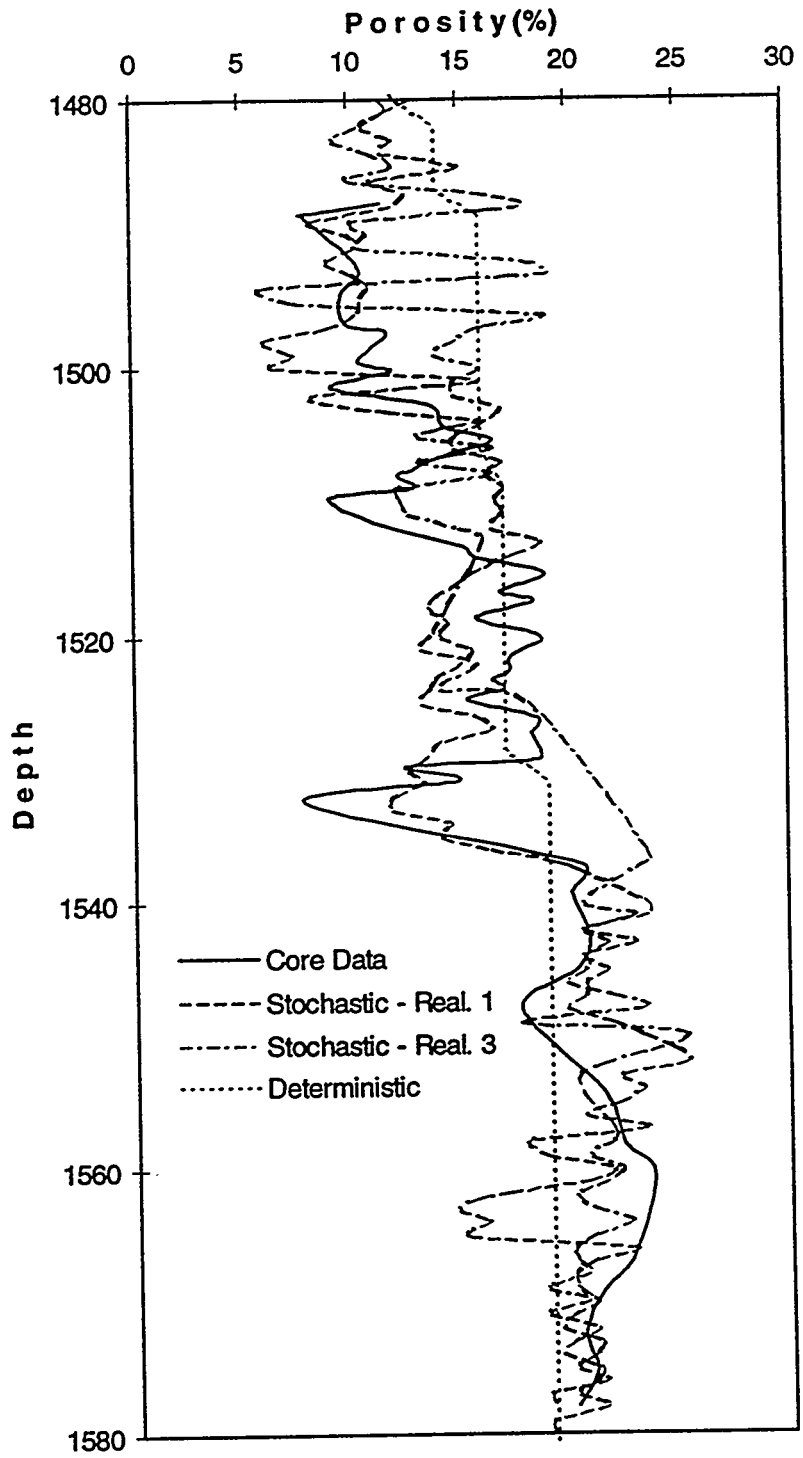

Figure 45

Porosity Comparison At Self Well No. 82 - Stochastic Model

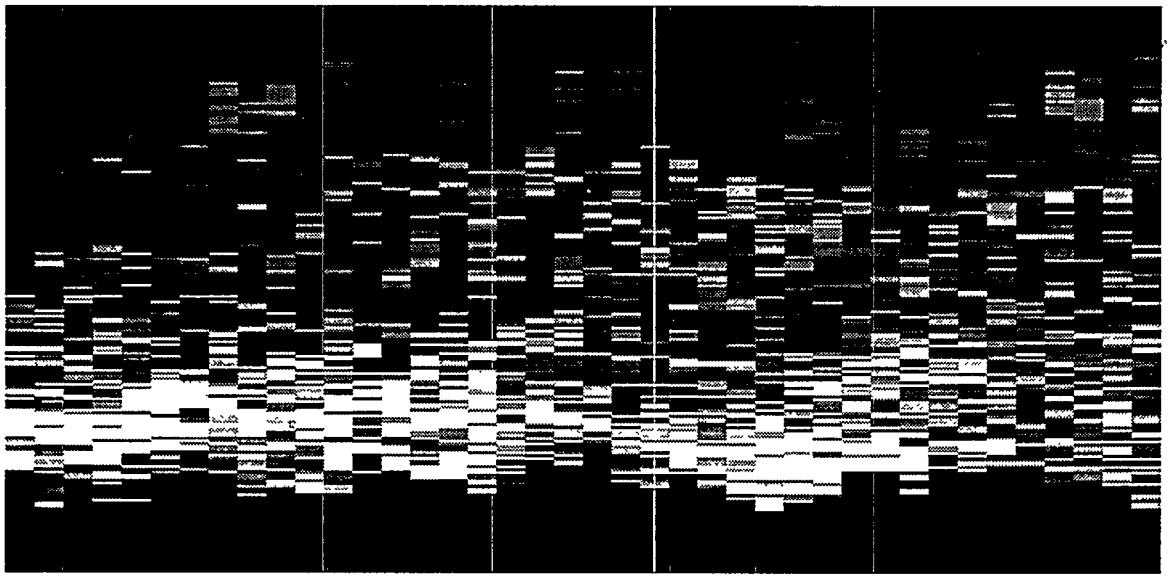

Realization No. 1

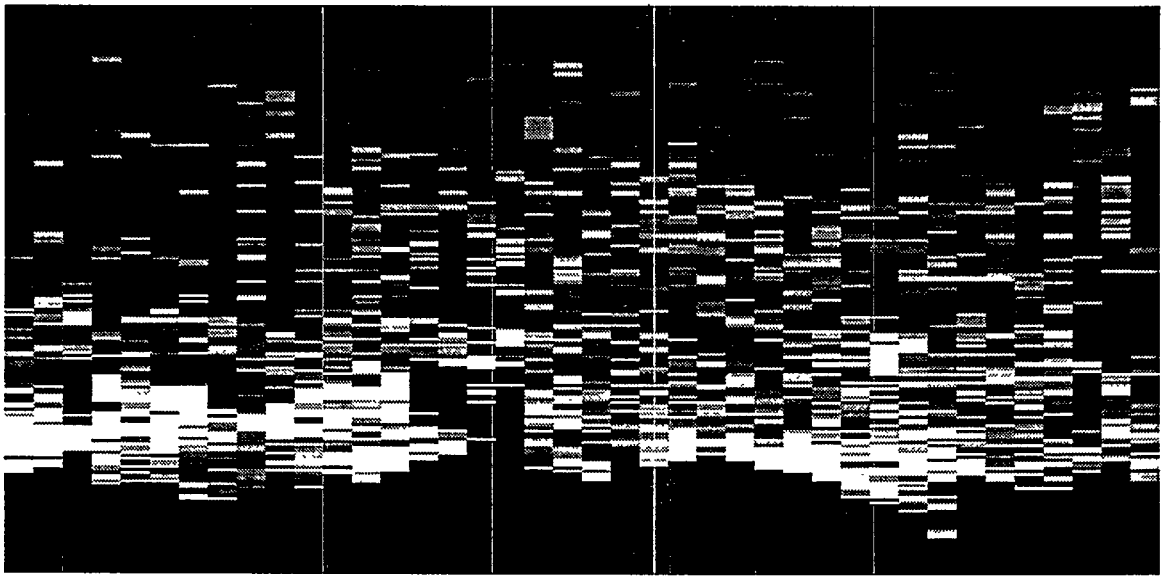

Realization No. 3

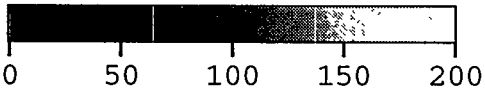

Figure 46

Permeability Distribution - North-South Cross Section - Stochastic Model

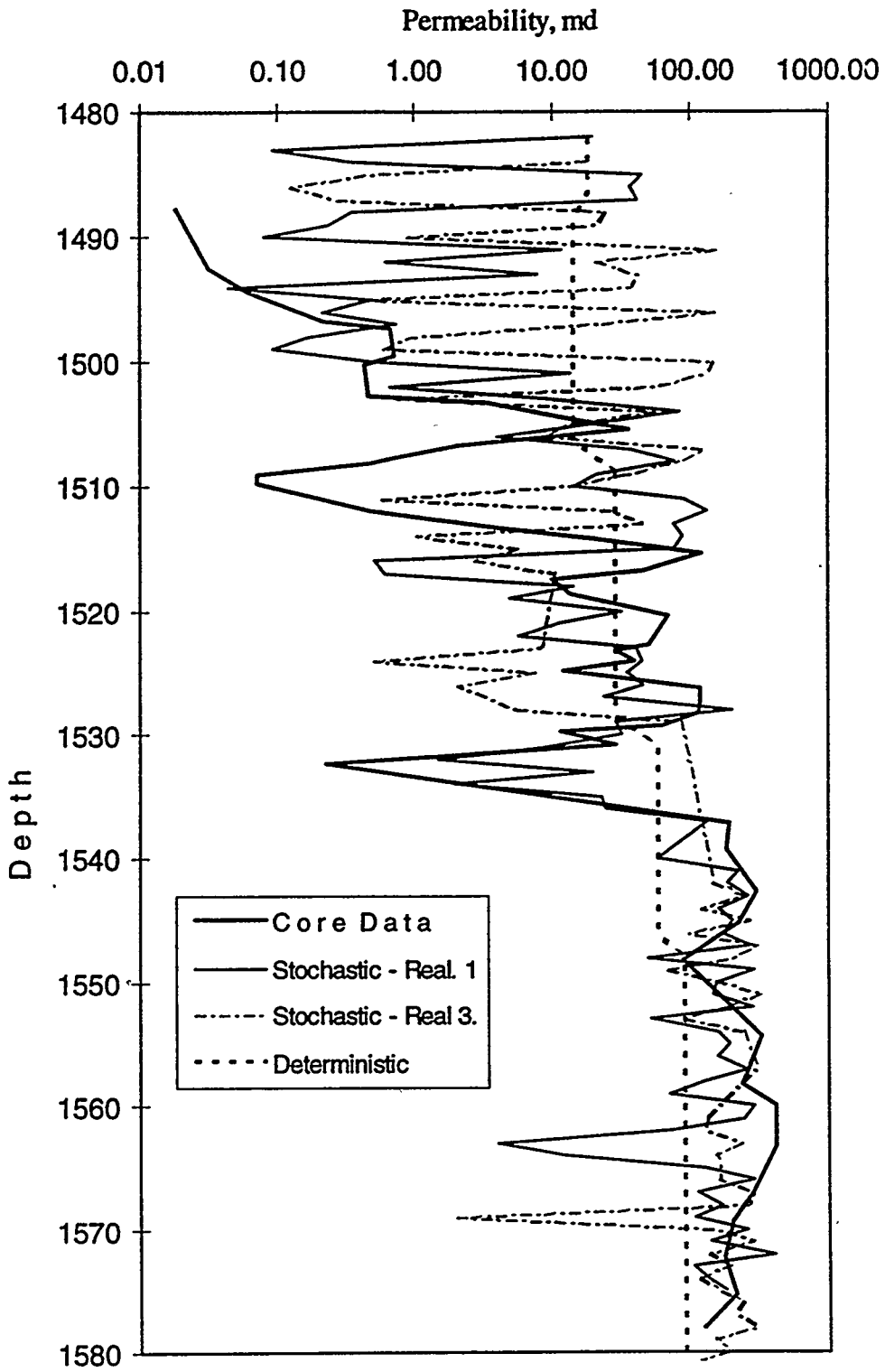

Figure 47

Permeability Comparison At Self Well No. 82 - Stochastic Model

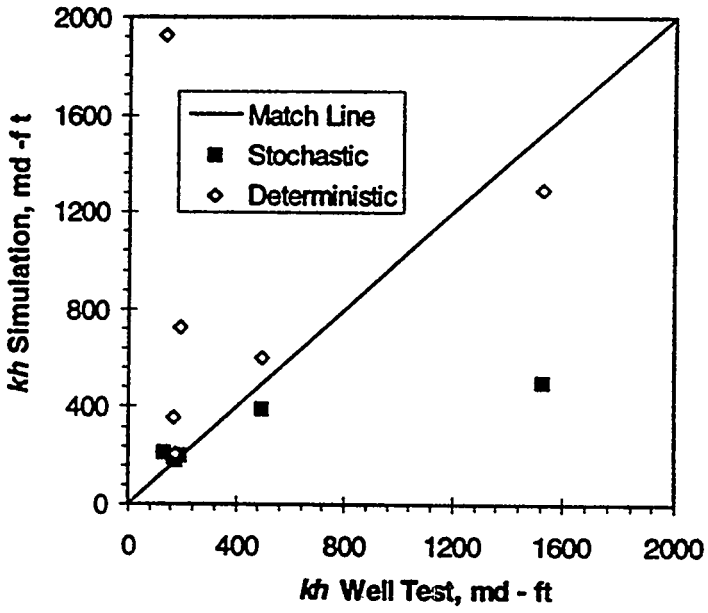

Figure 48
Permeability - Thickness (kh) Comparison - Stochastic Model

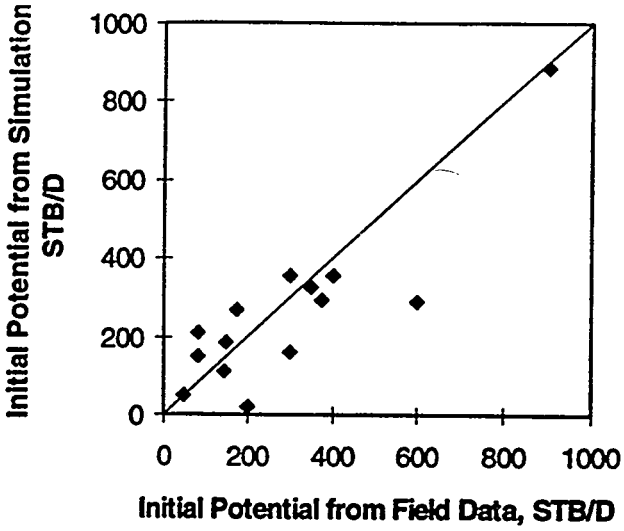

Figure 49

Initial Potential Comparison - Stochastic Model

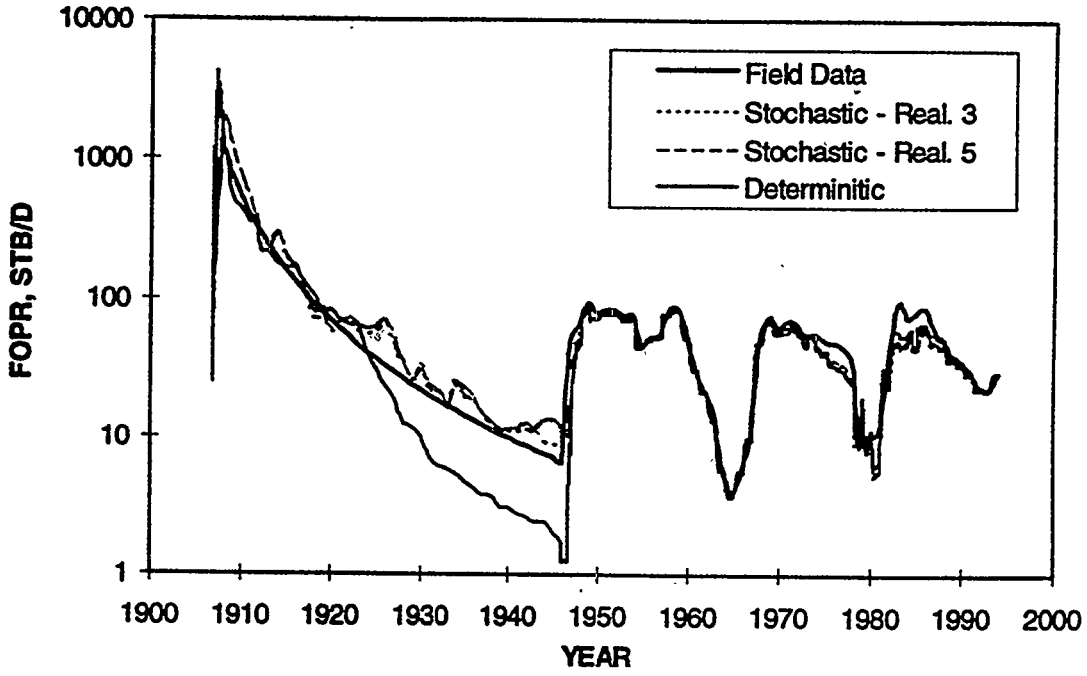

Figure 50

Field Oil Production Rate Comparison - Stochastic Model

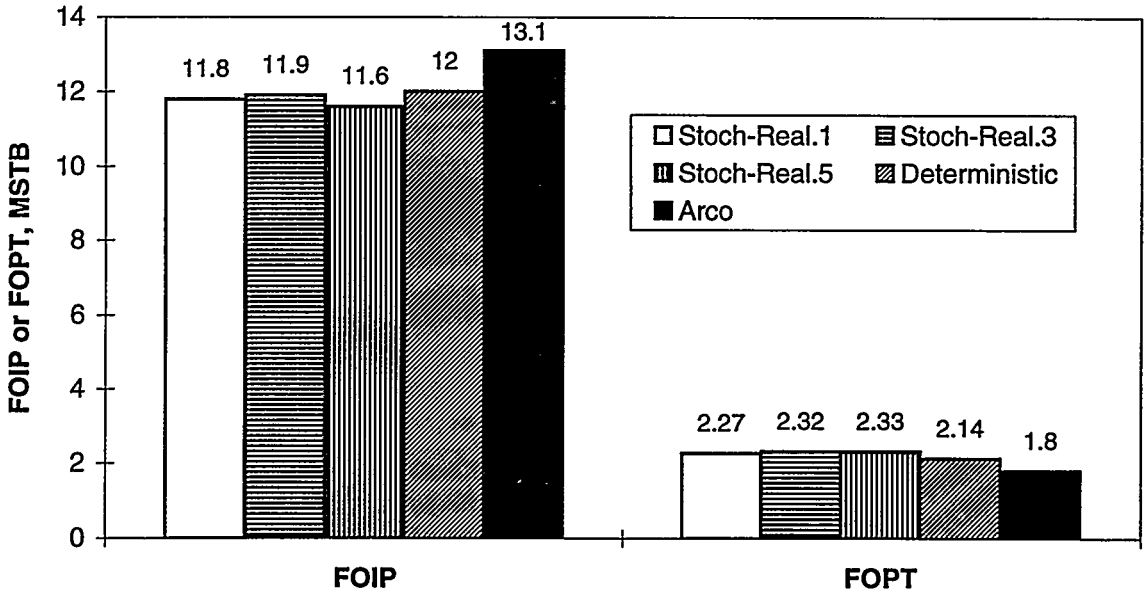

Figure 51

Original Oil In Place (FOIP) and Cumulative Oil Production (FOPT) At 1946 Comparison - Stochastic And Deterministic Models

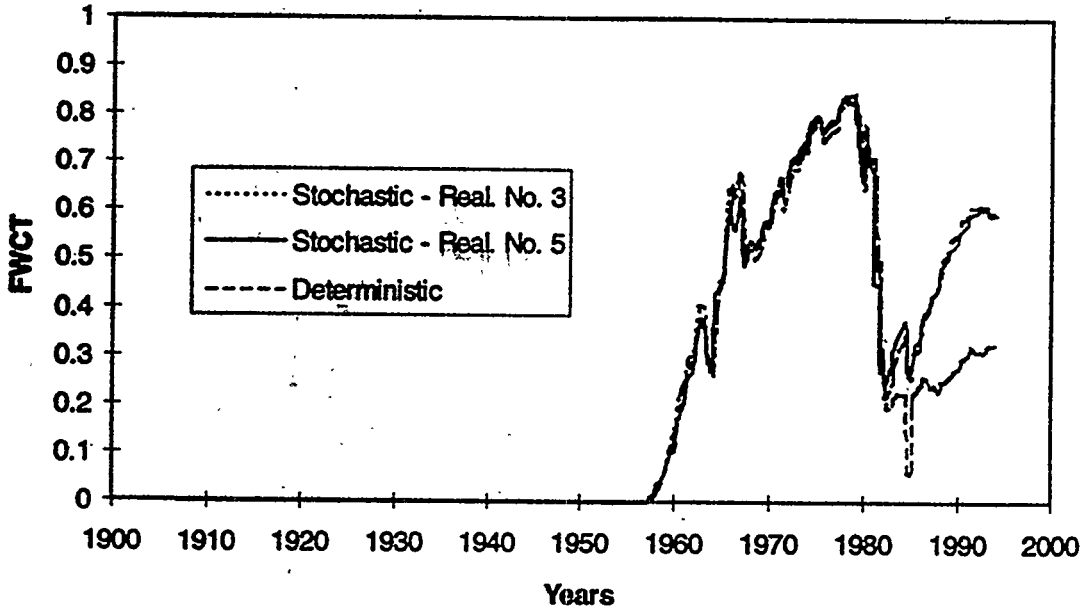

Figure 52

Field Water Cut Prediction For Stochastic And Deterministic Models

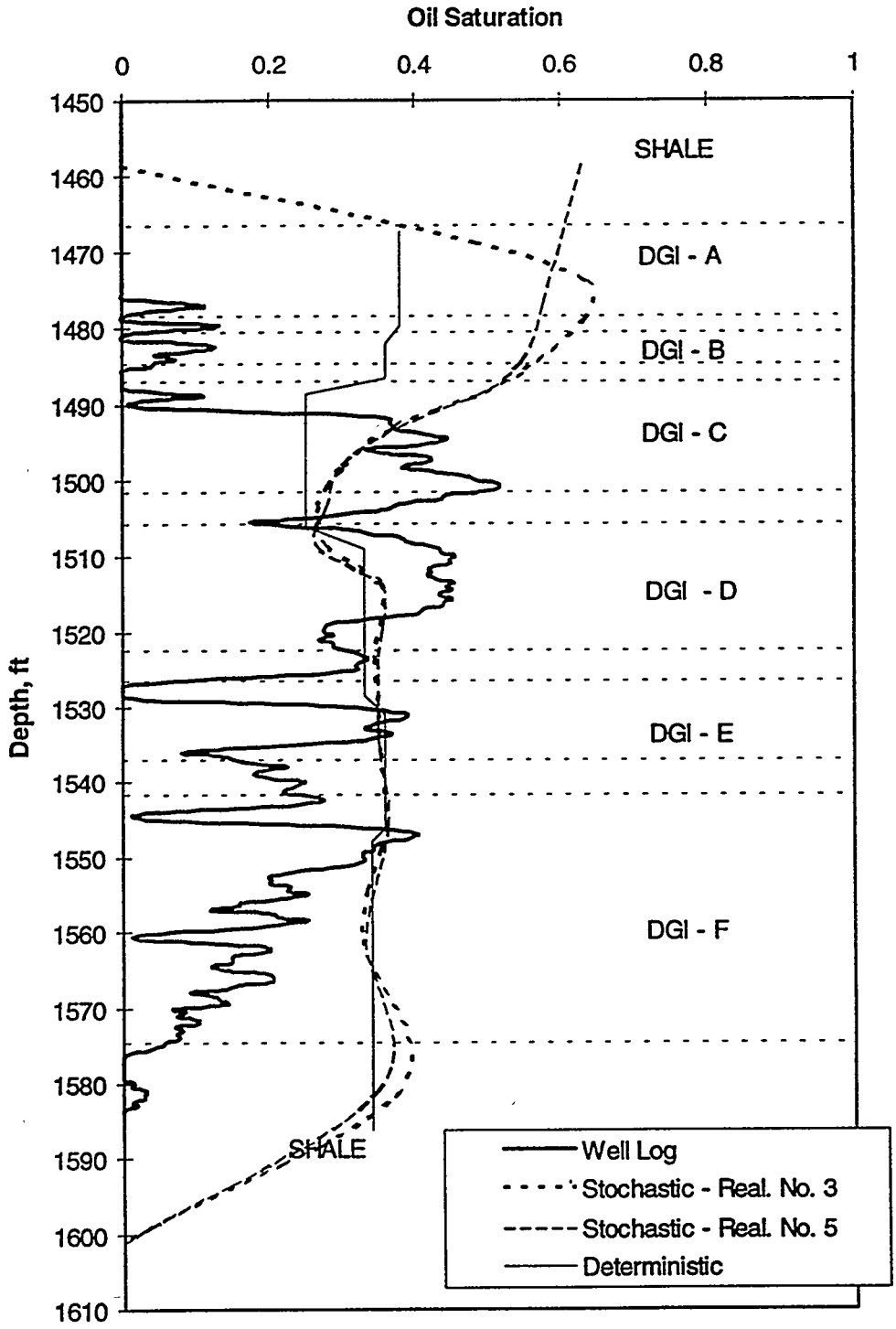

Figure 53

Oil Saturation Comparison At Self Well No. 82 - Stochastic And Deterministic Model

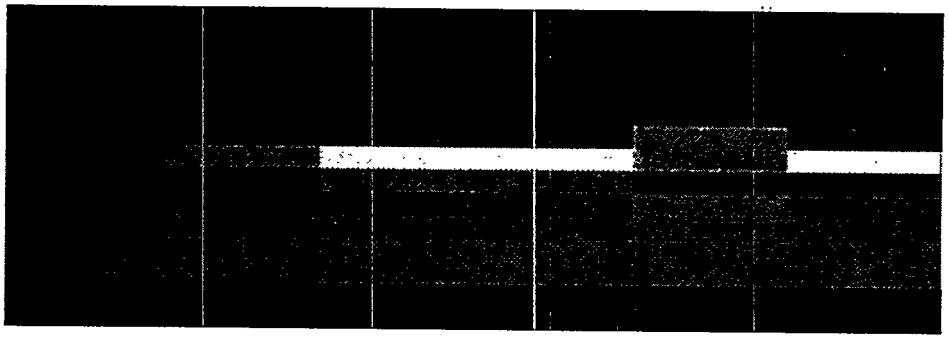

(A) Well 63 - 82

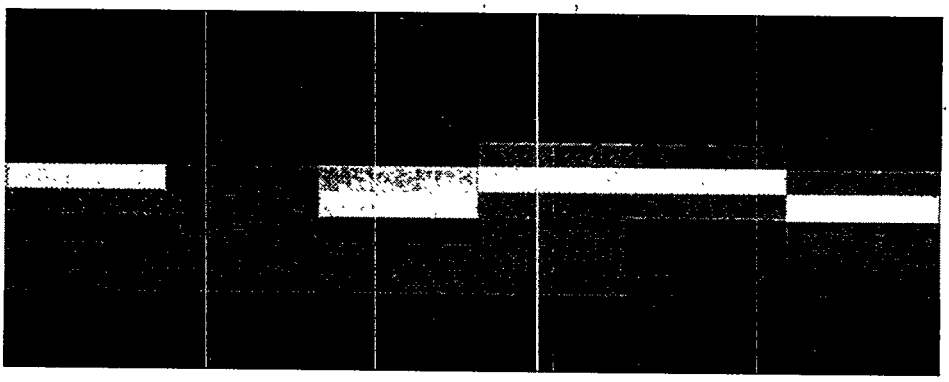

(B) Well 82 - 64

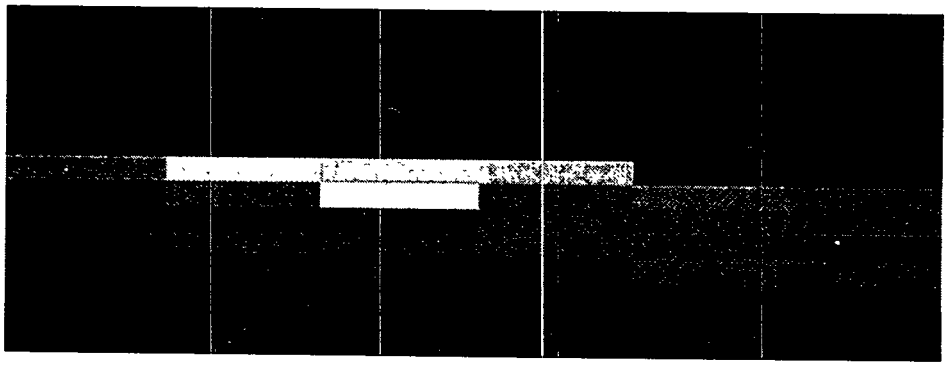

(c) Well 82 - 64

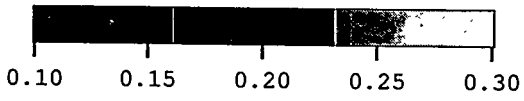

Figure 54

Porosity Distribution At The Tomogram Panels After Applying Correlations

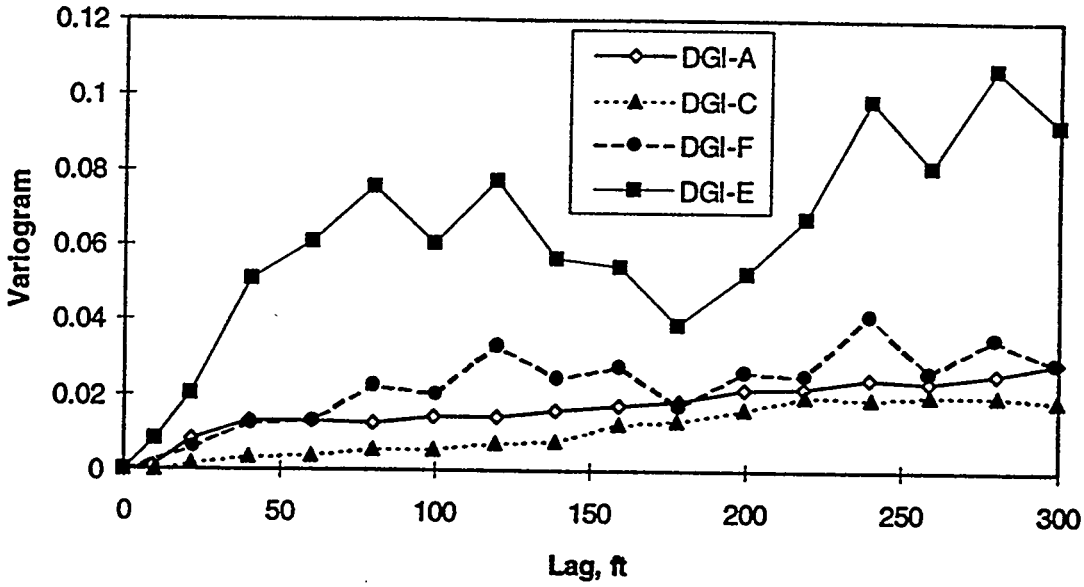

Figure 55.A

Horizontal Porosity Variogram Of The Tomogram Data (DGIs A, C, E, F)

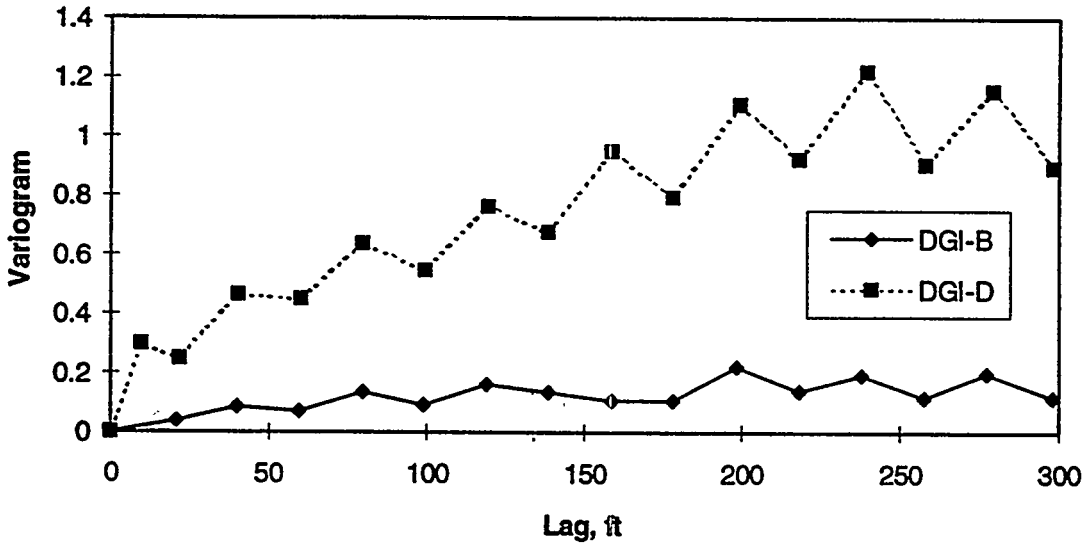

Figure 55.B
Horizontal Porosity Variogram Of The Tomogram Data (DGIs B And D)

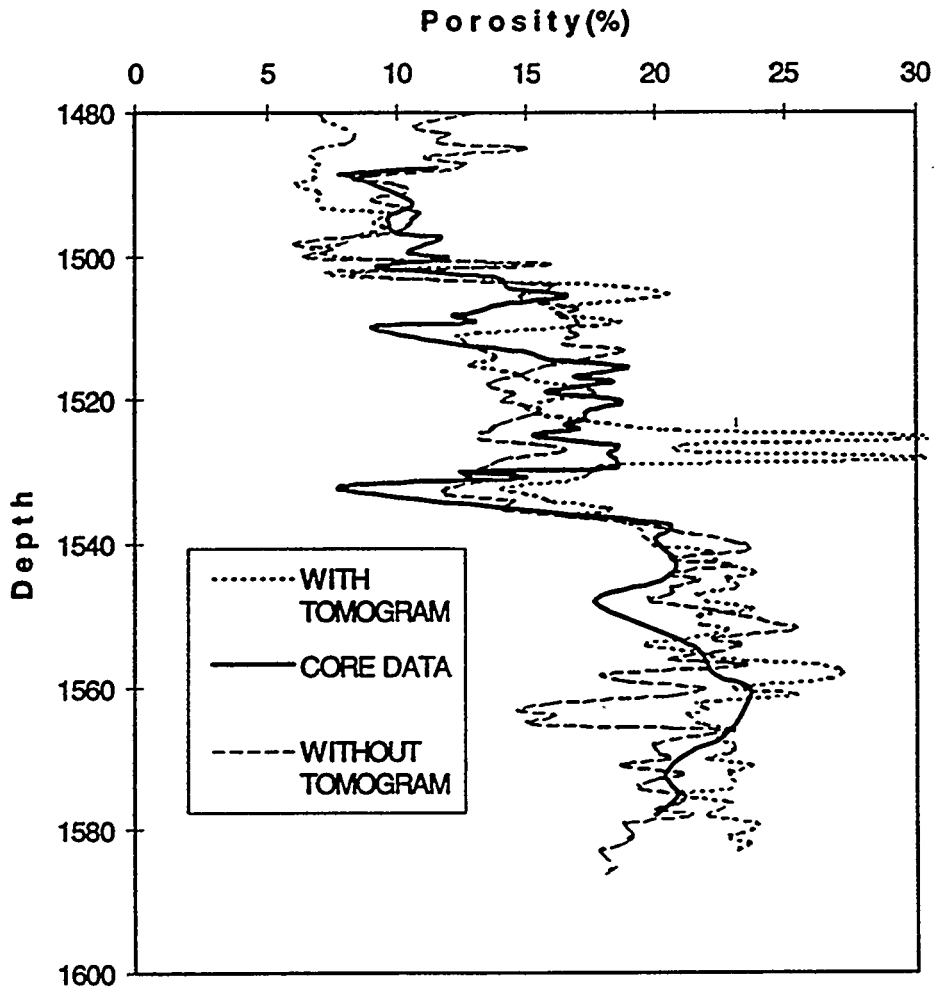

Figure 56

Porosity Comparison At Self Well No. 82

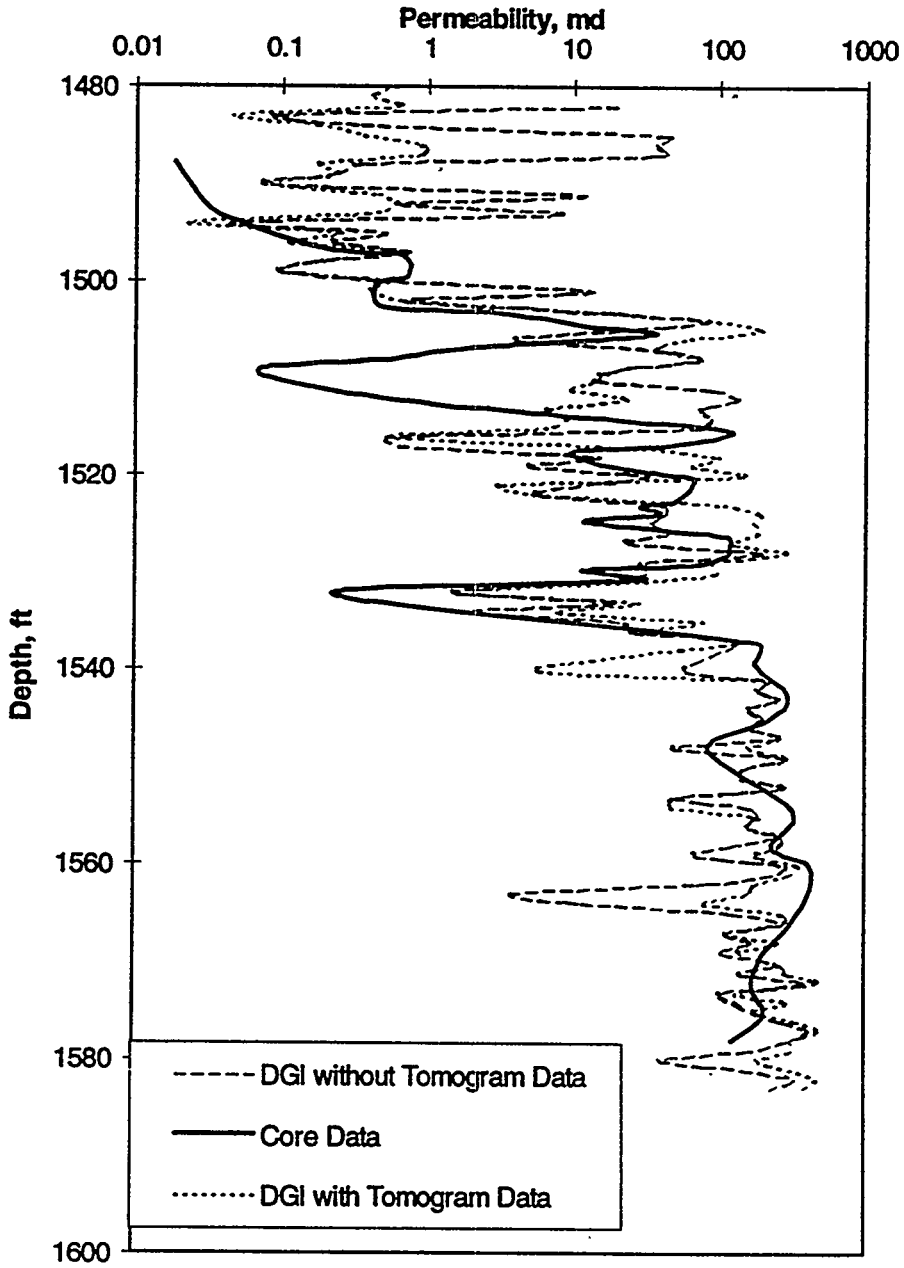

Figure 57
Permeability Comparison at Self Well No. 82

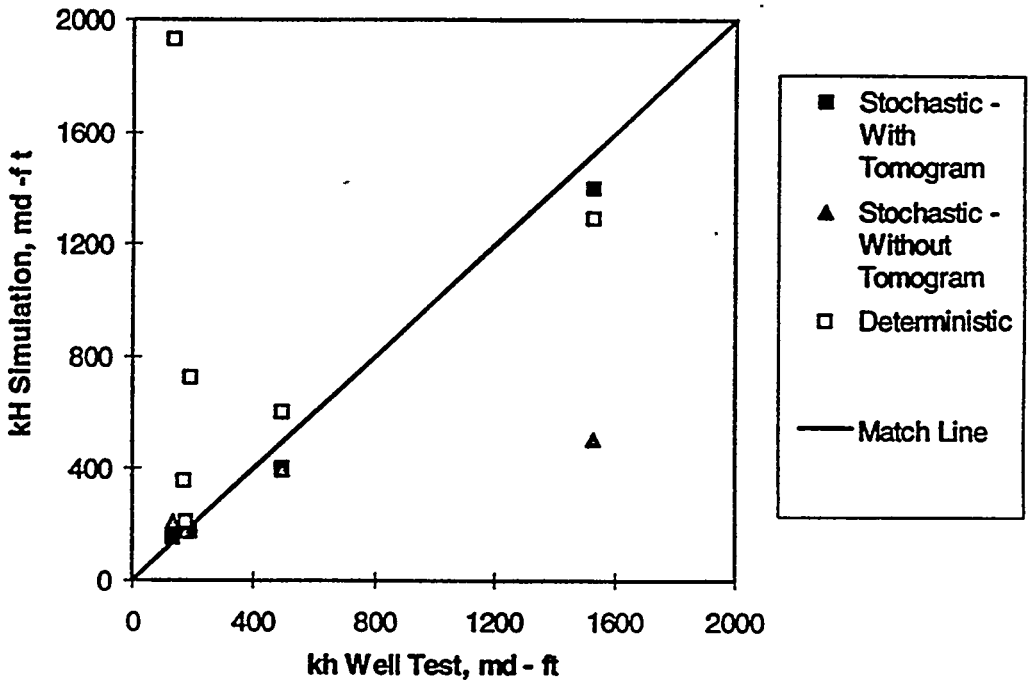

Figure 58
Permeability - Thickness (kh) Production Comparison - All Models

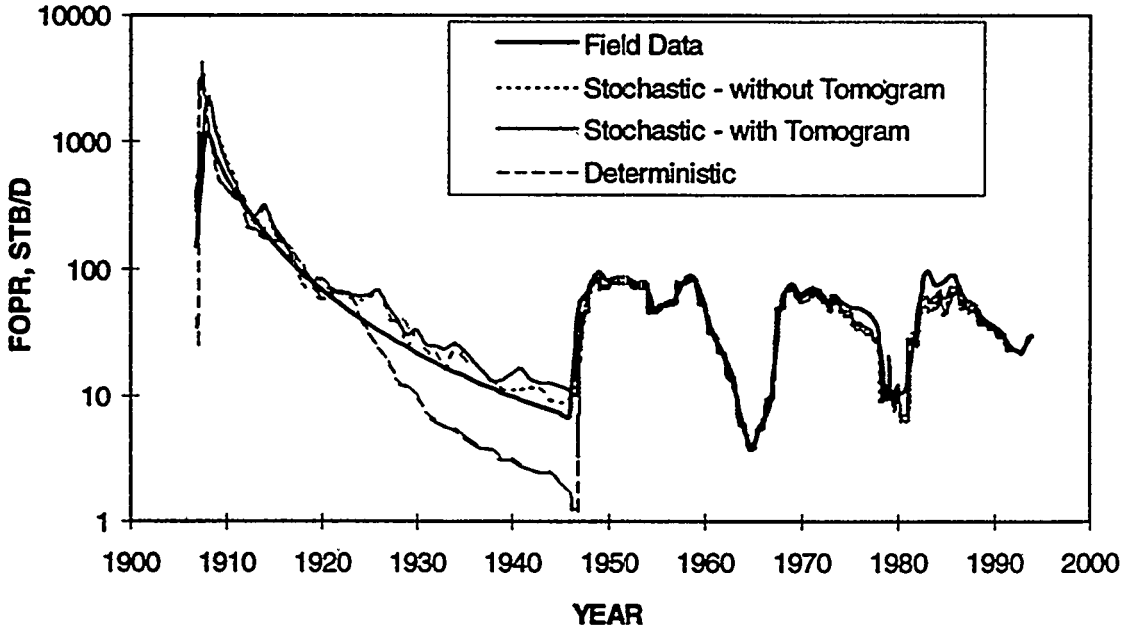

Figure 59

Comparison Of Field Oil Production Rate (FORP) - All Models

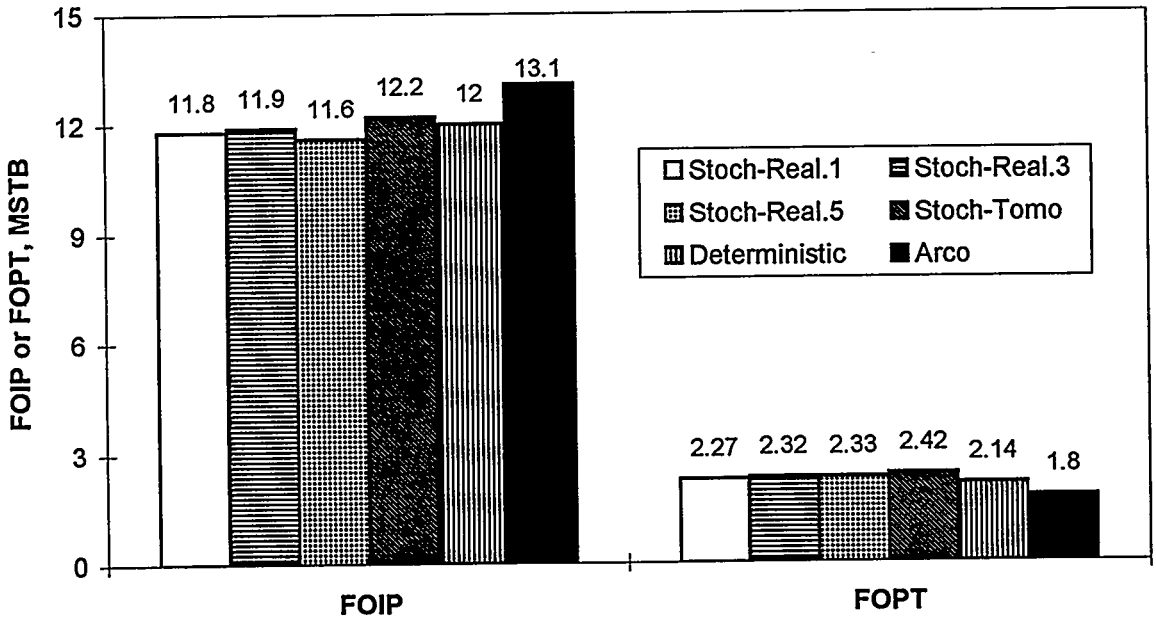

Figure 60

Comparison Of Original Oil Production Rate (FOIP) And Cumulative Production At 1946 For Different Models

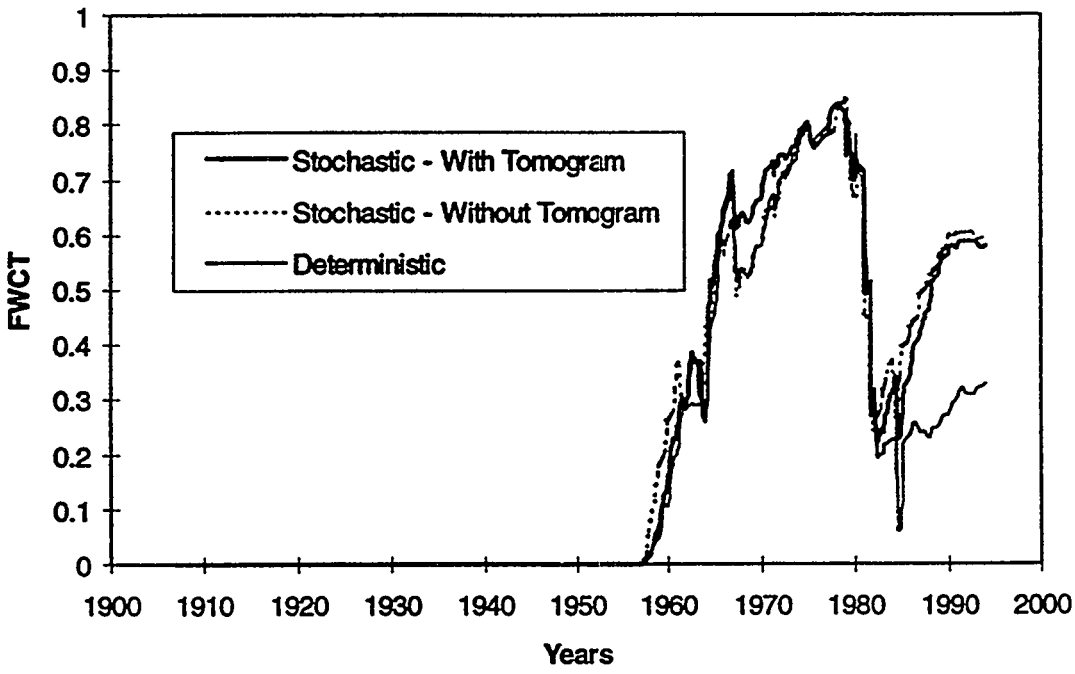

Figure 61

Comparison Of Field Water Cut - All Models

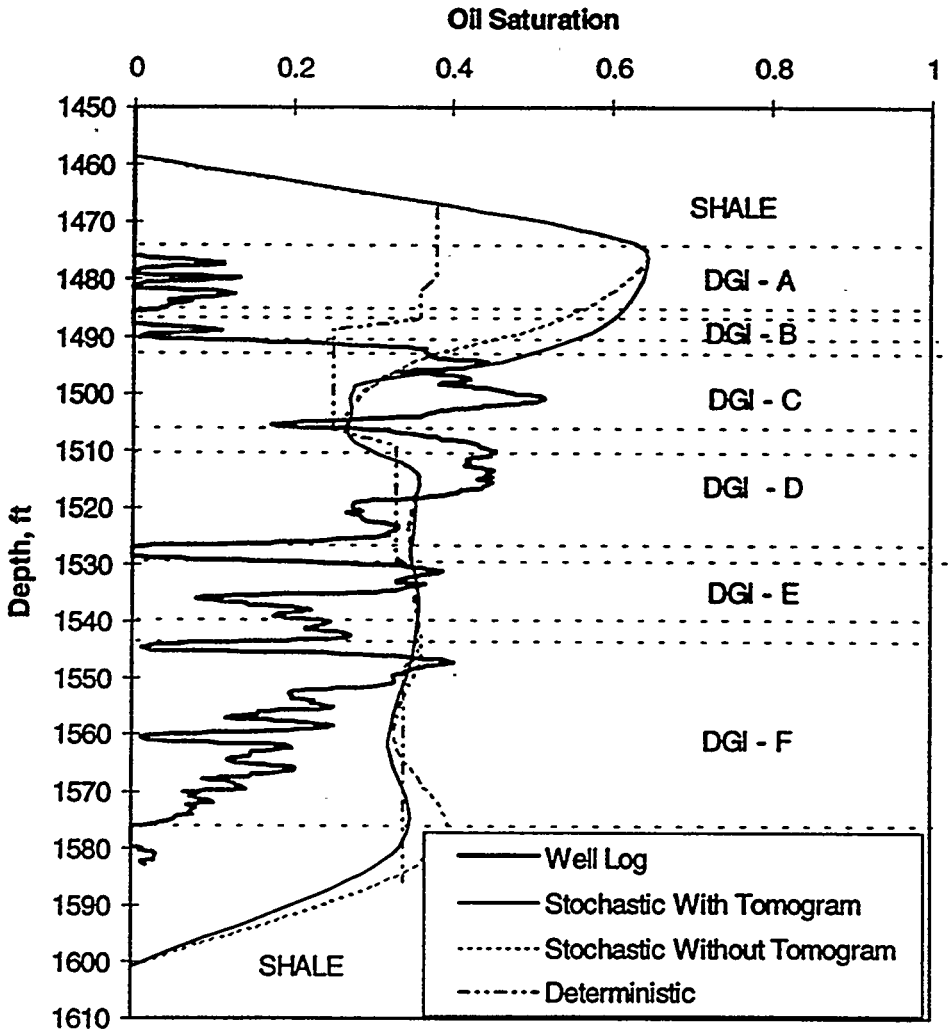

Figure 62

Comparison Of Oil Saturation At Self Well No. 82 - All Models

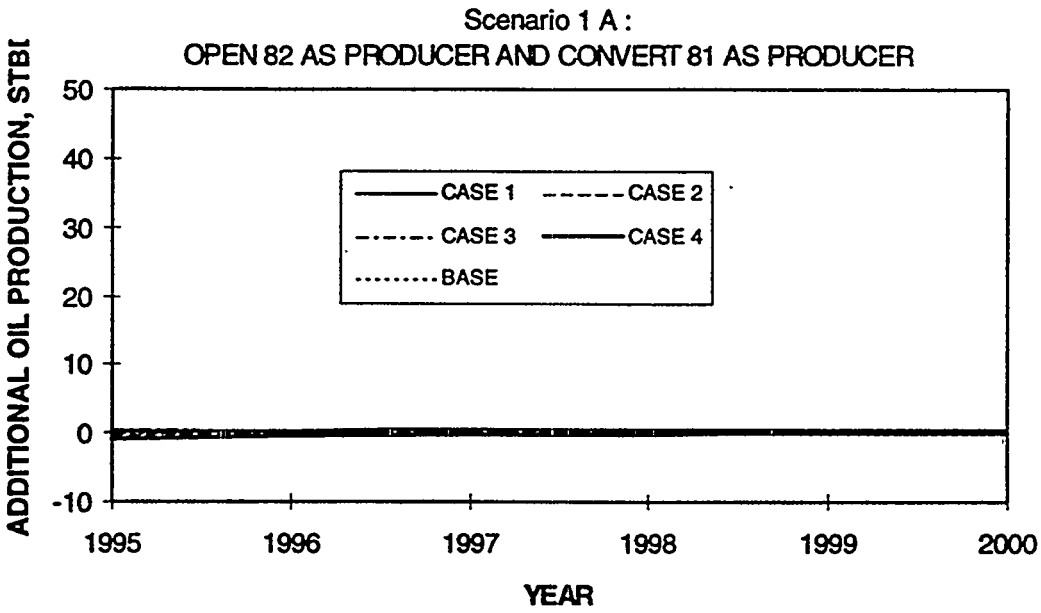

Figure 63.A

Increase Of Oil Production Using Scenario 1A

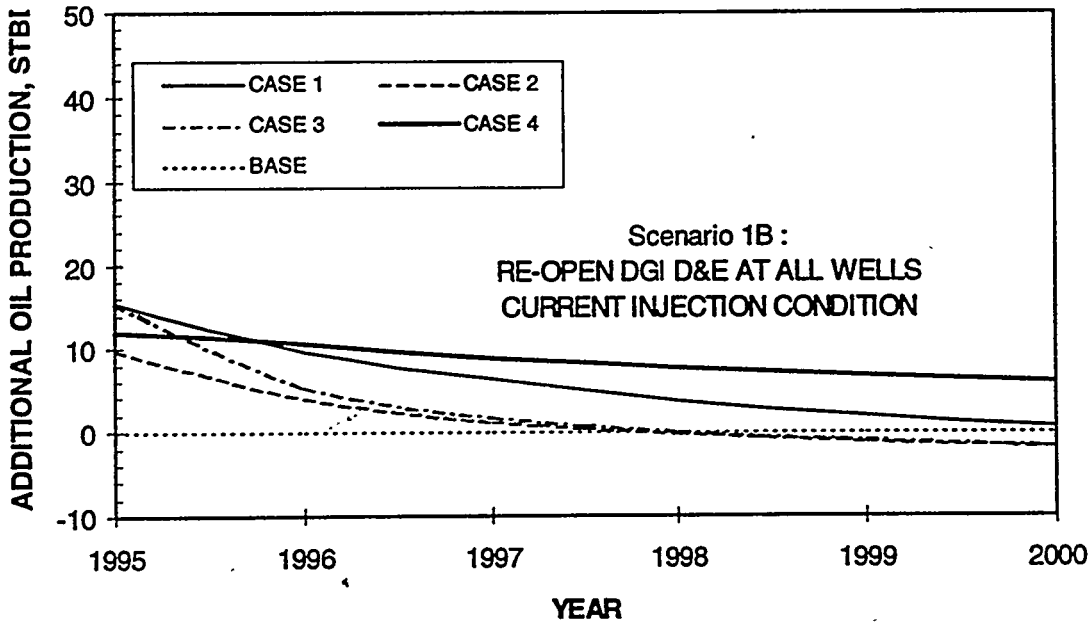

Figure 63.B

Increase Of Oil Production Using Scenario 1B

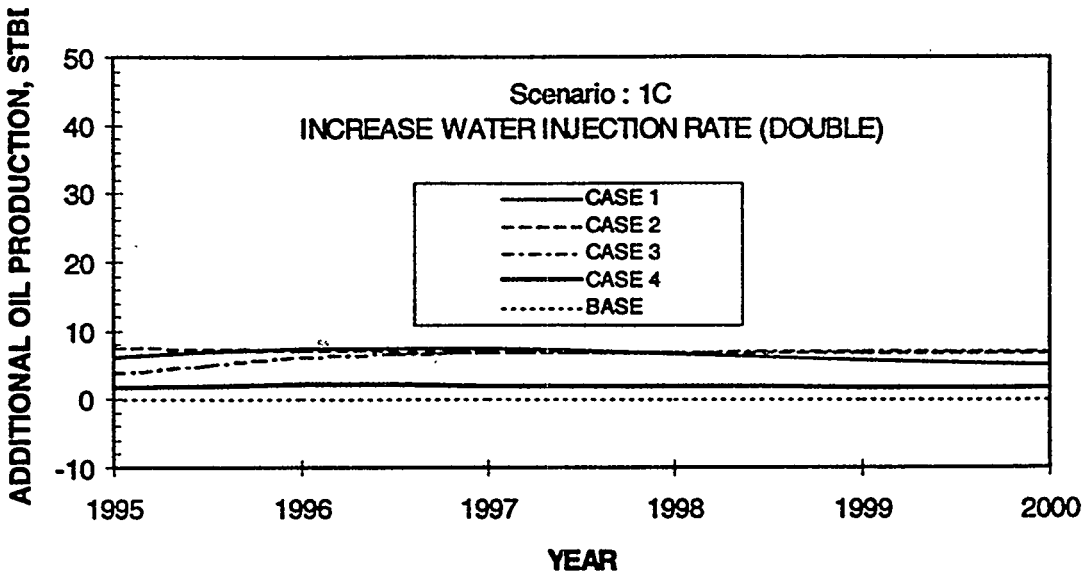

Figure 63.C
Increase Of Oil Production Using Scenario 1C

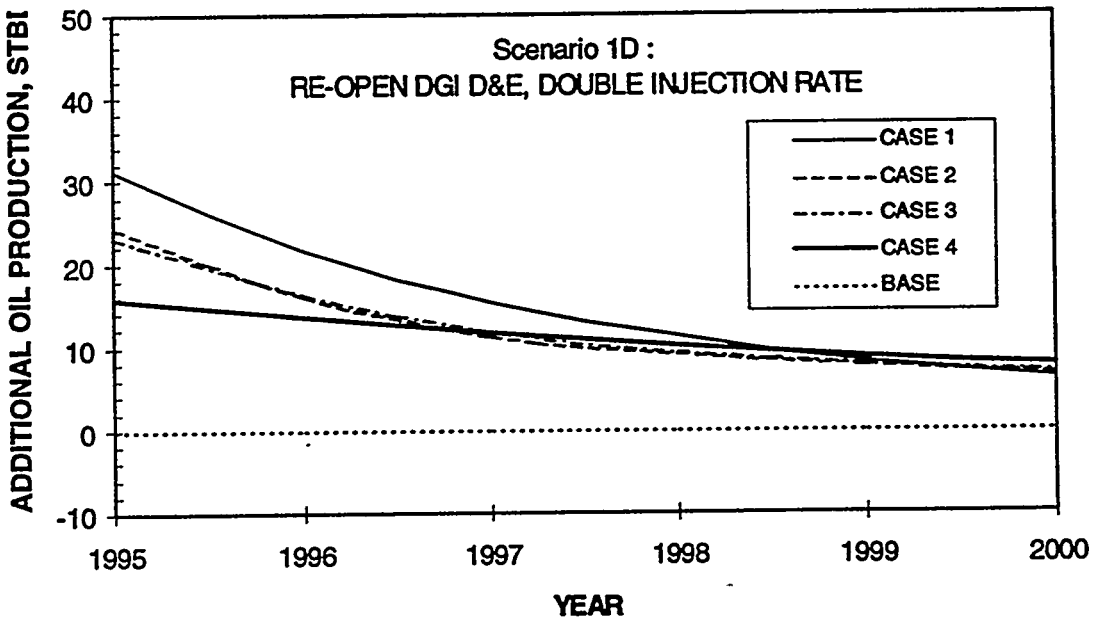

Figure 63.D

Increase Of Oil Production Using Scenario 1D

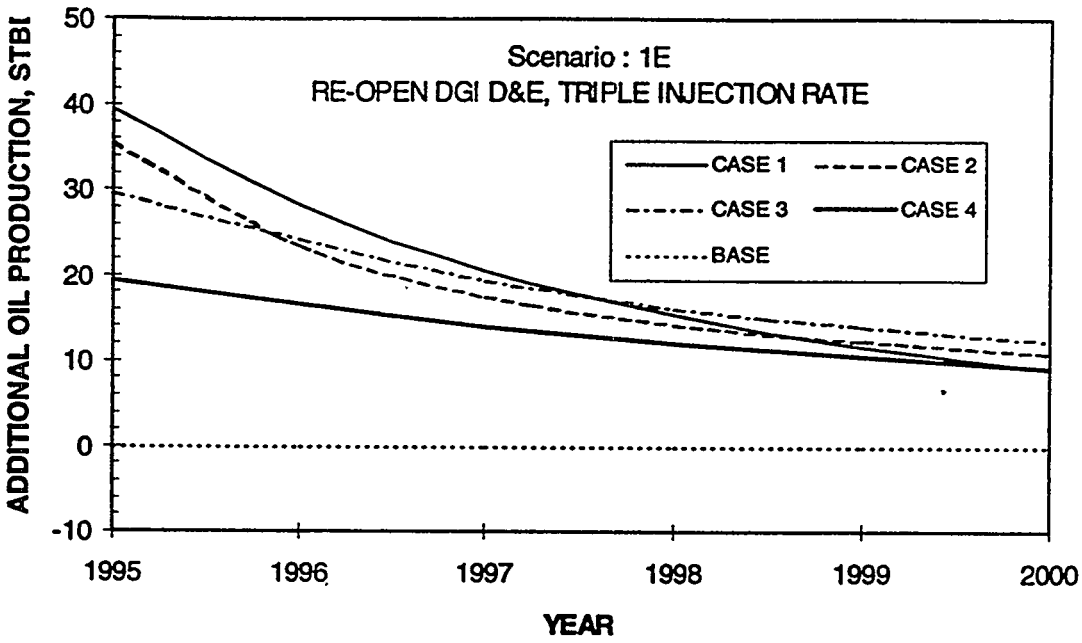

Figure 63.E

Increase Of Oil Production Using Scenario 1E

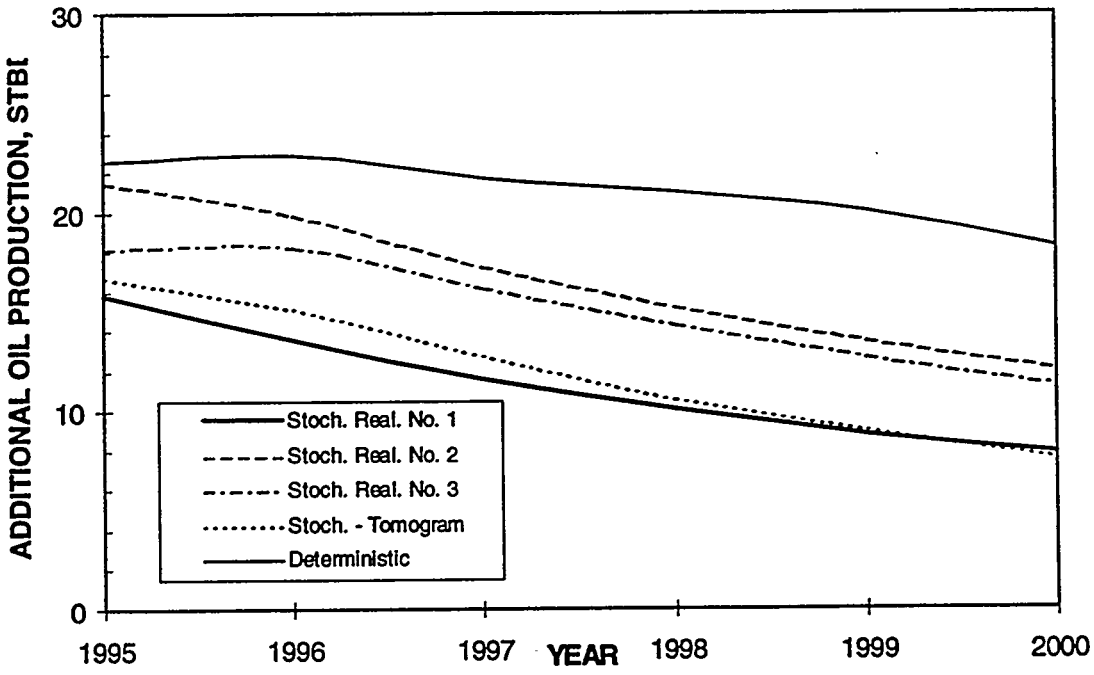

Figure 64

Comparison Of Additional Oil Production - All Models

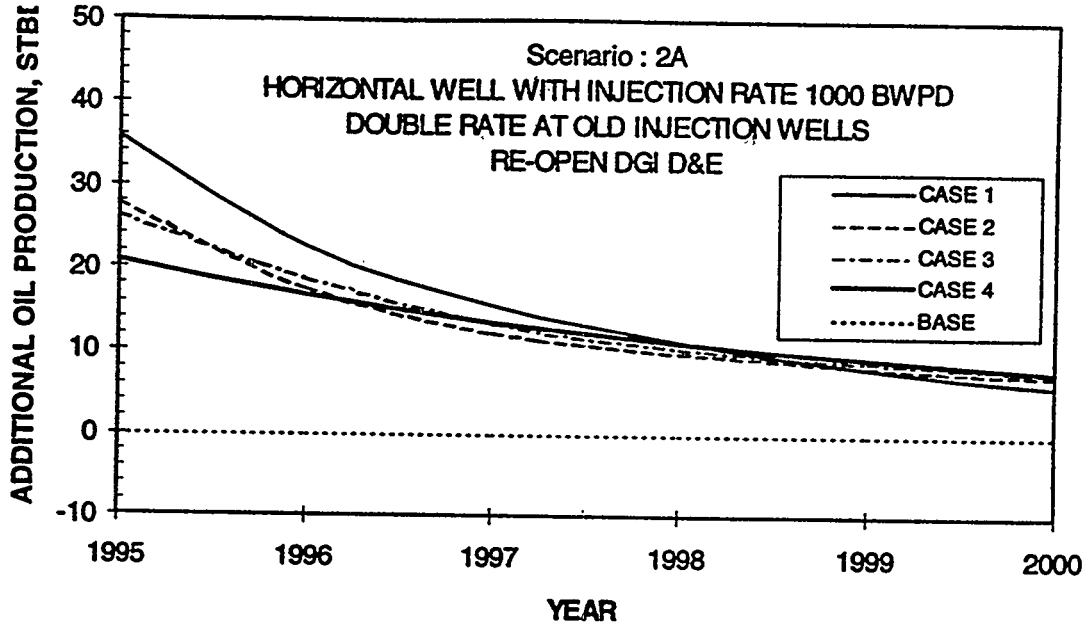

Figure 65.A

Increase Of Oil Production Using Scenario 2A

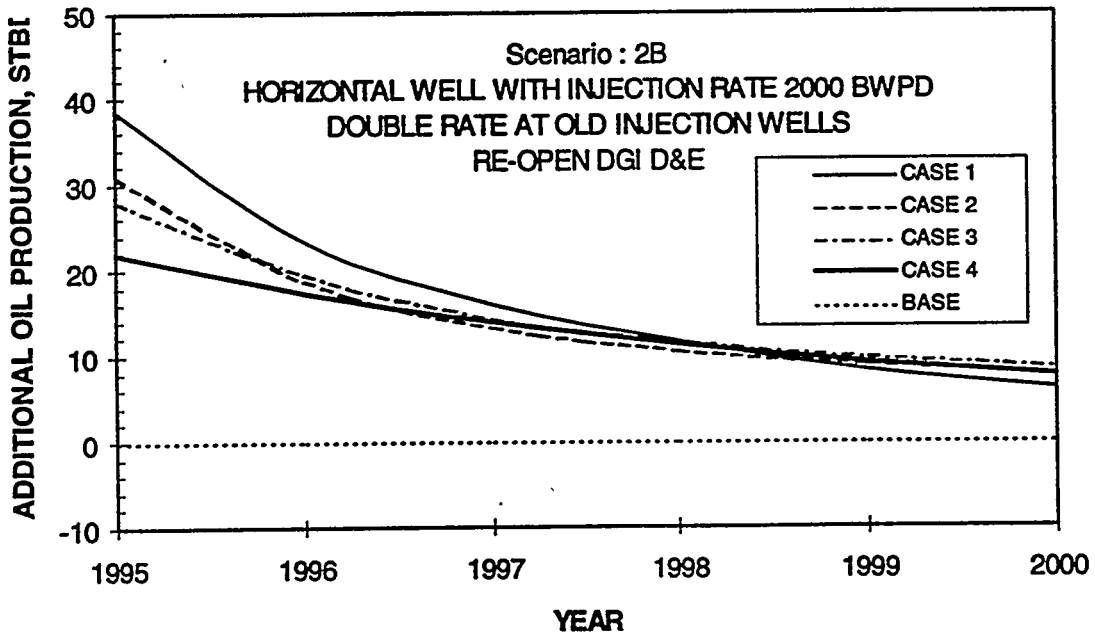

Figure 65.B

Increase Of Oil Production Using Scenario 2B

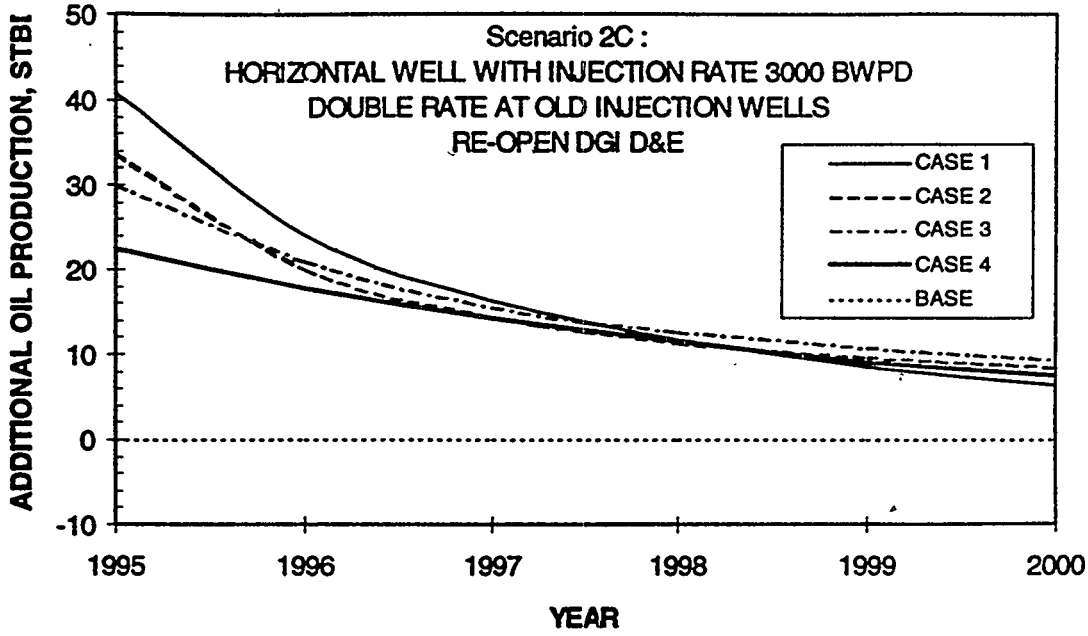

Figure 65.C
Increase Of Oil Production Using Scenario 2C

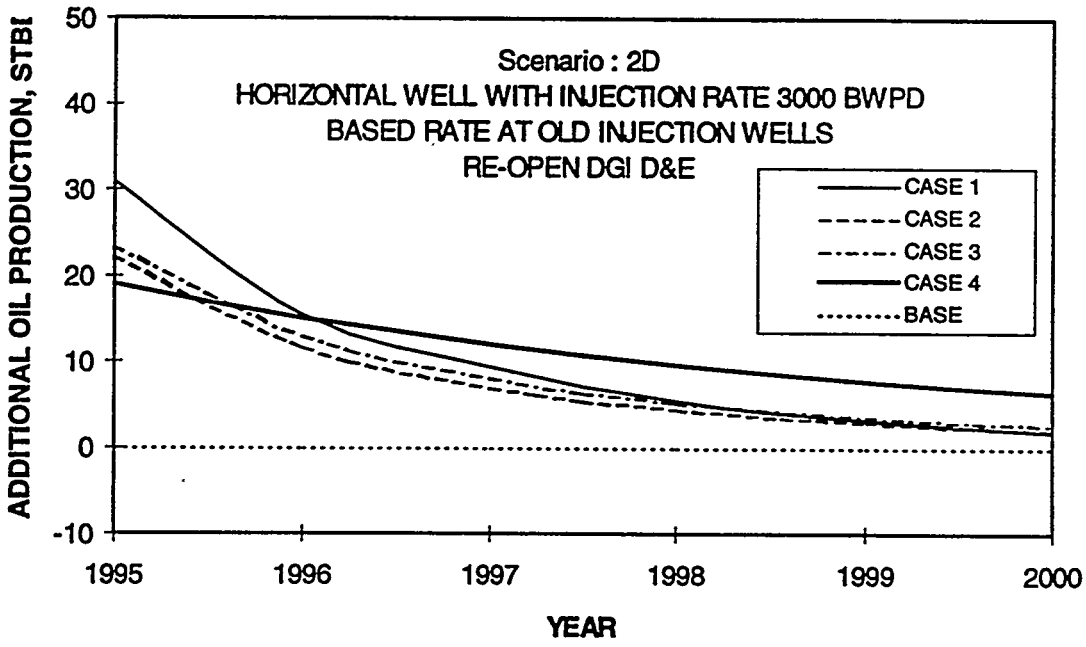

Figure 65.D

Increase Of Oil Production Using Scenario 2D

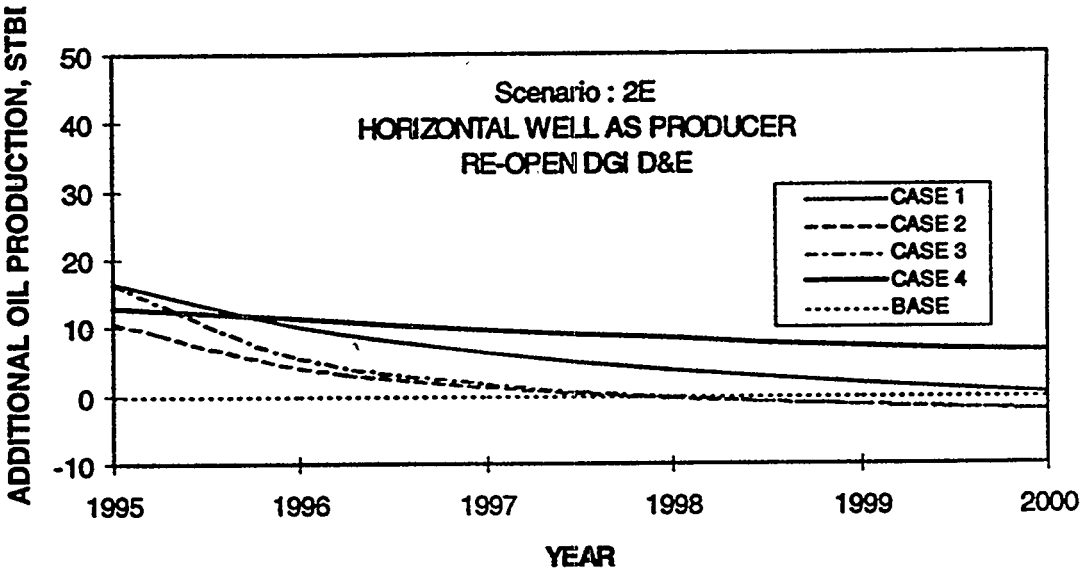

Figure 65.E

Increase Of Oil Production Using Scenario 2E

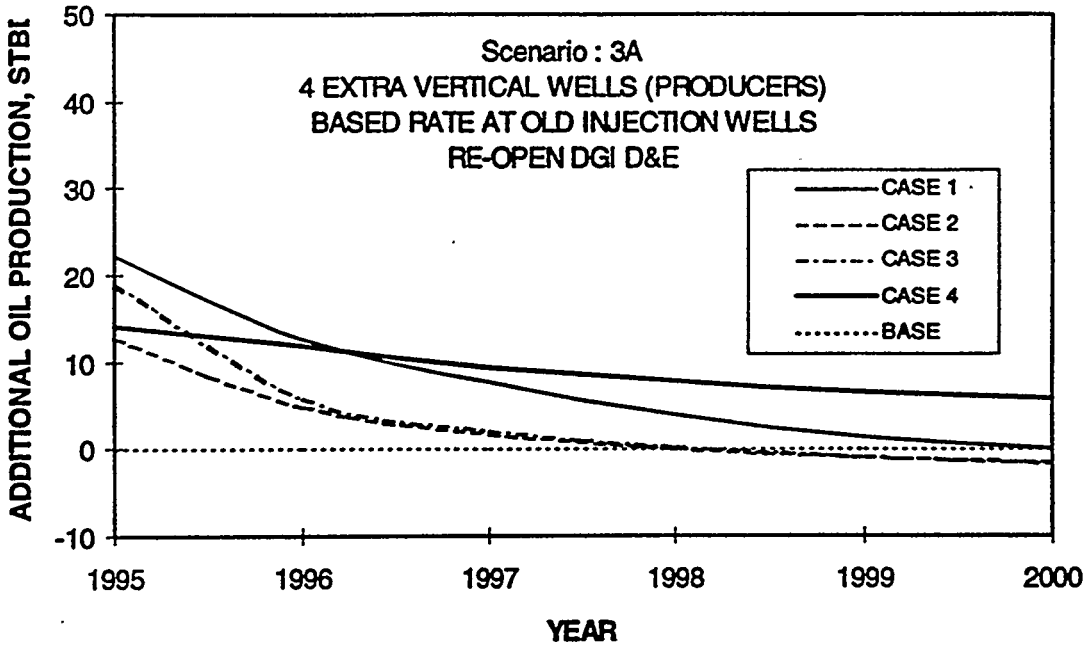

Figure 66.A

Increase Of Oil Production Using Scenario 3A

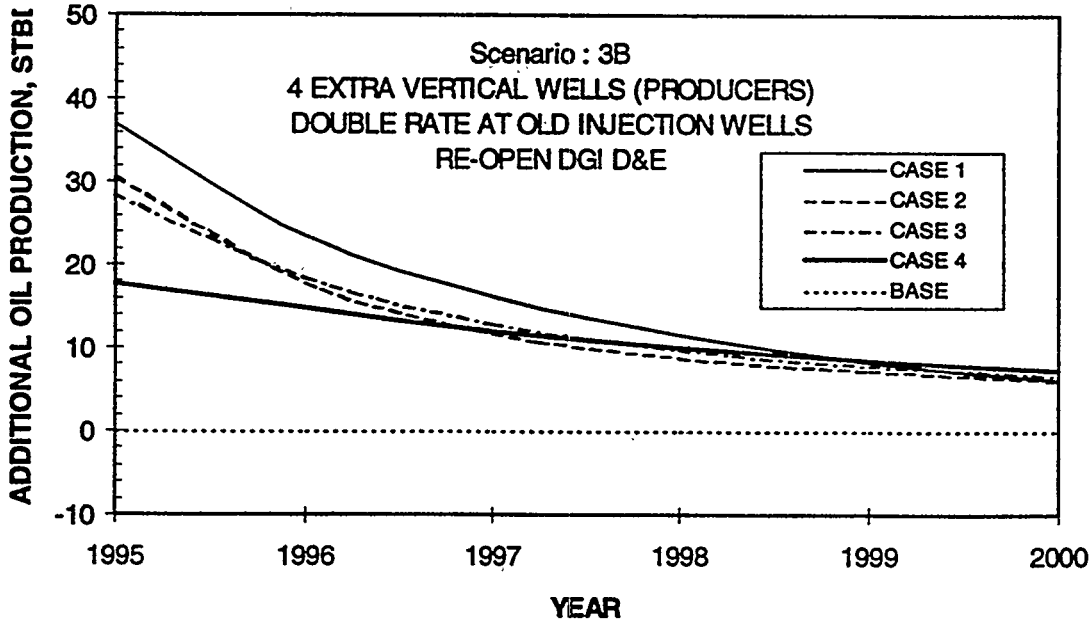

Figure 66.B

Increase Of Oil Production Using Scenario 3B

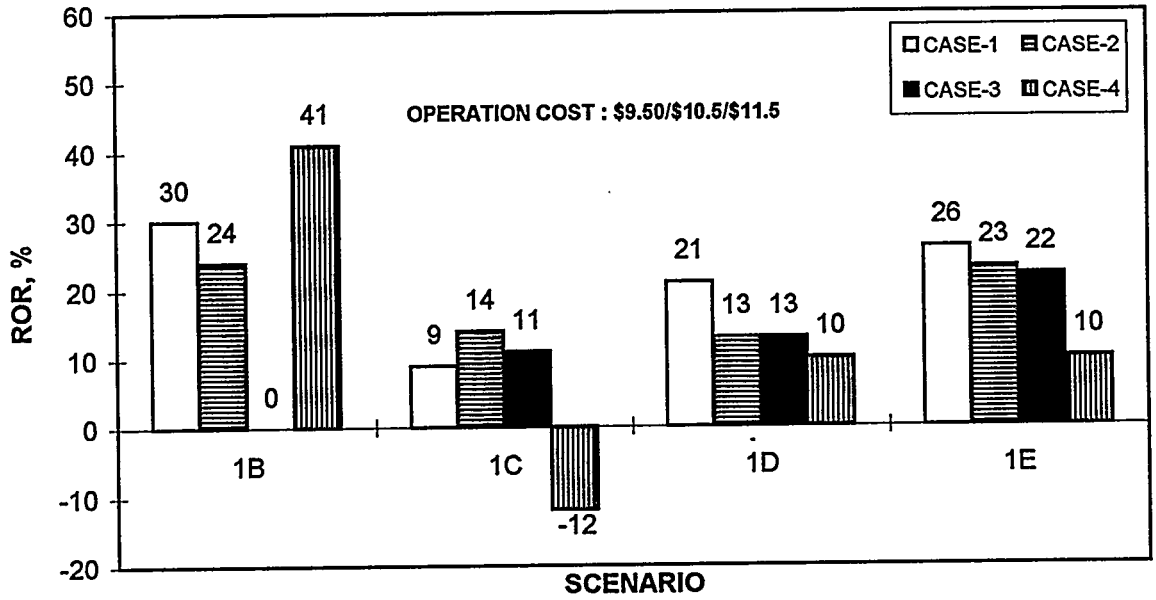

Figure 67

Rate Of Return Estimation For Different Case Study Stochastic Model Without Tomography Information

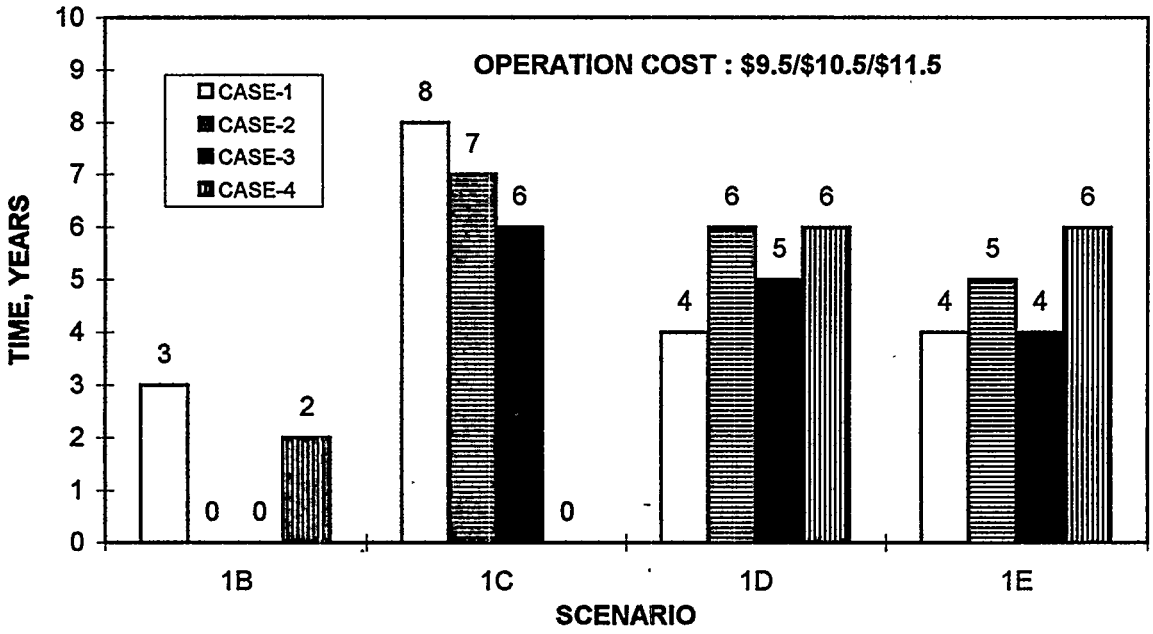

Figure 68

Pay Out Time Estimation For Different Cases Stochastic Model Without Tomography Information

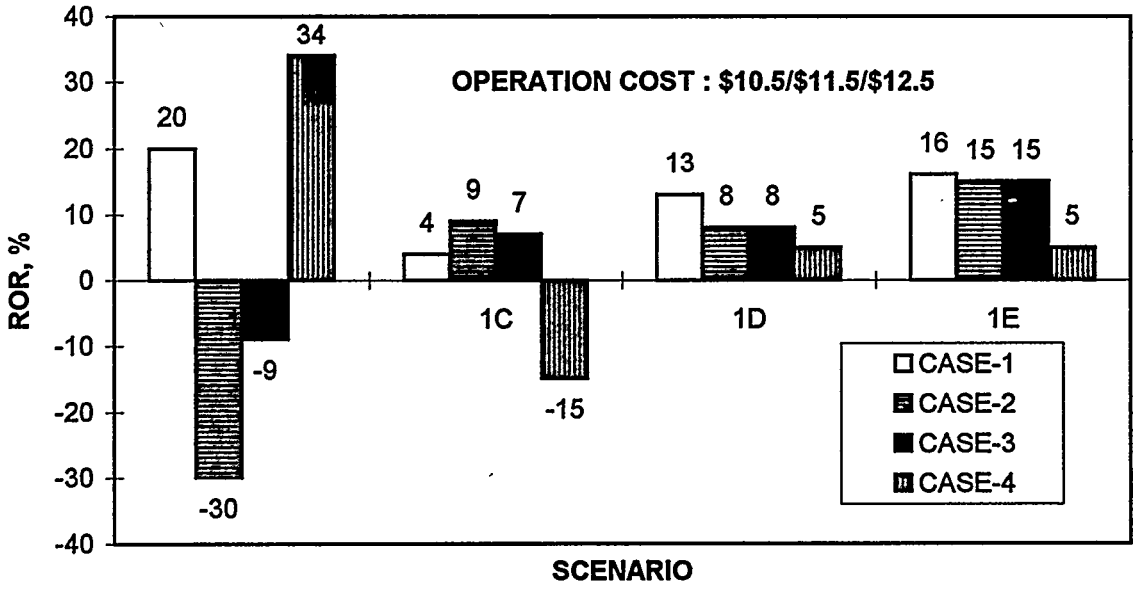

Figure 69

Rate Of Return Estimation For Higher Operating Cost Stochastic Model Without Tomography Information

☆U.S. GOVERNMENT PRINTING OFFICE: 1995 - 660-029/20021